T.C.
REPUBLIC OF TURKEY
HACETTEPE UNIVERSITY
GRADUATE SCHOOL OF HEALTH SCIENCES

MOLECULAR MOTOR CONTRACTILE MECHANISM OF RETINAL PERICYTES

Gülce KÜRELİ, MD

Neuroscience Program

DOCTOR OF PHILOSOPHY THESIS

ANKARA

2020

T.C.
REPUBLIC OF TURKEY
HACETTEPE UNIVERSITY
GRADUATE SCHOOL OF HEALTH SCIENCES

MOLECULAR MOTOR CONTRACTILE MECHANISM OF RETINAL PERICYTES

Gülce KÜRELİ, MD

Neuroscience Program

DOCTOR OF PHILOSOPHY THESIS

SUPERVISOR

Prof. Dr. Turgay DALKARA

ANKARA

2020

HACETTEPE UNIVERSITY

GRADUATE SCHOOL OF HEALTH SCIENCES

MOLECULAR MOTOR CONTRACTILE MECHANISM OF RETINAL PERICYTES

Gülce KÜRELİ

Supervisor: Prof. Dr. Turgay DALKARA

This thesis study has been approved and accepted as a PhD dissertation in "Neuroscience PhD Program" by the assessment committee, whose members are listed below, on 20.10.2020.

Chairman of the Committee :	*Prof. Dr. Bülent ELİBOL* *(Hacettepe Üniversitesi)*
Member :	*Prof. Dr. Şaban Remzi ERDEM* *(Başkent Üniversitesi)*
Member :	*Prof. Dr. Alp CAN* *(Ankara Üniversitesi)*
Member :	*Prof. Dr. Nikolaus Plesnila* *(Ludwig-Maximilians-Universität München)*
Member :	*Asst. Prof. Dr. Evren ERDENER* *(Hacettepe Üniversitesi)*

This dissertation has been approved by the above committee in conformity to the related issues of Hacettepe University Graduate Education and Examination Regulation.

Prof. Diclehan ORHAN, MD, PhD

Director

YAYIMLAMA VE FİKRİ MÜLKİYET HAKLARI BEYANI

Enstitü tarafından onaylanan lisansüstü tezimin/raporumun tamamını veya herhangi bir kısmını, basılı (kağıt) ve elektronik formatta arşivleme ve aşağıda verilen koşullarla kullanıma açma iznini Hacettepe Üniversitesine verdiğimi bildiririm. Bu izinle Üniversiteye verilen kullanım hakları dışındaki tüm fikri mülkiyet haklarım bende kalacak, tezimin tamamının ya da bir bölümünün gelecekteki çalışmalarda (makale, kitap, lisans ve patent vb.) kullanım hakları bana ait olacaktır.

Tezin kendi orijinal çalışmam olduğunu, başkalarının haklarını ihlal etmediğimi ve tezimin tek yetkili sahibi olduğumu beyan ve taahhüt ederim. Tezimde yer alan telif hakkı bulunan ve sahiplerinden yazılı izin alınarak kullanılması zorunlu metinlerin yazılı izin alınarak kullandığımı ve istenildiğinde suretlerini Üniversiteye teslim etmeyi taahhüt ederim.

Yükseköğretim Kurulu tarafından yayınlanan ***"Lisansüstü Tezlerin Elektronik Ortamda Toplanması, Düzenlenmesi ve Erişime Açılmasına İlişkin Yönerge"*** kapsamında tezim aşağıda belirtilen koşullar haricince YÖK Ulusal Tez Merkezi / H.Ü. Kütüphaneleri Açık Erişim Sisteminde erişime açılır.

- Enstitü / Fakülte yönetim kurulu kararı ile tezimin erişime açılması mezuniyet tarihimden itibaren 2 yıl ertelenmiştir. (1)
- Enstitü / Fakülte yönetim kurulunun gerekçeli kararı ile tezimin erişime açılması mezuniyet tarihimden itibaren **6** ay ertelenmiştir. (2)
- Tezimle ilgili gizlilik kararı verilmiştir. (3)

17/11/2020

Gülce KÜRELİ

[i]

---

[i] *"Lisansüstü Tezlerin Elektronik Ortamda Toplanması, Düzenlenmesi ve Erişime Açılmasına İlişkin Yönerge"*

(1) *Madde 6. 1. Lisansüstü tezle ilgili patent başvurusu yapılması veya patent alma sürecinin devam etmesi durumunda, tez **danışmanının** önerisi ve **enstitü anabilim dalının** uygun görüşü üzerine **enstitü** veya **fakülte yönetim kurulu** iki yıl süre ile tezin erişime açılmasının ertelenmesine karar verebilir.*

(2) *Madde 6. 2. Yeni teknik, materyal ve metotların kullanıldığı, henüz makaleye dönüşmemiş veya patent gibi yöntemlerle korunmamış ve internetten paylaşılması durumunda 3. şahıslara veya kurumlara haksız kazanç imkanı oluşturabilecek bilgi ve bulguları içeren tezler hakkında tez **danışmanının** önerisi ve **enstitü anabilim dalının** uygun görüşü üzerine **enstitü** veya **fakülte yönetim kurulunun** gerekçeli kararı ile altı ayı aşmamak üzere tezin erişime açılması engellenebilir.*

(3) *Madde 7. 1. Ulusal çıkarları veya güvenliği ilgilendiren, emniyet, istihbarat, savunma ve güvenlik, sağlık vb. konulara ilişkin lisansüstü tezlerle ilgili gizlilik kararı, **tezin yapıldığı kurum** tarafından verilir *. Kurum ve kuruluşlarla yapılan işbirliği protokolü çerçevesinde hazırlanan lisansüstü tezlere ilişkin gizlilik kararı ise, **ilgili kurum ve kuruluşun önerisi** ile **enstitü** veya **fakültenin** uygun görüşü üzerine **üniversite yönetim kurulu** tarafından verilir. Gizlilik kararı verilen tezler Yükseköğretim Kuruluna bildirilir.*
Madde 7.2. Gizlilik kararı verilen tezler gizlilik süresince enstitü veya fakülte tarafından gizlilik kuralları çerçevesinde muhafaza edilir, gizlilik kararının kaldırılması halinde Tez Otomasyon Sistemine yüklenir

***** *Tez **danışmanının** önerisi ve **enstitü anabilim dalının** uygun görüşü üzerine **enstitü** veya **fakülte yönetim kurulu tarafından karar verilir.***

ETHICAL DECLARATION

In this thesis study, I declare that all the information and documents have been obtained in the base of the academic rules and all audio-visual and written information and results have been presented according to the rules of scientific ethics. I did not do any distortion in data set. In case of using other works, related studies have been fully cited in accordance with the scientific standards. I also declare that my thesis study is original except cited references. It was produced by myself in consultation with supervisor (Prof. Dr. Turgay Dalkara) and written according to the rules of thesis writing of Hacettepe University Institute of Health Sciences.

Gülce KÜRELİ

ACKNOWLEDGEMENTS

I would like to thank to my parents Sezgi&İhsan, my sister Ece, other family members and friends for their endless support.

I thank to Hacettepe University Scientific Research Projects Coordination Unit for the financial support.

I have learned a lot from all members of the Institute of Neurological Sciences and Psychiatry, who were always very supportive, helpful and friendly. Hereby I thank to Anisa, Aslıhan B.V., Aslıhan T.S., Buket, Canan Ç.A., Canan K.B., Dilek, Doğa, Duygu, Eda, Elif, Emre Cem, Ecehan, Gökhan, Gül, Hülya, İlkay, İlksen, Melike, Merve, Mesut, Muhammet, Nevin, Nursel, Onur, Taha, Tuğba and Zafer. Special thanks to Atagün, Burak, Gökçe, Özlem and Zeynep for becoming another family to me.

I thank to professors Bülent Elibol, Emine Eren-Koçak, Hülya Karataş-Kurşun and Müge Yemişci-Özkan; Alp Can and Ş. Remzi Erdem for sharing their invaluable knowledge and experience during my PhD process.

This thesis was founded on the retinal techniques that I learned from Dr. Sinem Yılmaz-Özcan. She also contributed to gene knockdown. I would like to thank to her for being a great instructor.

Dr. Evren Erdener had invaluable contributions in the improvement of this thesis. He adapted and developed the techniques for 3D model preparation and FRET analysis. I have learned a lot from him about microscopy, image processing and analysis. I would like to thank to him for all his efforts and fruitful scientific discussions.

Last but not least, I would like to thank to Prof. Dr. Turgay Dalkara. He has always been a very supportive and dedicated supervisor. None of these could have been done without his experience and guidance.

ABSTRACT

Kureli, G., Molecular Motor Contractile Mechanism of Retinal Pericytes, Hacettepe University Graduate School of Health Sciences, Neuroscience Program, Doctor of Philosophy Thesis, Ankara, 2020. Although it is known that capillary pericytes function in the regulation of capillary tone and blood flow, the contractile proteins involved in these processes are unidentified. It is likely that α-SMA functions as a part of contractile apparatus in pericytes as it does in smooth muscle cells. Therefore, we examined the expression of α-SMA along the mouse retinal microvascular network together with the expression of Myh11 protein, which we identified as the potential myosin heavy chain isoform candidate based on the single cell transcriptomic data in the literature. We found that α-SMA is expressed by capillary pericytes, but depolymerization must be prevented for its demonstration in downstream segments, in contrast to Myh11, which highly colocalizes with α-SMA but is present throughout the microvascular tree. Immunofluorescent signals delineated close association of α-SMA and Myh11, which was also confirmed by high FRET efficiency, oriented as thin strands reminiscent of stress-fibers, conforming to a contractile function. The functional correspondence of this spatial association was evaluated by inhibition of actomyosin cross-bridge cycling with blebbistatin, which prevented noradrenaline-induced vasoconstriction. Alongside, a supportive mechanism in cellular contraction, actin polymerization, was assessed using markers identifying filamentous and globular forms of actin. After intravitreal noradrenaline application, actin polymerization was pronounced in downstream capillary pericytes, suggesting a need for actin polymerization for contractile force generation because they express α-SMA in low quantities. In conclusion, pericytes contract using actomyosin cross-bridge cycling, which is supplemented by actin polymerization in downstream pericytes.

Key Words: pericyte, actin, myosin, contractility, retina

This study is supported by Hacettepe University Scientific Research Projects Coordination Unit with the project number THD-2018-17247.

ÖZET

Küreli, G., Retinal Perisitlerin Moleküler Motor Kasılma Mekanizması, Hacettepe Üniversitesi Sağlık Bilimleri Enstitüsü Temel Nörolojik Bilimler Programı, Doktora Tezi, Ankara, 2020. Kılcal perisitlerin tonus ve kan akışının düzenlenmesinde görev yaptığı bilinmesine rağmen, bu süreçlerde yer alan kasılabilir proteinler henüz tanımlanmamıştır. Düz kas hücrelerinde olduğu gibi, α-SMA'nın perisitlerdeki kasılma aparatının da bir parçası olarak işlev görmesi muhtemeldir. Bu nedenle literatürdeki tek hücre-transkriptomik verilerine dayanılarak fare retinal mikrovasküler ağı boyunca, perisitlerdeki miyozin ağır zincir izoform adayı olarak belirlenen Myh11'inki ile birlikte α-SMA ifadesi incelenmiştir. α-SMA'nın aşağı segmentlerde gösterilebilmesi için depolimerizasyonun önlenmesi gerektiği, bunun aksine α-SMA ile yüksek oranda kolokalize olan Myh11'in tüm mikrovasküler ağ boyunca mevcut olduğu görülmüştür. α-SMA ve Myh11'in immünofloresan sinyaller ile gösterilen yakın ilişkisi yüksek FRET verimliliği ile de teyit edilmiş ve sinyallerin kasılma işlevi ile uyumlu, stres liflerini anımsatan ince iplikler olarak yerleştiği görülmüştür. Bu uzaysal ilişkinin işlevsel karşılığı, aktomiyozin çapraz köprü döngüsünün inhibitörü blebbistatin kullanılarak noradrenalin ile uyarılmış vazokonstriksiyonun önlenmesiyle değerlendirilmiştir. Bununla birlikte, hücresel kasılmada destekleyici bir mekanizma olan aktin polimerizasyonu, aktinin filamentöz ve globüler formlarını tanıyan belirteçler kullanılarak değerlendirilmiştir. İntravitreal noradrenalin uygulamasından sonra, aktin polimerizasyonu aşağı segmentlerdeki kılcal perisitlerde belirginleşmiş, bu da bu bölgedeki az miktarda α-SMA ifadesi nedeniyle kasılma kuvveti üretimi için aktin polimerizasyonuna ihtiyaç olduğunu düşündürmüştür. Sonuç olarak perisitlerin, aşağı segmentlerde aktin polimerizasyonu ile desteklenen aktomiyozin çapraz köprü döngüsünü kullanarak kasıldığı bulgusuna erişilmiştir.

Anahtar kelimeler: perisit, aktin, miyozin, kontraktilite, retina

Bu çalışma Hacettepe Üniversitesi Bilimsel Araştırma Projeleri Koordinasyon Birimi tarafından THD-2018-17247 numaralı proje ile desteklenmiştir.

TABLE OF CONTENTS

APPROVAL PAGE iii
YAYIMLAMA VE FİKRİ MÜLKİYET HAKLARI BEYANI iv
ETHICAL DECLARATION v
ACKNOWLEDGEMENTS vi
ABSTRACT vii
ÖZET viii
TABLE OF CONTENTS ix
SYMBOLS AND ABBREVIATIONS xi
LIST OF FIGURES xiii
LIST OF TABLES xv
1. INTRODUCTION 1
2. GENERAL INFORMATION 3
2.1. Pericytes 3
2.1.1. Pericyte Contractility and Blood Flow Regulation 5
2.2. Contractile Proteins 7
2.2.1. Actin 7
2.2.2. Myosin II 13
2.3. Retinal Vasculature 20
3. MATERIALS AND METHODS 22
3.1. Animals 22
3.2. Intravitreal Delivery of Substances 22
3.3. Whole Mount Retina Preparation 24
3.4. Fluorescent Labeling 25
3.5. Immunofluorescent Labeling 26
3.6. Imaging and Analysis 29
3.7. Statistical Analysis 31
3.8. Förster Resonance Energy Transfer (FRET) 32
4. RESULTS 37
4.1. Pericytes are Contractile 37
4.2. Organization of α-SMA Fiber Bundles Suggests a Contractile Function 38
4.3. Contribution of Actomyosin Coupling to Pericyte Contraction 39
4.3.1. Myh11 Protein Labeling Highly Colocalizes with α-SMA Expression In Pericytes 39

4.3.2. Myh11 Expression is Independent from Retinal Vascular Order, Fixative Type and α-SMA Staining Pattern 42

4.3.3. Blebbistatin Disrupts Actomyosin Mediated Constriction in Retinal Microvascular Segments 46

4.3.4. Analysis of α-SMA and Myh11 Interaction in Pericytes with FRET 48

4.4. Role of Actin Polymerization in Pericyte Contraction 49

4.4.1. Actin Isoforms in Pericytes 49

4.4.2. Phalloidin and DNase I Labeling as Indicators of Actin Polymerization State 52

4.4.3. NA Induces Actin Polymerization in Retinal Pericytes 54

5. DISCUSSION 58

6. CONCLUSION AND REMARKS 67

7. REFERENCES 68

8. APPENDICES

APPENDIX-1: Ethical Approval for Thesis Studies

APPENDIX-2: Thesis Originality Report

9. CURRICULUM VITAE

SYMBOLS AND ABBREVIATIONS

°C	Celsius degree
µL	Microliter
µM	Micromolar
g	Gram
kDa	Kilodalton
kg	Kilogram
mg	Milligram
mL	Milliliter
mm	Millimeter
nm	Nanometer
α-SMA	α-Smooth Muscle Actin
Acta2	Actin Alpha 2, Smooth Muscle
ADP	Adenosine Diphosphate
ATP	Adenosine Triphosphate
ATP	Adenosine Triphosphatase
BBB	Blood Brain Barrier
BRB	Blood Retina Barrier
Ca^{2+}	Calcium ion
CNS	Central Nervous System
dH_2O	Distilled water
DMSO	Dimethyl sulfoxide
DNase I	Deoxyribonuclease I
EC	Endothelial cell
ECM	Extracellular Matrix
ELC	Essential Light Chain
FRET	Förster Resonance Energy Transfer
F-actin	Filamentous actin
G-actin	Globular actin

IQR	Interquartile Range
JND	Juxtanuclear Diameter
JNDR	Juxtanuclear Diameter Ratio
L/min	Liter/Minute
Mg^{2+}	Magnesium ion
MLC	Myosin light chain
MLCK	Myosin light chain kinase
MLCP	Myosin light chain phosphatase
MHC	Myosin heavy chain
Myh11	Myosin heavy chain 11, smooth muscle
NG2/Cspg4	Neural glial antigen 2/Chondroitin sulphate proteoglycan 4
NVC	Neurovascular Coupling
NVU	Neurovascular Unit
PBS	Phosphate Buffered Saline
PDGF-B	Platelet-derived growth factor-B
PDGFR-β	Platelet-derived growth factor receptor beta
PFA	Paraformaldehyde
Pi	Inorganic phosphate
RBC	Red Blood Cell
RLC	Regulatory light chain
RNase	Ribonuclease
ROI	Region of Interest
SD	Standard Deviation
siRNA	small interference RNA
vSMC	Vascular smooth muscle cell

LIST OF FIGURES

Figure	Page
2.1. Pericyte morphology varies along microvasculature.	4
2.2. Pericytes on upstream and downstream vessels might be contributing to NVC differentially.	6
2.3. Sequence differences of actin isoforms.	8
2.4. Actin treadmilling activity.	10
2.5. Organization of actin filaments in vSMCs.	12
2.6. Structure of myosin II.	14
2.7. Actin-myosin cross-bridge cycling.	16
2.8. Regulation of myosin activity.	17
2.9. Blebbistatin's mechanism of action.	20
2.10. Retinal trilaminar vascular network.	21
3.1. α-SMA labeling is unaffected by antibody concentration and vasoconstrictor application.	28
3.2. Principle of retinal vascular branch order determination.	30
3.2. Basic principle of FRET.	33
3.3. Principle of spectral unmixing.	36
4.1. 3D modeling of a contracted pericyte from Z-stack image of NA treated retina labeled with antibody against α-SMA.	37
4.2. α-SMA fiber bundles are differentially organized in pericytes from third, fourth and sixth retinal vascular orders.	38
4.3. Myh11 immunolabeling closely follows α-SMA immunostaining in retinal microvessels.	40
4.4. Myh11 negative control.	40
4.5. Demonstration of α-SMA and Myh11 shown with deconvolution.	41
4.6. Demonstration of α-SMA and Myh11 with STED.	41
4.7. Demonstration of α-SMA and Myh11 with nanobodies.	42
4.8. Despite gradual tapering in α-SMA labeling toward downstream capillaries, Myh11 labeling covers all microvasculature in the superficial retinal vascular layer.	43
4.9. Myh11 labeling continues all along the superficial layer, revealing the capillary loops.	43

4.10. Myh11 labeling uninterruptedly continues in the intermediate and deep layers of retinal vasculature. 44

4.11. Myh11 labeling is unaffected by fixation method. 45

4.12. Knocking down α-SMA expression did not modify Myh11 organization. 46

4.13. Blebbistatin prevents NA-induced vasoconstrictions in downstream retinal vascular branches. 48

4.14. FRET efficiency between antibodies against α-SMA and Myh11 in retinal pericytes. 49

4.15. Phalloidin labeling largely overlaps with α-SMA immunostaining. 51

4.16. Noradrenaline stimulation induces actin polymerization in microvessels. 53

4.17. Noradrenaline induces F-actin polymerization in downstream retinal pericytes 55

4.18. High F/G signal ratio is associated with decreased capillary diameter. 57

5.1. Activation of α_1-adrenergic receptors triggers a cascade of events that lead to cellular contraction 66

LIST OF TABLES

Table **Page**

2.1. List of mouse genes coding MHC isoforms. 15

1. INTRODUCTION

Pericytes are contractile microvascular mural cells. In vascular segments proximal to the microvasculature (upstream segments), the primary mural cell type is the vascular smooth muscle cell (vSMC), whose actomyosin contractile machinery and its support by actin polymerization, have been well characterized (1). In contrast, reservations have been voiced regarding pericyte contractility *in vivo* (2-4) and their role in cerebral and retinal blood flow regulation (5, 6), especially for the ones located on downstream capillaries. Therefore, deeper insight into the contractile mechanisms of central nervous system (CNS) pericytes located on various microvascular segments is required for a better understanding of the physiological and pathological processes involving pericyte contraction.

Pericytes share several common features with vSMCs although they have distinct properties and display varying phenotypes along the microvascular tree (7). Prompted by *in vitro* cell culture studies suggesting presence of actin polymerization-mediated as well as actomyosin-mediated contraction in pericytes (8), we sought to explore whether or not pericytes use a similar contractile apparatus to vSMCs and cultured pericytes under *in vivo* conditions as well and how this phenotype varies along the course of microvasculature between the up- and downstream pericytes. Therefore, we tested the following hypotheses:

- Organization of actin bundles is suggestive of a contractile function
- Retinal pericytes express Myh11 and it colocalizes with α-SMA
- Actin and myosin in pericytes interact and are functionally coupled
- Actin polymerization is a supportive mechanism to actomyosin mediated pericyte contraction

We found that the pattern of α-Smooth Muscle Actin (α-SMA) immunostaining was suggestive of a contractile function, with a variation in orientation of the bundles along the vasculature. We also detected the smooth muscle isoform of myosin heavy chain (Myh11) in retinal pericytes, which highly overlapped with α-SMA immunostaining, suggesting presence of an actomyosin

coupling-mediated contractile machinery. We supported this histological finding by pharmacological inhibition of myosin ATPase (Adenosine Triphosphatase), an enzyme involved in actomyosin mediated contraction with blebbistatin administered prior to a vasoconstrictive agent, noradrenaline (NA) (1, 9). Inhibition of myosin ATPase prevented constriction of downstream retinal microvascular segments, supporting the idea that pericyte contractility is mediated by actomyosin cross bridge cycling. We also investigated actin polymerization in pericytes, an adjunctive contractile mechanism in smooth muscle cells (1, 10). After the induction of retinal pericyte contraction by intravitreal NA, we found that filamentous/globular (F/G) actin ratio, a microscopy-based index of actin polymerization, was increased in downstream pericytes, suggesting a supplementary role for F-actin polymerization in pericyte contractility as in vSMCs.

2. GENERAL INFORMATION

2.1. Pericytes

Pericytes are vascular mural cells located around microvessels, including the pericapillary arterioles, capillaries and postcapillary venules. They were first described by Rouget (1879) (11) and, hence, initially named as “Rouget cells”. Later Zimmermann (1923) (12) re-named them as pericytes due to their prominent position around the microvasculature (13). A distinctive feature of these cells is their typical microscopic appearance reminiscent of a “bump on a log”. Another characteristic feature of pericytes is that they are ensheathed by two layers of basement membrane that they share with the neighboring endothelial cells (ECs) (14).

Pericytes are in close interaction with each other and also with neighboring ECs, both structurally and functionally, through gap junctions placed on their interdigitating, “peg and socket” type of cytoplasmic extensions penetrating through the basement membrane into the ECs. Signaling pathways involving PDGF-B, TGF-β, angiopoietins, sphingosine-1-phosphate and Notch play roles in pericyte EC interaction (15). PDGF-B/PDGFR-β (Platelet-Derived Growth Factor-B/Platelet-Derived Growth Factor Receptor-beta) signaling pathway is crucial for pericyte survival, proliferation and migration. In models of defective PDGF-B/PDGFR-β signaling, pericyte coverage decreases, causing endothelial hyperplasia, microaneurysms and hemorrhages (13). By way of these interactions, pericytes also aid in the maintenance of blood-brain barrier (BBB) / blood-retina barrier (BRB). ECs were shown to have increased transcytosis by electron microscopy in the absence of pericytes (16, 17).

Pericytes comprise a heterogenous cell population differing in their expression profiles and morphology depending on their developmental stage or position along the vascular axis (13). They are also heterogenous in terms of their origin, deriving from ectoderm (neural crest) or mesoderm (14). Morphological

heterogeneity of pericytes is illustrated in Figure 2.1. Pericytes around precapillary arterioles and at bifurcation points of capillaries are of wrapping, ensheathing or mesh type, conforming to a contractile function. Those lying along the capillaries are named as midcapillary or thin-strand/helical pericytes based on their morphology with thin and long extensions. Some researchers argue that they do not have a contractile function but take part in regulation of BBB/BRB maintenance (2). Those around postcapillary venules display a stellate morphology, and they are thought to regulate leukocyte trafficking across vascular wall.

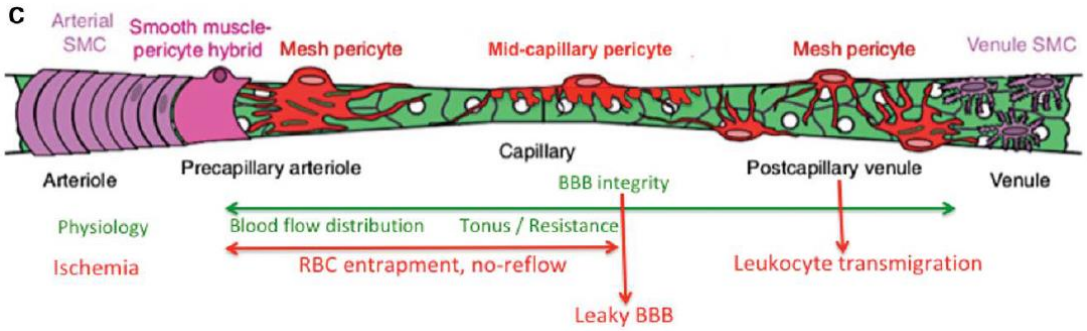

Figure 2.1. Pericyte morphology varies along microvasculature. Pericytes attain mesh-like morphology around precapillary arterioles, helical or thin-strand morphology around middle-capillary region and mesh/stellate-like morphology around postcapillary venules. Variations in structure are thought to be correlated with function. Insult to pericytes at different locations are associated with no-reflow phenomenon, BBB permeability and leukocyte infiltration (18).

Many pericyte-specific markers have been proposed: PDGFR-β, NG2/Cspg4 (Neural glial antigen 2/Chondroitin sulphate proteoglycan 4), CD13 (alanyl membrane aminopeptidase), desmin, vimentin, and recently Kir 6.1 (Potassium inwardly rectifying channel, subfamily J, member 8) (13, 19). However, none of these markers are specific to pericytes, as they are also expressed by other cell types in CNS: PDGFR-β, NG2, desmin and vimentin are expressed by vSMCs. Oligodentrocyte precursor cells are NG2 positive. It should also be noted that some of the mentioned putative markers are contractile proteins such as desmin and vimentin, which are intermediate filament proteins expressed by smooth muscle cells (20). A recent study utilizing RNA-seq and in situ hybridization suggested two novel pericyte marker

candidates (vitronectin and interferon-induced transmembrane protein), which are not validated for routine use yet (21).

As pericytes and vSMCs share almost all of the proposed pericyte markers, differentiation of these two cell types must not solely depend on a single marker expression, but a combination of markers or a combination of immunologic detection with morphological definition criteria and localization along the vascular tree (13, 14).

2.1.1. Pericyte Contractility and Blood Flow Regulation

Pericytes are contractile cells, just like the other upstream vascular mural cell, vSMCs, which form circular bands around larger upstream vessels. Although these two cell types have much in common, pericytes morphologically differ from vSMCs with their longer and thinner processes incompletely covering the vessel, intermittent localization of their soma, a soma/nucleus protruding out the vessel wall and being embedded within two layers of basement membrane (22). They reach the highest density in mammalian body in CNS with a pericyte to endothelial cell ratio of 1:3-1:1 (23). As CNS vasculature is unique in having blood flow regulation with fine spatial resolution and BBB/BRB properties, the high pericyte density is thought to underlie these functional specializations. Moreover, pericytes are also involved in angiogenesis, removal of toxic metabolites, inflammation, regeneration and limitation of EC proliferation (19, 24).

Pericytes are one of the members of the neurovascular unit (NVU), along with neurons, astrocytes and ECs. Each component of the NVU closely communicates to provide neurovascular coupling (NVC) for delivering more blood flow as neural activity increases, a vital vascular response called functional hyperemia (13). This phenomenon is the physiological basis for blood oxygen level dependent (BOLD) signal in fMRI (functional Magnetic Resonance Imaging) (25). Close interaction of pericytes with the other members of the NVU makes it a crucial player in NVC.

Although Fernández-Klett et al. (5) initially reported that functional hyperemia was not mediated by dilation of microvessels in case of pharmacologically

induced seizure activity, Hall et al. (26) later clearly demonstrated capillaries actively dilated about one second before arterioles during sensory stimulation in mouse cortex *in vivo*. Supporting the idea that capillaries actively participate in NVC, most of the perivascular nerve endings in CNS end around capillaries, rather than arterioles (24). On the other hand, Rungta et al. (27) showed that upstream vessels dilate before downstream capillaries in olfactory bulb upon stimulation, although red blood cell (RBC) velocity increases faster in downstream capillary segments still supporting the active role of capillary/thin-strand pericytes in NVC. Therefore, pericytes on upstream and downstream vessels might be contributing to NVC differentially. Pericytes on the upstream microvessels have been shown to relax and contract in response to neural activity to match tissue blood flow demand, contributing to the NVC at the microcirculatory level (26, 27) (Figure 2.2.). Whereas, downstream pericytes has the capability to adjust their stiffness, hence, they are thought to modify capillary blood flow by changing the distal capillary resistance (27-29).

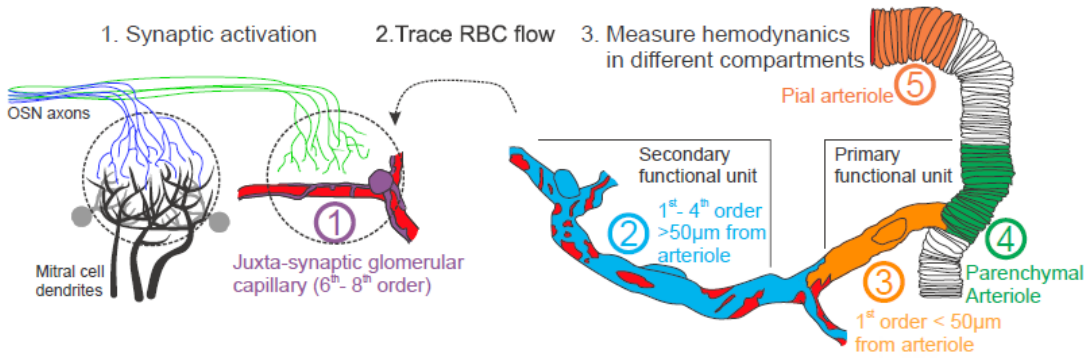

Figure 2.2. Pericytes on upstream and downstream vessels might be contributing to NVC differentially. Rungta et al. (27) divided vascular network of olfactory bulb into functional units. The unit 1, which is the closest one to synaptic activity, represents capillary pericytes. With synaptic activation, upstream units display faster luminal diameter increases, although downstream units reach higher RBC flux rates earlier. This is attributed to the differential organization of contractile fiber bundles, which are organized circularly in upstream segments to change the luminal diameter primarily, and helically in downstream segments, being attributed to the vascular wall resistance changes easing the flux of blood cells (27).

In addition to coupling through gap junctions with neighboring cells, responsiveness of pericytes to vasoactive mediators such as catecholamines,

endothelin-1, thromboxane, ATP, nitric oxide, prostaglandins, and the end products of neural activity such as potassium, adenosine and lactate (24) can set the pericyte contractility in a coordinated way with other components of the NVU. The responsiveness of pericytes to these mediators has been shown *ex vivo*, in isolated rat retina and cerebellar slices (30) and also *in vivo* in the cortex (5).

In case of a dysfunction in NVC, a mismatch between blood flow and tissue demand arises. This situation is observed in diseases involving microvasculature, such as Alzheimer's disease (31), diabetic retinopathy (32), and acute ischemic stroke (18). The current treatment approach for acute ischemic stroke is recanalization either by mechanical removal of the thrombus (thrombectomy) or thrombolysis with tissue plasminogen activator. Although both approaches are effective in recanalizing large vessels, microcirculatory dysfunction persists, hampering complete tissue reperfusion. This condition, named as no-reflow phenomenon blocks the passage of RBCs and leads to ineffective oxygen extraction, although plasma may continue to flow (33, 34). This blockage was initially thought as a result of swollen ECs and astrocyte endfeet but it was later realized to be mainly caused by persistent pericyte contraction, triggered by reactive oxygen species and sustained elevation of intrapericytic calcium (35-37).

2.2. Contractile Proteins

2.2.1. Actin

Actin, the evolutionarily conserved microfilament protein, is the most abundant protein (20% of the total cellular protein) in mammalian cells except for a few cell types. (16, 38, 39). As a structural protein, its turnover is very slow, counted by weeks in muscle cells (39). Only 7% of the F-actin is formed from newly synthesized monomers, otherwise, the primary source is polymerization of the existing pool of G-actin (40).

Actin has 6 different mammalian isoforms which are coded by different genes and highly similar in amino acid sequence (95% homology): α-skeletal muscle actin,

α-cardiac muscle actin, α-smooth muscle actin, γ-smooth muscle actin, γ-cytoplasmic actin and β-cytoplasmic actin. Most of the difference stems from the amino acid sequences at the N-terminal region, which alters the binding properties of isoforms to actin binding proteins (16, 41) (Figure 2.3.). This differential binding is thought to differentiate between muscular and cytoplasmic isoforms, as well as differential distribution of the isoforms within cytoplasm (41, 42). Cytoplasmic actin isoforms are ubiquitously expressed while muscle isoforms are cell type specific. Knockouts of α-skeletal (43) and cardiac muscle (44) and β-actins (45) are not compatible with life in transgenic mice. α-smooth muscle actin knockouts are viable, but develop vascular aneurysms and blood pressure regulation problems (46), whereas γ-cytoplasmic actin knockouts have hearing problems (47). Isoforms coexisting in a cell are thought to be differentially distributed by their different binding dynamics or by targeting of transcripts. Distribution of the isoforms is cell type specific: For example, α-skeletal muscle actin is confined to sarcomeres whereas γ-cytoplasmic actin is found in other cellular localizations in the muscle (42). Between the cytoplasmic isoforms, β-cytoplasmic actin is considered as the more dynamic one, being targeted to active membranous regions such as growth cones of neurons. (48). β-cytoplasmic actin also colocalizes with myosin II in contractile rings of dividing cells (41).

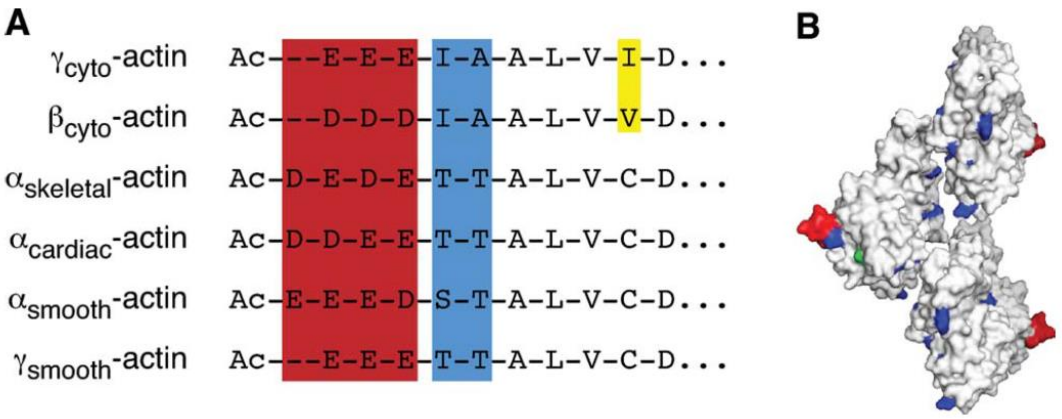

Figure 2.3. Sequence differences of actin isoforms. A shows alignment of actin isoforms by N terminal and B shows isoform sequence differences on an F-actin model. Red sequences vary most between all isoforms, whereas blue sequences mainly vary between muscle and cytoplasmic isoforms. Yellow indicates substitutions within cytoplasmic isoforms and green within muscle isoforms (42).

Cytoplasmic and smooth muscle isoforms of actin were detected in cultured pericytes (49). Although capillary pericytes were previously reported not to express α-SMA (2, 50), the presence of α-SMA, the main contractile isoform in vSMCs in downstream capillary pericytes has recently been disclosed only after prevention of F-actin depolymerization, suggesting that α-SMA filaments are actively (de/re)-polymerized (36, 37). The latter studies also showed that short interfering RNA (α-SMA-siRNA) suppressed α-SMA expression preferentially in high branch order capillary pericytes and prevented their contraction, conforming to the existence of a smaller pool of a-SMA involved in contraction of downstream capillary pericytes. These findings were confirmed by recent single-cell RNA sequence of the cells of brain vasculature (51), which reported a large amount of α-SMA mRNA was located in vSMCs, whereas low hits were detected in pericytes (52).

Actin Polymerization

Actin is found in polymerized (polymeric/filamentous(F)) or depolymerized (monomeric/globular(G)) forms. There is a highly dynamic balance between these two forms in live cells and the balance can rapidly shift towards the polymerized form to promote contractility upon mechanical or chemical stimulation. F-actin polymerization is one of the universal cellular mechanisms providing contractility and cell motility; therefore, it may also play a role in pericyte contraction as it does in vSMCs (1). Blockage of actin polymerization induces relaxation in vascular tissue without affecting myosin light chain phosphorylation (53).

Actin filaments are asymmetric in terms of polymerization and depolymerization; growth being the net effect at the barbed (+) end by binding of ATP-bound G-actin monomers and, depolymerization at the pointed (-) end by detachment of ADP-bound G-actin monomers (39) (Figure 2.4.). This polarity is determined by the orientations of the four domains of actin (42) and the ends take their names from the orientation of myosin filaments on actin (39). While actin monomers are stabilized by bound nucleotides, nucleotides bound to monomers are stabilized by Mg^{2+} in the environment. ATP hydrolysis-induced conformational

changes affect the binding properties of F-actin with other monomers and actin binding proteins (38).

Steady-state polymerization-depolymerization activity is called as treadmilling and its rate is slower than 1 subunit per second (39, 54). However, in activity dependent cases, durability of filaments ranges from seconds to days, depending on the activity, for example, having a faster turnover in lamellipodia and more stable state in myofibrils. Polymerization rate is also affected by local monomer concentrations. The concentrations are heterogenous in polarized cells, and local translation events contribute to this heterogeneity (55).

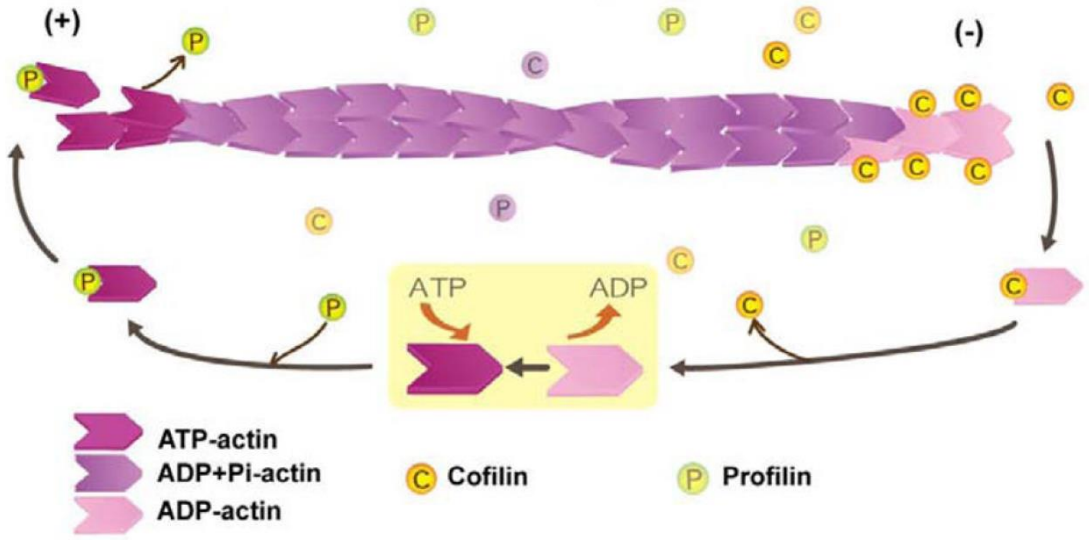

Figure 2.4. Actin treadmilling activity. ATP binding induced conformational changes in actin monomers promotes polymerization of actin filaments at the barbed (+) end, whereas hydrolysis of ATP promotes net depolymerization at the pointed (-) end. Conformational changes also affect interaction of actin with actin binding proteins, such as cofilin promoting monomer dissociation and profilin promoting monomer association (38).

Organization of Actin in vSMCs

As vSMCs are taken as the proxy cells to understand the contractile machinery, it is crucial to understand their organization. Actin filaments are attached to focal adhesion points (dense plaques) containing α-actinin, mediating communication between intra and extracellular environments via integrins to

provide stiffness to the cell membrane. This mechanosensing is important both to transmit the intracellular forces to outside and to sense external mechanical pressure (56). The strong connections to extracellular matrix generate the contractile force necessary to narrow the vessel lumen (constrict) (1). Phosphorylation of focal adhesion associated proteins (e.g. vinculin, paxillin, talin) upon stimulation starts a reaction that results in actin polymerization (56). The intracellular attachment points are called as dense bodies and contain α-actinin.

Four of the actin isoforms, α-smooth muscle actin (α-SMA) (60%), γ-smooth muscle actin and γ-cytoplasmic actin (20%) as well as β-cytoplasmic actin (20%) are expressed in vSMCs (1). Contractile and cytoskeletal actin filaments are organized differentially in vSMCs (56). α-SMA and γ-smooth muscle actin, the latter of which is more abundant in gastrointestinal smooth muscle cells, are located on contractile structures of vSMCs called stress fibers (1). Stress fibers are less organized structures compared to sarcomeres of skeletal muscles (57) and are also observed in pericytes (58). β-actin isoform is organized around dense bodies, whereas γ-cytoplasmic actin is mainly localized to the cortical region of the cell. (56) (Figure 2.5.). β and γ cytoplasmic actins are considered as the cytoskeletal actin isoforms and constitute the more dynamic population of actin to be polymerized upon stimulation with vasoconstrictive mediators (16). A similar organization of actin isoforms was also observed in cultured bovine retinal microvascular pericytes (59), except that pericytes do not express γ-smooth muscle actin isoform (60).

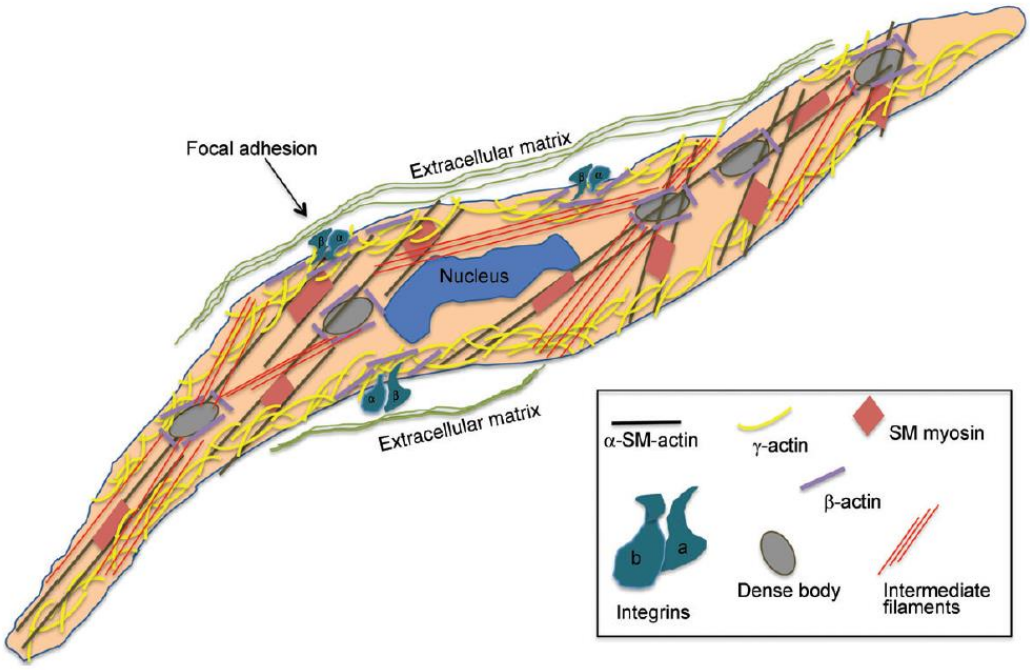

Figure 2.5. Organization of actin filaments in vSMCs. γ-cytoplasmic actin is concentrated in cortical/submembranous regions, whereas β-cytoplasmic actin is concentrated mainly around dense bodies. α-SMA stretches between focal adhesion points and dense bodies, colocalizing with myosin filaments, giving rise to contractile components of the cell (1).

Intracellular F-actin stress fibers are known to transmit F-actin-mediated forces to the extracellular environment for an integrated cellular contraction (1, 8). However, the involvement of these F-actin based mechanisms in downstream capillary contraction requires further *in vivo* evidence because α-SMA is expressed in low quantities in pericytes unlike vSMCs.

Pharmacological Tools for Studying Actin

Natural toxins are commonly used to investigate actin polymerization. Latrunculins are derived from a sea sponge (61). They bind G-actin monomers in a 1:1 ratio and prevent polymerization, shifting the actin state towards depolymerization (62). Cytochalasins are derived from fungi and their action is complementary to that of latrunculins. They bind to barbed (+) end of actin filaments, preventing polymerization and inducing a net depolymerization (63, 64).

Phalloidin is an F-actin stabilizer obtained from the mushroom *Amanita phalloides*, preventing depolymerization (65, 66). It is mostly used for isoform-nonspecific actin labeling by its fluorescently conjugated form. Sea sponge-derived jasplakinolide, which induces and stabilizes polymerization of actin, is mostly used in live studies rather than for labeling (67). Phalloidin binds actin in a 1:1 ratio and interacts with two neighboring monomers in a filament, shifting the equilibrium towards polymerization. Its affinity is unaffected by the length of actin filaments or interaction state with tropomyosin and myosin because its molecular size is very small (0.6 nm) (65, 66, 68).

While phalloidin binds filamentous actin, Deoxyribonuclease I (DNase I) enzyme has a natural affinity for monomeric actin (69). It binds to G-actin with 1:1 ratio and its enzymatic activity is inhibited upon binding. Its fluorescently conjugated forms are used in combination with phalloidin to visualize monomeric and polymeric states of actin.

2.2.2. Myosin II

Myosin is the principal cellular motor protein. It has been phylogenetically classified into 35 subclasses (70), two of which being functionally the most well-characterized: Myosin I, functioning in vesicular transport and myosin II, functioning in cellular contraction, cell motility, division, migration and neuronal plasticity (71-73). Besides having two heavy chains, myosin II bears one regulatory light chain (MLC20/RLC) and one essential light chain (MLC17/ELC) near the neck region of each heavy chain, which acts as a force-transmitting lever (73) (Figure 2.6.). Head region of the heavy chain, which is highly conserved across species (74), harbors the actin-binding site and ATP catalytic activity required for actomyosin mediated contraction (72). Mg-ATPase activity of myosin head increases upon binding to actin (71). Tail regions conform to a coiled-coil conformation lining up in a filamentous structure (thick filaments) (72). The number of myosin heavy chain (MHC) isoform genes in human genome is 16 (75) (Table 2.1.). Among them, type 11 is considered to be smooth muscle specific, whereas 9, 10 and 14 are found in non-muscle cell types,

such as fibroblasts. Pericytes also express myosin II (19), but the predominant isoform is yet undetermined.

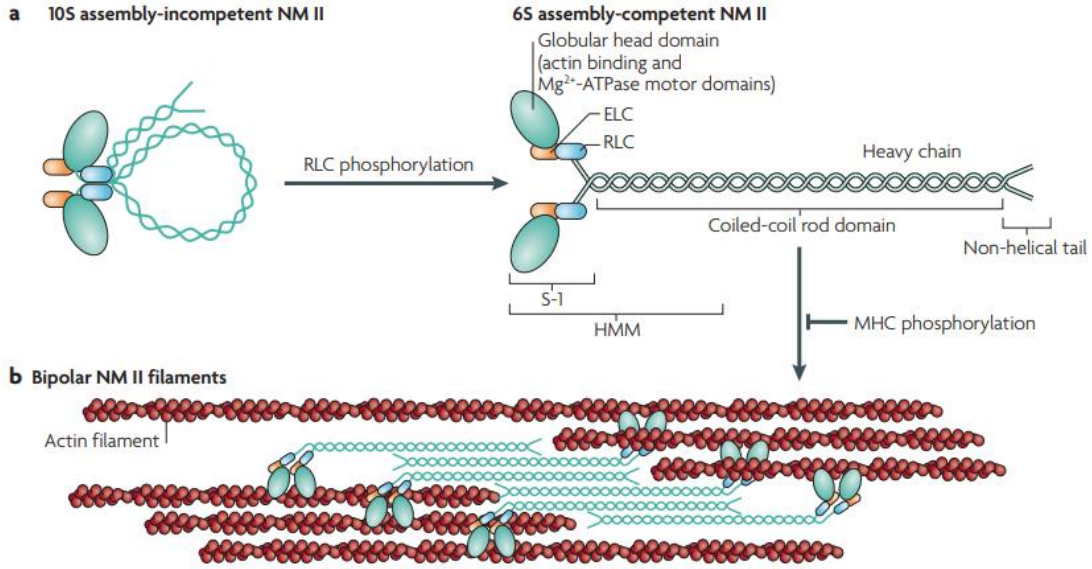

Figure 2.6. Structure of myosin II. Myosin II is a hexamer, composed of two heavy and 4 light chains, 2 being essential (ELC) and 2 being regulatory (RLC). Myosin heavy chains (MHCs) have three functional divisions: head, neck and tail. Head region carries actin interaction sites and Mg-ATPase activity. Neck region is apposed to light chains and acts as a force-transmitting lever. Tail regions of two MHCs exist in a coiled-coil conformation. Another subdivision nomenclature of MHC is based on enzymatic cleavage sites. Cleavage by α-chymotrypsin divides MHC into two, giving rise to heavy meromyosin (HMM) and light meromyosin (LMM). HMM is further divided by papain into S1 and S2 regions, S1 containing functional head and neck domains. Phosphorylation of vertebrate non-muscle and smooth muscle RLCs induces a conformational change allowing actin-myosin interaction (76).

Table 2.1. List of mouse genes coding MHC isoforms.

Myh1	Mus musculus myosin, heavy polypeptide 1, skeletal muscle, adult
Myh2	Mus musculus myosin, heavy polypeptide 2, skeletal muscle, adult
Myh3	Mus musculus myosin, heavy polypeptide 3, skeletal muscle, embryonic
Myh4	Mus musculus myosin, heavy polypeptide 4, skeletal muscle
Myh6	Mus musculus myosin, heavy polypeptide 6, cardiac muscle, alpha
Myh7	Mus musculus myosin, heavy polypeptide 7, cardiac muscle, beta
Myh7b	Mus musculus myosin, heavy chain 7B, cardiac muscle, beta
Myh8	Mus musculus myosin, heavy polypeptide 8, skeletal muscle, perinatal
Myh9	Mus musculus myosin, heavy polypeptide 9, non-muscle IIa
Myh10	Mus musculus myosin, heavy polypeptide 10, non-muscle IIb
Myh11	Mus musculus myosin, heavy polypeptide 11, smooth muscle
Myh13	Mus musculus myosin, heavy polypeptide 13, skeletal muscle
Myh14	Mus musculus myosin, heavy polypeptide 14, non-muscle IIc
Myh15	Mus musculus myosin, heavy chain 15

Human MYH16 gene has no counterpart in mouse genome (52).

As pericytes show heterogeneity in α-SMA expression along the microvasculature, whether or not MHC isoform exhibits a parallel heterogeneity is also unknown. In an early study, pericytes on peripheral capillaries were found to express non-muscle MHC isoforms but not the smooth muscle isoform (20). In a later study (77), midcapillary pericytes in the brain and retina were reported to express scarce amounts of non-muscle MHC and no smooth muscle isoform. In contrast to these early studies limited by available antibodies at that time, recent single-cell transcriptomic studies have disclosed that pericytes express non-muscle MHC isoforms (Myh9, Myh10, Myh14), smooth muscle MHC isoform (Myh11) and to a lesser extent, cardiac muscle MHC isoforms (Myh6, Myh7) (52).

Actomyosin Cross-Bridge Cycling

Actin-myosin cross-bridge cycling is accepted as the main contractile mechanism for muscle cells (Figure 2.7.). Upon actin-myosin interaction, power stroke moves myosin along actin filament (73). ATP binding to myosin head is essential for detachment of myosin head from actin filament. When bound ATP is hydrolyzed, the cycle restarts and myosin head can bind actin once again.

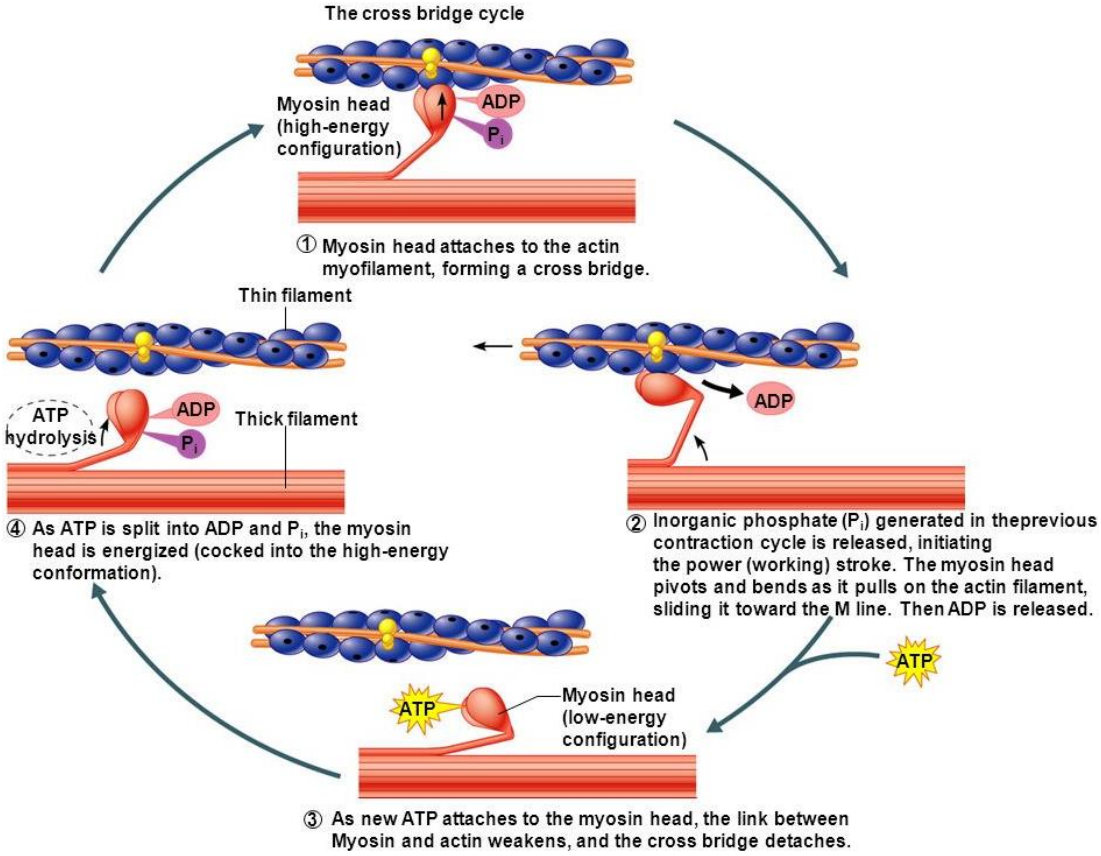

Figure 2.7. Actin-myosin cross-bridge cycling (78).

Phosphorylation of RLC by myosin light chain kinase (MLCK), which is activated by cytosolic calcium elevation, is a major regulatory mechanism for vertebrate smooth muscle or non-muscle, but not for sarcomeric (skeletal and cardiac muscle) myosin II's (72, 79). Phosphorylation induces a conformational change in thick filaments, enabling binding to actin (see Figure 2.6.). RLC phosphorylation is also enhanced by inhibition of myosin light chain phosphatase (MLCP), which dephosphorylates RLC by phosphorylation through small G protein RhoA/Rho kinase

pathway, further sensitizing myosin to calcium (80) (Figure 2.8.). It may directly phosphorylate and activate MLCK too (81). Rho kinase also regulates actin polymerization via activation of LIM kinase, which phosphorylates cofilin, preventing depolymerization (82). Rho activation is also known to promote pericyte contractility in cultures (83). Phosphorylation of MHC, on the other hand, is a poorly understood phenomenon (72). Phosphorylation of non-muscle MHCs is associated with filament disassembly *in vitro* (76).

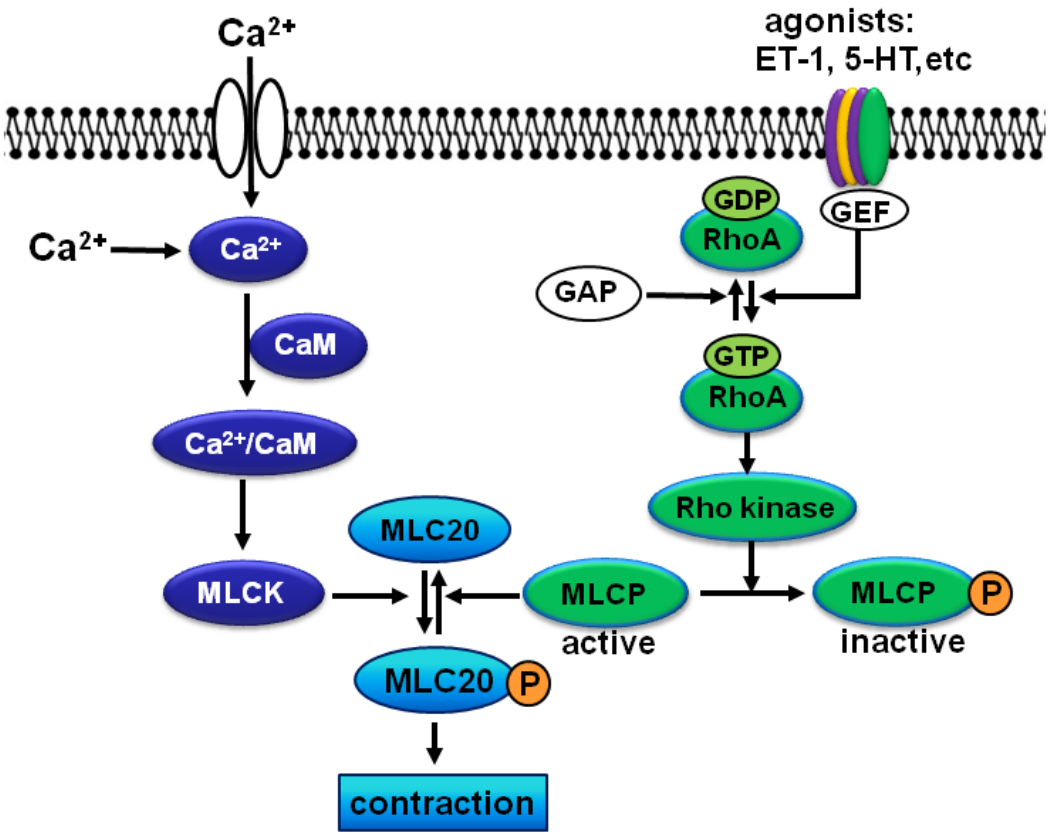

Figure 2.8. Regulation of myosin activity. In vertebrate smooth muscle cells, contraction is regulated through RLC phosphorylation. Phosphorylation by Ca^{2+}/Calmodulin activated MLCK enhances actin binding of myosin head to actin. Another mechanism works through RhoA/Rho kinase pathway, which phosphorylates MLCP, thereby preventing dephosphorylation of RLC and promoting contractile state of myosin. Ca^{2+}: Calcium, CaM: Calmodulin, MLCK: Myosin Light Chain Kinase, MLC-20: Regulatory Light Chain (RLC), MLCP: Myosin Light Chain Phosphatase, ET-1: Endothelin-1, 5-HT: 5-hydroxytryptamine, GTP: Guanosine Triphosphate, GDP: Guanosine Diphosphate, GAP: GTPase-activating Protein, GEF: Guanine nucleotide Exchange Factor (84).

Striated muscle myosin II's are inherently not regulated by phosphorylation but through intracellular calcium levels via troponin-tropomyosin system (72). Tropomyosin has 7 actin binding sites and is coiled around actin filaments, regulating the interaction of myosin with actin. In skeletal muscle, troponin T, I and C proteins take part in thin filaments along with actin and tropomyosin, C component acting as a Ca^{2+} sensor. Upon Ca^{2+} binding, tropomyosin slides and reveals actomyosin interaction sites. In smooth muscle cells, however, caldesmon protein acts as the Ca^{2+} sensor instead of troponin. At low cellular Ca^{2+} concentrations, caldesmon binds to actin-tropomyosin complex and prevents myosin binding. When Ca^{2+} levels rise, binding affinity of caldesmon to Ca-Calmodulin complex overweighs and detaches caldesmon from actin-tropomyosin complex allowing myosin binding (85). The presence of an immunologically SMC-related tropomyosin form in both capillary and venular pericytes has been shown suggesting an analogous mechanism to SMC contraction, although its expression seems lower than those of in vSMCs (20).

Organization of Myosin II in vSMCs

In contrast to regular sarcomeric organization of myosin filaments in striated muscles, the organization of myosin II in vSMCs takes place in structures called stress fibers, as mentioned above (85). One myosin filament is surrounded by about 15 actin filaments in SMCs, in contrast to 6-8 actin filaments in striated muscle. In addition to the smooth muscle isoform, vSMCs also express non-muscle myosin, whose function is still uncertain (1).

It is possible that pericytes contract using the same mechanisms as vSMCs. Supporting this idea, actin and myosin isoforms have been detected in stress fibers of pericytes (58). Additionally, inhibitors of actomyosin complex have been shown to inhibit pericyte contraction *in vitro* (8). However, cultured pericytes may act differently and may not exactly represent *in vivo* conditions. For example, stress fiber formation is promoted as contact surface and focal adhesions increase under culture conditions (86). Therefore, further studies are required to disclose the presence of a functional actomyosin coupling mechanism in pericytes *in vivo* as well as in

morphologically different pericyte subtypes located on up- or downstream microvasculature.

Pharmacological Blockers of Myosin II

There are several pharmacological agents to understand myosin's function. Among them blebbistatin is the only universal myosin inhibitor, since it inhibits all mammalian myosin II isoforms (73), although with different affinities (87). Blebbistatin has the highest affinity for skeletal muscle myosin II, lowest for smooth muscle myosin II and intermediate affinities for cardiac and non-muscle myosins (73). It binds to the head region between actin and ATP binding sites, and keeps myosin II in an actin detached state, by stabilizing ADP+Pi intermediate products (88) (Figure 2.9.). (-) Enantiomer is the active form and has the inhibitory effect (89). Other inhibitors of myosin II acting through ATPase cycle are isoform specific, such as N-benzyl-p-toluene sulphonamide and 2,3-Butanedione monoxime, which are specific for skeletal muscle myosin II (90). Another inhibitory mechanism for myosin II acts through MLCK inhibition by agents such as ML-7, ML-9 and MLCK inhibitor 18 (91).

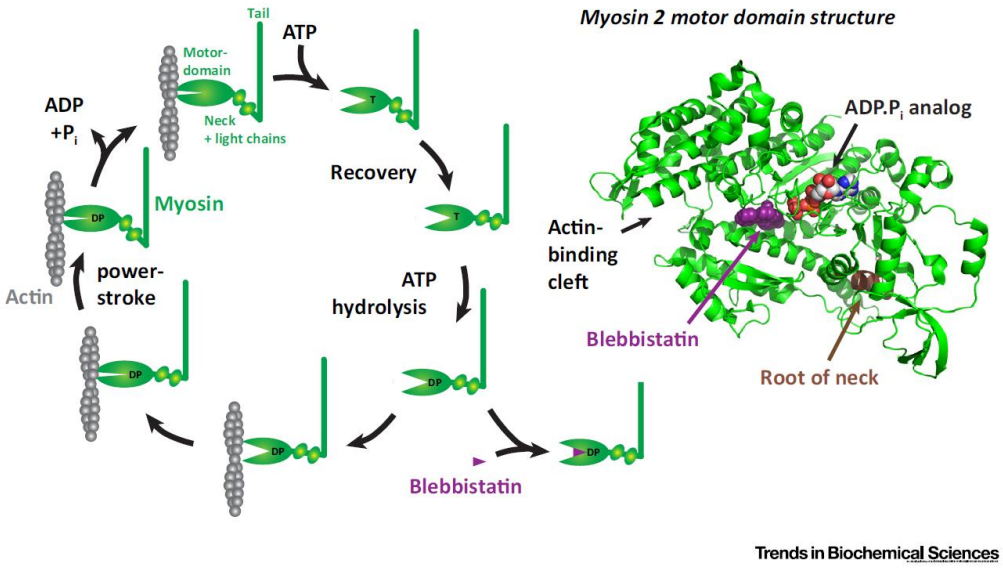

Figure 2.9. Blebbistatin's mechanism of action. Myosin II inhibitor blebbistatin, binds to the MHC's head domain between actin and ATP binding sites (right), and keeps myosin in an actin-detached state (left) by binding to ADP-bound open-state myosin, interfering with actin-myosin cross-bridge cycling (73).

2.3. Retinal Vasculature

Retina represents an ideal tissue to study pericytes, because of its common origin with cerebral tissue and highest pericyte:endothelial cell ratio in mammalian body (23, 92). Moreover, trilaminar organization of retinal vascular branches enables visualization of the entire vascular tree on a single plane, from arteriolar to venular end (93). This feature contrasts to cerebral tissue, whose vessels run along irregular paths, radiating at varying angles, making it hard to trace the microvasculature by branching order.

Retina is considered as a part of mammalian CNS, because they have the same embryological origin (13). It is composed of 10 layers: inner limiting membrane, nerve fiber layer, ganglion cell layer, inner plexiform layer, inner nuclear layer, outer plexiform layer, outer nuclear layer, outer limiting membrane, photoreceptor layer, retinal pigment epithelium. The vascular supply of retina is provided by two sources: choroidal vessels supplying the outer 1/3 and branches of central retinal artery supplying the inner 2/3 of retina. Branches of the central retinal artery comprise a trilaminar vascular network comprised of superficial, intermediate and deep layers (94) (Figure 2.10.). Retinal vasculature lacks autonomic input possibly to protect visual activity from changing systemic sympathetic tonus (95).

Just like the cerebral tissue, retina requires high energy supply, and the blood flow through the retinal vessels is regulated by NVC, especially in the intermediate layer, which is largely composed of capillaries, suggesting a significant role for capillary pericytes in flow regulation (96, 97).

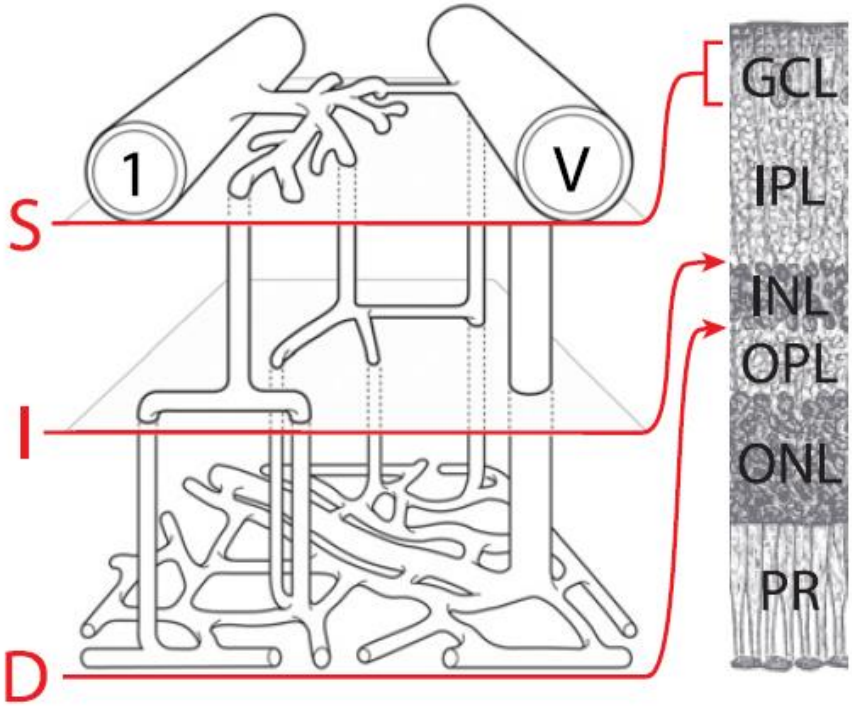

Figure 2.10. Retinal trilaminar vascular network. The network is formed by branches of the central retinal artery, is composed of superficial (S), intermediate (I) and deep (D) layers. Superficial layer is embedded within ganglion cell layer (GCL). Intermediate layer is positioned between inner plexiform layer (IPL) and inner nuclear layer (INL), while deep layer is positioned between INL and outer plexiform layer (OPL). ONL: Outer nuclear layer, PR: Photoreceptors (94).

3. MATERIALS AND METHODS

3.1. Animals

60 male and female *Swiss albino* mice weighing 25-35 g were kept in plexiglass cages and exposed to 12 hours of light-dark cycles. Food and water were provided *ad libitum*. Contralateral eye of each animal was used for vehicle injection. Experimental procedures on mice were approved by Hacettepe University Animal Experimentations Local Ethics Board (Registration number: 2018/20).

3.2. Intravitreal Delivery of Substances

1-1.5 g/kg urethane was injected intraperitoneally via a xylazine coated syringe and the depth of anesthesia was checked by toe pinch reflex. The mouse was placed under a stereomicroscope (Nikon, SMZ 745T) and the head was stabilized with a nosepiece, which allows movement around the longitudinal axis of the head. This provides alignment of the eyes under the microscope for effective intravitreal delivery of substances by injection. Oxygen saturation, pulse rate and rectal temperature were monitored and maintained within physiological limits during the procedure.

In contrast to urethane anesthesia, ketamine-xylazine provides temporary anesthesia for 30-45 minutes, which is long enough for the procedure, and viability of the animal is maintained. Therefore, it was the preferred anesthesia method in procedures involving repeated injections in consecutive days (siRNA injection). A mixture of 100 µL xylazine (Xylazinbio 2%, 8.7 mg/kg), 200 µL ketamine (Ketasol, 100 mg/mL, 87 mg/kg) and 2 mL 0.9% saline was injected intraperitoneally with 10 µL per g of the animal dosage.

We chose intravitreal delivery as the drug administration route in order to avoid systemic effects of NA. The intravitreal injections of NA and its vehicle (5% dextrose) were achieved via 33 G Hamilton Neuros Syringe (1701 RN, Hamilton). A

1.5 mm portion of the needle was left outside of the protective sleeve and inserted through ora serrata, avoiding damage to lens and retina (98). After vehicle injection, the syringe was cleaned thoroughly with repeated washes in distilled water before use for NA injection.

The induction of pericyte contraction was achieved by intravitreal delivery of 1 µL of 100 µM Noradrenaline (Cardenor, Norepinephrine tartrate, Defarma). As the volume of intraocular fluids in mice is about 4 µL (99), a dilution factor of 5 was calculated for substances delivered intravitreally (yielding approximately a 20 µM intravitreal concentration). The same volume of vehicle was injected into the contralateral eye. Previously 5% dextrose was the recommended diluent due to higher stability of NA. More recent studies reported similar stabilities in both 5% dextrose and saline, and recommended saline to prevent hyperglycemia in hypotensive patients (100, 101). However, because in our study the total applied volume of NA solution is too low, 5% dextrose was preferred to be on the safe side in terms of stability, as only minute concentrations of NA were used. Diluted solutions were stored at +4°C, for maximum 2 months, and protected from light (101).

30 seconds after the injection, eyes were removed with the aid of a surgical blade, since the routine forceps-assisted enucleation technique leads to an increase in the intraocular pressure and hence retinal detachment along with escape of vitreous body through the puncture site. Removal and immersion into fixative were immediately (within two minutes) carried out due to short half-life of NA (102). Mice were euthanized by cervical dislocation after eyeball extraction.

± Blebbistatin (Abcam), is a cell permeable and reversible inhibitor of myosin II ATPase cycle activity (88, 103). Blebbistatin in powder form is reconstituted in DMSO as it is a hydrophobic molecule, and stored at -20°C. To prevent cytotoxic effects of DMSO, its final concentration should not exceed 1% (73). The concentration of DMSO in delivered mixture was 2.5%, diluted to 0.5% with vitreous volume dilution factor. When diluted in physiological saline, the mixture must be mixed well and equilibrated to room temperature in order to prevent precipitate formation. Mixture

in saline must be freshly prepared each time 1 hour before use. 1 µL of 250 µM (yielding approximately 50 µM final concentration) inhibitor was delivered intravitreally 40 minutes prior to the application of NA in relevant groups. This concentration is above the solubility limit of blebbistatin, but slow precipitation kinetics of the molecule allows the use of blebbistatin in effective concentrations once the mixture is prepared in prewarmed conditions before the formation of precipitates (73). Phototoxicity and fluorescence problems related to the toxin do not arise as the retinas are illuminated after fixation. Contralateral eyes were injected with the same volume of saline prior to NA injection as vehicle. Any chemical interaction between NA and blebbistatin as well as their vehicles is not expected due to a 40-minute interval between injections.

To knock-down the transcripts of α-SMA encoded by Acta2 gene, small interference RNA (siRNA) was injected intravitreally into the target eye. The injection solution was prepared in RNase free conditions, by cleaning the working chamber and instruments with 70% ethanol, 10% bleach and then RNAse solution. JetPEI transfection agent (Polyplus) was used to deliver siRNAs to the intracellular compartments. In line with the recommendations of the kit, 3 µL JetPEI was mixed with 12.5 µL 10% glucose and 9.5 µL nuclease free water and vortexed. 3.76 µL Acta2-siRNA was mixed with 12.5 µL 10% glucose and 8.74 µL nuclease free water and vortexed. JetPEI containing solution was added on top of the siRNA containing one, and incubated at room temperature for 15 minutes after being vortexed. 1-2 µL of the mixture was injected intravitreally to the target eye, and the effect was evaluated 48 hours later.

3.3. Whole Mount Retina Preparation

Fixation was provided by the immersion of eyes into 100% ice-cold methanol. The eyes were kept in methanol at -20°C for one hour (36). Fixation process was ended by transfer into phosphate-buffered saline (PBS, Sigma). Fixed eyeballs were kept in PBS at +4°C until retina extraction. In some cases, eyeballs were fixed in 4% paraformaldehyde (PFA) at +4°C for one hour, for comparison of fixation methods.

Fixed eyeballs were transferred to a petri dish containing PBS at room temperature. All the following procedures were carried out under a stereomicroscope. Skin and its appendages, lacrimal gland and extraocular muscles surrounding the eyeballs were removed by a fine scissor. A minimal piece of surrounding tissue was purposefully left over to provide a handling spot for external manipulations with forceps.

A hole was created at the corneal margin with a 26 G needle. One of the tips of a Vannas Spring Scissor (FST) was inserted through this hole to make a circular cut along ora serrata, enabling the removal of cornea, followed by the removal of lens and vitreous body together with help of a fine forceps. Four radial cuts were made with a fine spring scissor to flatten out the retina. Following the flattening, retina can be detached from the underlying sclerochoroidal tissue with the aid of a fine forceps and very gentle handling. Separated retina was transferred to a round-bottom centrifuge tube containing 200 µL PBS. They can be used immediately or stored at +4°C for 3-5 days.

3.4. Fluorescent Labeling

The use of methanol as a fixative necessitates only very gentle permeabilization, as methanol itself also permeabilizes lipid structures. Therefore, whole mount retinas were washed and permeabilized with 0.1% PBS-Triton-X 100 (Merck), 3 times, 5 minute each. Differential staining of filamentous (F-actin) and globular (G-actin) forms of actin was achieved by two natural compounds conjugated with different fluorophores, Phalloidin-Alexa Fluor 568 conjugate (Biotium, 00044) and Deoxyribonuclease I-Alexa Fluor 488 conjugate (Thermofisher, D12371) respectively. Phalloidin is a natural toxin purified from the mushroom Amanita phalloides, which stabilizes F-actin regardless of the isoform (104). Deoxyribonuclease I (DNase I) has a natural affinity for G-actin in an isoform-nonspecific manner and can be used for fluorescent labeling when conjugated to a fluorophore (55, 105). Both compounds were diluted in PBS at 1:200 ratio and applied to tissue for 40 minutes, at room temperature. After washing with PBS 3

times, 5 minute each, retinas were mounted on glass slides with a 50/50 % PBS/Glycerol mounting medium containing the nuclear marker Hoechst 33258 (Invitrogen, 1:1000 dilution).

Fluorophore conjugated lectins can be used in the demonstration of basement membranes thanks to their natural affinity to carbohydrate moieties. After washing and permeabilizing retinas in the same way, Fluorescein lectin (Vector Labs, FL-1171-1) was diluted in PBS, with a 1:200 concentration and applied to tissue for 8 hours or overnight at +4°C. After washing with PBS, 3 times for 5 minutes, retinas were mounted on glass slides with mounting medium containing Hoechst 33258. Spacers made out of intentionally broken coverslips were used in order to prevent squeezing of the vascular lumina in retinal preparates (106).

3.5. Immunofluorescent Labeling

Whole mount retinas were washed and permeabilized with 0.1% PBS-Triton-X 100 (Merck), 3 times, 5 minute each. Background blocking was achieved by 10% Normal Goat Serum in PBS.

Primary antibody against Myh11 (Abcam, ab82541) was diluted in blocking solution with 1:400 concentration and incubated at room temperature for 4 hours. After washing with 0.1% PBS-Triton X, 3 times, 5 minutes each, Cy2 or Alexa Fluor-555 conjugated goat-anti rabbit secondary antibody (Jackson Immunoresearch) diluted in blocking solution with 1:200 concentration was applied for 1 hour at room temperature. Retinas were washed with 0.1% PBS-Triton X for 3 times, 5 minutes each.

For double labeling with α-SMA, two different primary antibodies were used depending on the fluorescent channel of Myh11 secondary antibody. When Cy2, was used as the fluorophore for Myh11, α-SMA primary antibody conjugated to Cy3 (Sigma, C6198) was used. It was diluted in blocking solution with 1:300 concentration and incubated overnight at +4°C. When Cy3 was used as the fluorophore for Myh11, an unconjugated primary antibody against α-SMA (Sigma, A5228) was used. As this is

an antibody produced in mouse, Fab fragments were used instead of secondary antibody to prevent nonspecific background staining. In this case, 1 µL of α-SMA unconjugated primary antibody was incubated with 1.25 µL of Alexa Fluor 488 conjugated goat-anti mouse Fab fragment (Jackson Immunoresearch) in 10 µL PBS for 1 hour at room temperature. After the addition of 288 µL 10% Normal Mouse Serum in PBS to achieve 1:300 antibody concentration, the mixture was incubated at room temperature for one more hour. After the removal of the secondary antibody used for Myh11 labeling, the mixture was put over whole mount retinas and incubated overnight at +4°C. Tissues were washed 3 times, 5 minutes each, with PBS after the overnight incubation of either α-SMA antibodies, and mounted with mounting medium containing Hoechst 33258.

Complete or partial lack of α-SMA labeling was recently associated with depolymerization of actin filaments, and this problem was partly overcome by rapid methanol fixation (36,37). Despite this improvement, the labeling of α-SMA tapers towards downstream retinal vascular branches. Considering the paucity of α-SMA protein levels in downstream segments, we questioned whether this amount can be visualized with higher antibody concentration, and whether contractile stimulus changes labeling by epitope masking. To this end, we examined retinal pericytes labeled with higher α-SMA antibody concentration (1:100) and also compared vehicle vs 50 µM NA treatment. In all cases, labeling efficiency was unchanged and visualization was successful with comparable laser intensity use (%0.1-5, increasing towards downstream branches). NA treatment did not induce any change in labeling efficiency either, and labeling was traceable down to 7-8th orders in all cases (Figure 3.1.).

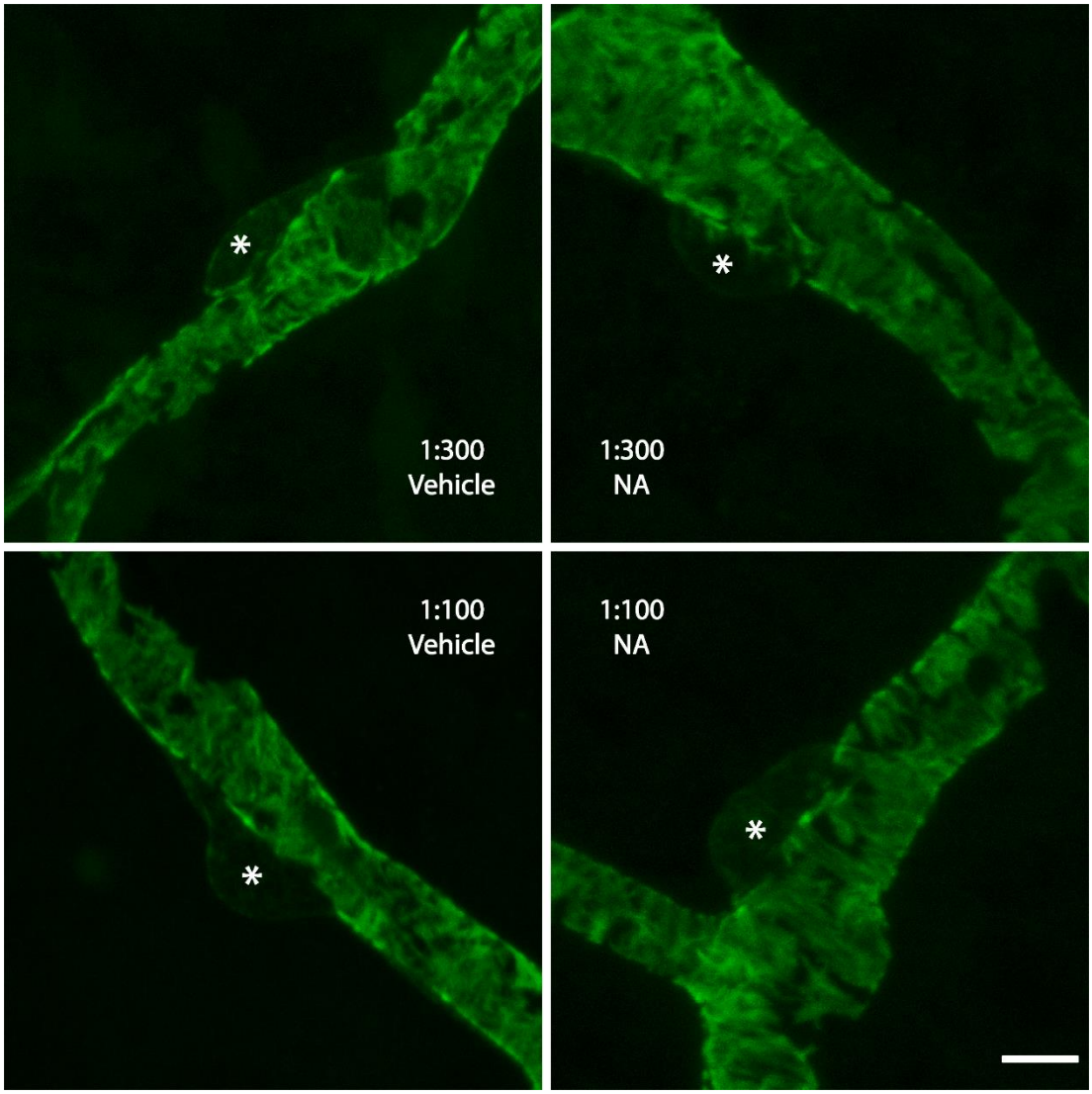

Figure 3.1. α-SMA labeling is unaffected by antibody concentration and vasoconstrictor application. Pericytes labeled with antibody against α-SMA from fifth order branches are shown. Neither the antibody concentration (1:300 vs. 1:100) nor the vasoconstrictive stimulus state (vehicle vs. NA) affected labeling intensity and traceability of labeling. All images were acquired with the same imaging parameters, except for the first image, in which laser intensity was 0.5% instead 1%. Scalebar: 5 µm. Z-stack maximum projection images of 3.5-7.5 µm thick vascular sections.

β-actin labeling was performed by overnight incubation with a monoclonal antibody (Sigma, A5441; 1:100 dilution) and Alexa Fluor 488-conjugated Fab fragment (Jackson Immunoresearch) primary-secondary complex, prepared as described for α-SMA above, at +4°C after blocking with 10% normal goat serum.

Nanosecondary antibodies (nanobodies) are produced from camelid heavy chain antibodies (107). Being only of 15 kDa size, these secondary antibodies provide better tissue penetration and resolution. Alexa Fluor-488 conjugated anti-rabbit IgG nanosecondary (Chromotek, srb488) (1:500 dilution in blocking solution, 1:350 for FRET) was used to label the primary antibody against Myh11, in combination with Cy3 conjugated antibody against α-SMA, to achieve higher resolution and closer interaction distance in FRET experiments. In FRET experiments, the labeling order was reversed so that, acceptor fluorophore carrying antibody was applied before donor fluorophore carrying antibody (108). The rest of the double labeling protocol otherwise remained the same.

3.6. Imaging and Analysis

Analyses for blebbistatin experiments were performed on Fluorescein-lectin labeled whole-mount retinas. Primary branches of the central retinal artery were defined as the first order retinal microvessels (see Figure 3.2. for a sample scheme of retinal vascular branch orders), and vascular orders equal to or higher than 2 at the superficial retinal vascular layer were evaluated. Analyzed vessels were branches of a randomly selected first order retinal vessel, whose entire network can be imaged uninterruptedly. The images were acquired by combined tile-scan and Z-stack (10 layers each) modes of Leica TCS SP8 confocal laser scanning microscope (25X/0.95 water objective). Because pericyte soma position with reference to the vessel wall significantly changes with imaging plane, we measured the pericyte-associated diameters at the juxtanuclear sections perpendicular to vessel axis (see 4.18.A). Rarely, when the difference between values measured from two sides of a pericyte nucleus was relatively high, mean of the two values was used (7). These values were divided by the initial diameter of each vascular segment for an intrinsic baseline correction and this value was taken as the “juxtanuclear diameter ratio”. For a homogenous dataset formation, a single pericyte with a clearly visualized soma was attributed per vascular branch. Pericytes on the microvascular wall were identified

based on their “bump-on-a-log” morphology and surrounding lectin-labeled basement membrane.

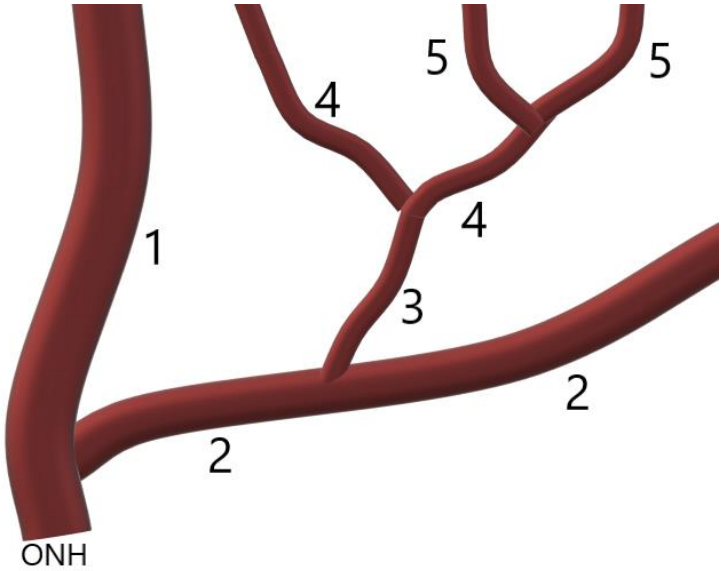

Figure 3.2. Principle of retinal vascular branch order determination. ONH: Optic Nerve Head, which denotes the region where central retinal artery branches off.

For F/G-actin signal intensity measurement, all images were acquired with Leica TCS SP8 confocal laser scanning microscope (63X/1.40 oil objective) with the comparable imaging parameters and in Z-stack mode to cover the whole vascular thickness. Stacks were composed of images acquired with 0.7 µm-wide steps along Z axis. Signal intensities were measured on maximum projection images (8-bit) encompassing the entire vessel along the z axis with ImageJ (NIH) software. Digitized microscopic images were selected by simple randomization for evaluation and the investigator was always blind to the treatment. The pericyte covered microvascular segments were marked as a Region of Interest (ROI) with a 20 µm axial length along the pericyte, soma being at the central position and the vascular width lying perpendicularly to the axis (see Figure 4.17.A). Signals were normalized by subtracting the background signals for each channel obtained from the maximum projection image. The ratio of normalized F-actin signal to normalized G-actin signal (F/G-actin) was used as an index of actin polymerization (16). The formula used for this calculation is given below (Formula 3.1.), ROI indicating the value measured in

ROI and background indicating the value measured from background for each actin state:

$$F/G\ actin\ signal\ ratio = \frac{F_{ROI} - F_{background}}{G_{ROI} - G_{background}} \quad (3.1.)$$

Most of F-actin is produced by polymerization of the existing G-actin pool, and only a minute fraction is synthesized de novo (55). Because the eyes were immediately fixed after the stimulation of contraction, any contribution from de novo synthesis was considered as negligible. Therefore, evaluation was based on the assumption that the resulting changes were a result of an exchange between F and G- actin populations. Pericytes on the microvascular wall were identified based on their "bump-on-a-log" morphology and processes highlighted by F-actin labeling with phalloidin (109).

Pericyte-associated vascular diameter changes were measured from the same individual pericytes as F/G-actin signal ratios were calculated. Diameter measurements were done with the same principle as mentioned above.

3D modeling was made consecutively on ImageJ, Slicer and Paraview softwares, using Z-stack compilation of images acquired with 0.2 µm-wide steps.

For images which do not require quantitative analysis, imaging parameters varied and Z-stack thicknesses are indicated in figure legends for each case.

3.7. Statistical Analysis

In the analysis of blebbistatin dataset, extreme outliers of JNDR, which lie more than 3.0 times the interquartile range (IQR) below the first quartile or above the third quartile, were defined per vascular order group and removed from the initial dataset. Dataset was split up by vascular order and, the parametric assumption criteria were evaluated based on coefficient of variation, skewness, normality tests, histogram and detrended plots. Mann-Whitney U or Independent samples *t*-tests were used depending on parametric assumption testing. Accordingly, mean and SD

or median and IQR were used as central tendency and dispersion measures; and error bar and box plot graphs were used in demonstration of these measures for parametric and nonparametric cases, respectively.

In F/G actin signal ratio analysis, extreme outliers of F/G signal ratio values, which lie more than 3.0 times the interquartile range below the first quartile or above the third quartile, were defined per vascular order group and removed from the initial dataset. Dataset was split up by vascular order and, the parametric assumption criteria were evaluated based on coefficient of variation, skewness, normality tests, histogram and detrended plots. Mann-Whitney U and Kruskal-Wallis tests were used for hypothesis testing as none of the vascular order groups had normal distribution and met parametric assumptions.

ROC analysis was used to determine the cutoff value of F/G-actin signal ratio differentiating contracted cells from non-contracted ones in related vascular order groups, which exhibited significant signal differences. False positivity rate was accepted as 15% for cutoff value determination. Groups of pericytes separated by the predetermined cutoff value, were compared by JNDRs. Mann-Whitney U test was used for hypothesis testing due to the skewed distribution of values.

Hypothesis testings were done one-sided (CI: 95%). All statistical analyses were performed with IBM SPSS© 23 software.

3.8. Förster Resonance Energy Transfer (FRET)

FRET is a non-radiative type of energy transfer from an excited donor fluorophore to a nearby acceptor fluorophore (110). The emission window of the donor must overlap with the excitation window of the acceptor fluorophore. Resonance energy transfer occurs when the distance separating two fluorophores is 1-10 nm (111) (Figure 3.3.). Distances less than 1 nm results in quenching, whereas larger distances than 10 nm are not suitable for energy transfer (112).

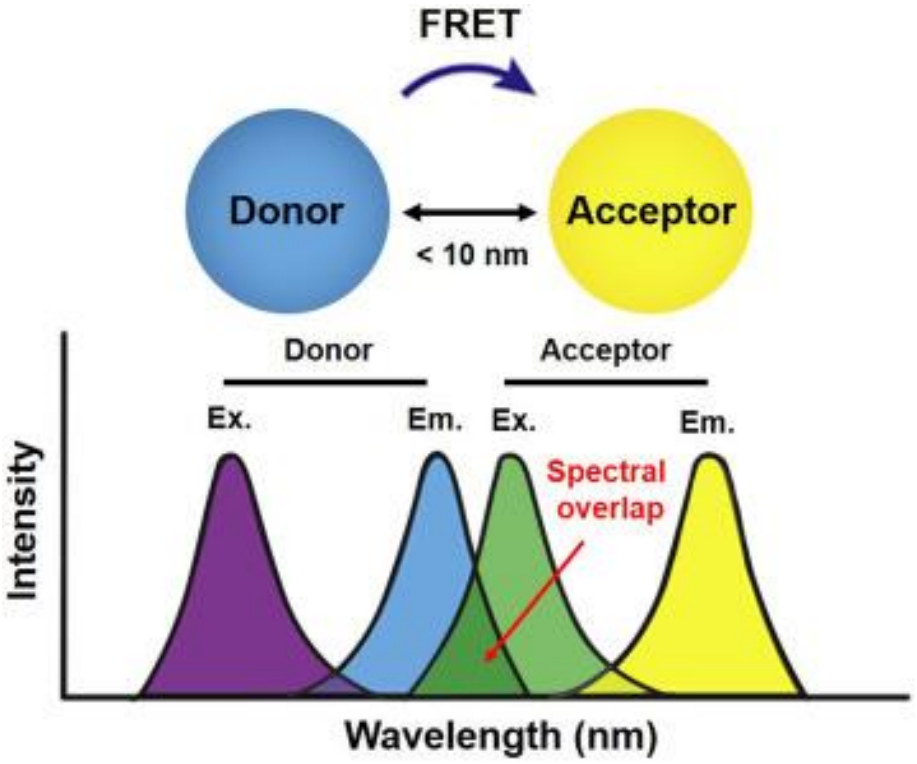

Figure 3.3. Basic principle of FRET. FRET occurs when two fluorophores, of which one has an emission spectrum (donor) that overlaps with the other's excitation spectrum (acceptor), are in 1-10 nm distance (113).

FRET is an all-or-none phenomenon (110). The probability of FRET is calculated by the following equation (Formula 3.2.), where *R* is the distance between two fluorophores, and R_0 is the distance where the probability of the energy transfer is 50% (typically 3-8 nm) (112):

$$E = \frac{{R_0}^6}{R^6 + {R_0}^6} \qquad (3.2.)$$

Either fluorescent proteins or fluorophore dyes can be used as FRET pairs. There are some widely accepted FRET pairs, such as CFP-YFP, Cy3-Cy5. Suitable FRET pairs have higher R_0 values. FRET efficiency gives a clue about the proximity of two fluorophores; therefore, this technique is mentioned in the literature as the "spectroscopic ruler". As the lateral resolution of light microscopy is around 200 nm, FRET aids in the evaluation of interaction and colocalization of proteins having distances below resolution limits.

FRET was utilized in this study to show the close interaction between actin and the head of myosin heavy chain. Alexa Fluor-488 (donor) and Cy3 (acceptor) was chosen as the FRET pair (114) and the fluorophores were used to label Myh11 and α-SMA respectively.

There are several different techniques to conduct FRET, such as acceptor photobleaching (AB), sensitized emission (SE) and fluorescent lifetime imaging (FLIM). FRET-AB is the preferred method of FRET for fixed cells or tissues (115). In FRET-AB, acceptor fluorophore is photobleached permanently, which is expected to increase the fluorescence intensity of the donor (dequenching) within a defined ROI (112). However, in this technique any movement in the imaged area must be avoided, as this leads to movement artifacts, which may lead to misreading of the intensity changes (110).

Another challenge in applying FRET-AB with antibodies is the large size of the fluorophores (112). As the approximate size of an antibody is 10-15 nm, the size of a primary-secondary antibody complex becomes 30 nm, which decreases the possibility of energy transfer when the labeled antibody complexes fall in opposite directions. Besides the distance, dipole orientation of the fluorophores is another factor affecting FRET probability. To minimize the distance between fluorophore pair, a directly conjugated antibody and a nanosecondary antibody were used in this study.

In our study, application of FRET-AB was also limited by the technical properties of the confocal microscope in our facility, which lacks a red-far red excitation laser. Alexa Fluor-488-Cy3 was chosen therefore as the FRET pair. However, cross-excitation and cross-bleaching of the donor during acceptor photobleaching led to erroneous efficiency calculation, as it is calculated by the formula below (Formula 3.3.):

$$FRET\ efficiency = \frac{D_{post} - D_{pre}}{D_{post}} \qquad (3.3.)$$

Therefore, AB was an intensity measurement-dependent technique which was hampered by movement artifacts, cross-excitations and spectral bleed-throughs. SE, which utilizes donor-only and acceptor-only samples prepared under the same conditions with the FRET sample which includes both donor and acceptor, is also based on an intensity dependent calculation and hence can be affected by heterogeneities in labeling an imaging plane.

Unlike these techniques, spectral unmixing utilizes intrinsic fluorescent spectral properties of the fluorophores, and hence is unaffected by intensity-borne errors. Therefore, an excitation-emission (ExEm) spectral unmixing approach was used to avoid cross-excitation and cross-emission (spectral bleedthrough) artifacts encountered in intensity-based approaches (116) (Figure 3.4.). Donor-only, acceptor-only and donor-acceptor samples were prepared simultaneously under same conditions, without the use of nuclear marker Hoechst 33258. All samples were imaged in lambda-scan mode of Leica LasX software, using 488 nm and 552 nm lasers separately, with 5 nm wide windows of 3 nm steps within the range of 492-680 nm. RT 15/85 beamsplitter for reflectance microscopy was used to avoid spectral losses filtered out by dichroic mirrors. Acquired spectral images were processed with Fiji and analyzed with FRETTY plugin.

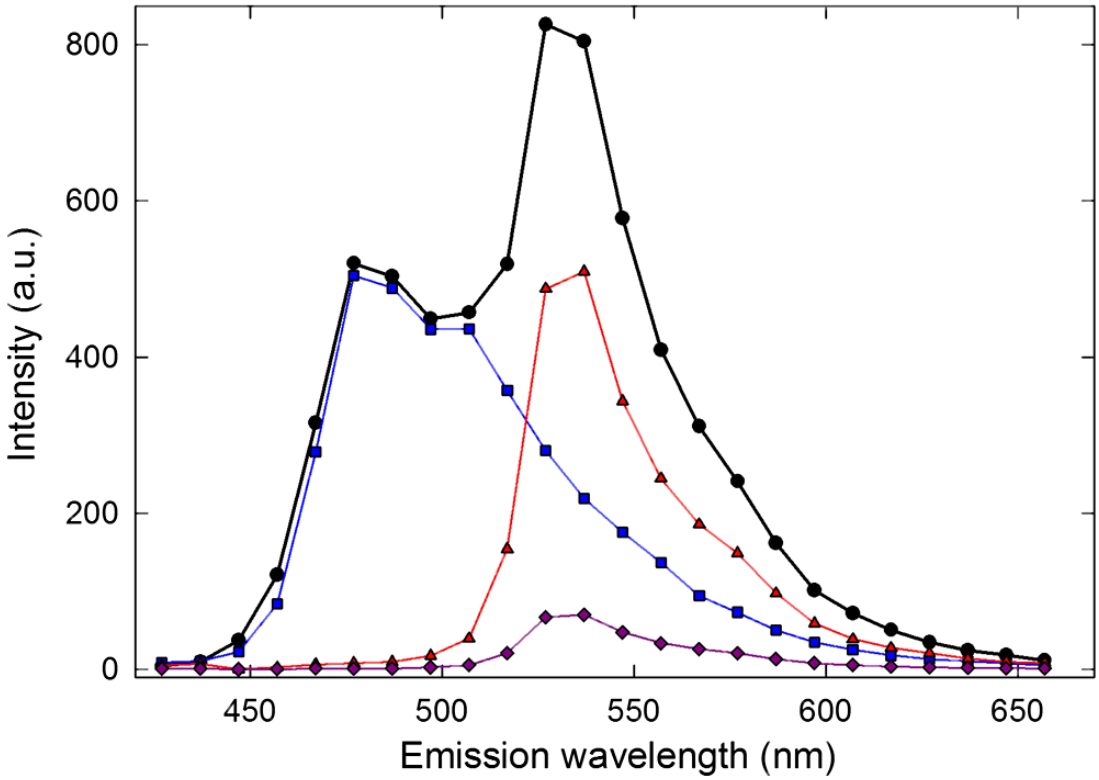

Figure 3.4. Principle of spectral unmixing. Black line shows the spectrum acquired when the FRET sample was excited by donor-exciting laser. When the line is decomposed, it can be seen that the second peak, which is the anticipated FRET signal, is actually a combination of donor bleedthrough (blue line), acceptor spectrum caused by cross-excitation (purple line), and the actual FRET signal (red line). Spectral unmixing approach aims to overcome these issues by such decomposing algorithms (116).

4. RESULTS

4.1. Pericytes are Contractile

To study pericyte contractility in the superficial layer of retina, we injected NA into the vitreous body. By 3D constructions produced from imaging of contracted pericytes with help of α-SMA immunolabeling, we identified two types of contraction pattern: one characterized with a steep decrease in luminal diameter from the periphery of pericyte toward the soma at the center (node-like) (Figure 4.1.), where both walls moved toward each other, being maximal under the soma; and the other, characterized with slight displacement (indentation) of the soma into the lumen, causing a less steep but diffuse diameter change along the pericyte (tide-like), similar to descriptions of pericyte contraction induced by focal electrical stimulation along the capillary segments by Ivanova et al. (117).

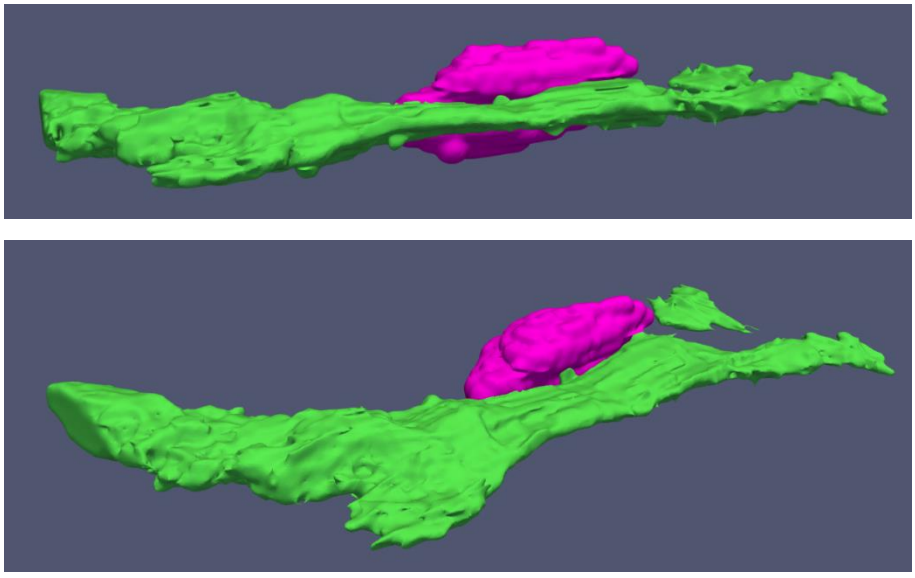

Figure 4.1. 3D modeling of a contracted pericyte from Z-stack image of NA treated retina labeled with antibody against α-SMA. The image was processed with ImageJ, Slicer and Paraview softwares to build a 3D reconstruction. This image shows steep reduction in luminal diameter from periphery toward pericyte soma, being maximal under the soma. Magenta: Pericyte nucleus, Green: capillary lumen. Thanks to Dr. Evren Erdener for his valuable efforts in image preparation.

4.2. Organization of α-SMA Fiber Bundles Suggests a Contractile Function

High resolution imaging of α-SMA labeled retinal pericytes, revealed the protein's organization and orientation within cytoplasm and processes. The organization of the fiber bundles were mainly circumferential in upstream pericytes, similar to vSMCs, whereas towards downstream branches, the orientation of (relatively shorter) bundles became less circumferential, running oblique or parallel to the longitudinal capillary axis, complying to nodal and tide-like contraction patterns respectively (Figure 4.2.).

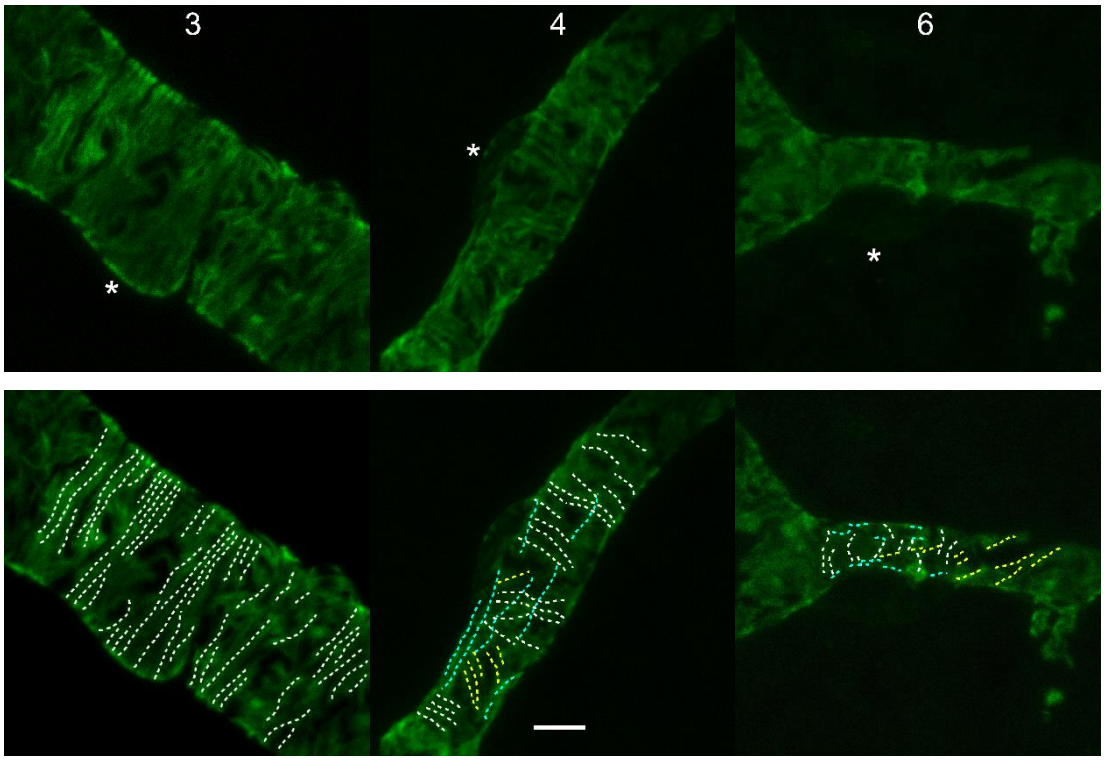

Figure 4.2. α-SMA fiber bundles are differentially organized in pericytes from third, fourth and sixth retinal vascular orders. The organization of the α-SMA labeling within the cytoplasm of pericyte processes suggest a vectoral structure, functioning in capillary diameter changes. Note that in the third order, bundles regularly run rather circumferential (white), while in the fourth order bundle orientation becomes irregular with some bundles running oblique (yellow) or parallel (cyan) to the longitudinal capillary axis, and the irregularity further increases in the sixth order. Asterisks denote the localization of pericyte somas. Scalebar: 5 µm. Z-stack maximum projection images of 7.5, 8.7, and 6 µm thick vascular sections, respectively.

4.3. Contribution of Actomyosin Coupling to Pericyte Contraction

Actin-myosin cross-bridge cycling is the main cellular mechanism that provides vSMC contraction. We explored whether this mechanism is also active in pericytes, the downstream mural cells on microvessels thought to replace vSMCs. We used immunofluorescent identification of α-SMA and Myh11 as well as pharmacological inhibition of myosin ATPase to evaluate actin-myosin interaction in retinal pericytes.

4.3.1. Myh11 Protein Labeling Highly Colocalizes with α-SMA Expression in Pericytes

Considering that most pericytes are contractile and has many features in common with upstream vSMCs, it is likely that pericyte contraction is also mediated by actomyosin cross-bridge cycling. We first searched the presence of myosin along with α-SMA in pericytes by immunohistochemistry. We chose Myh11 isoform of myosin based on pericyte single cell transcriptomics data (52) and used antibodies against smooth muscle isoform of myosin heavy chain. We found that Myh11 was continuously expressed in all pericytes located on from the first to the last branch order microvessels. Although it was not possible to track α-SMA in high branch order downstream pericytes, this was not the case for Myh11 immunolabeling. Both immunoreactivities highly overlapped, suggesting an intimate co-localization of both proteins (Figure 4.3.). Myh11 immunostaining was specific but not a staining artifact, as shown by omitting the incubation step with primary antibody against Myh11 in the immunostaining protocol (Figure 4.4.).

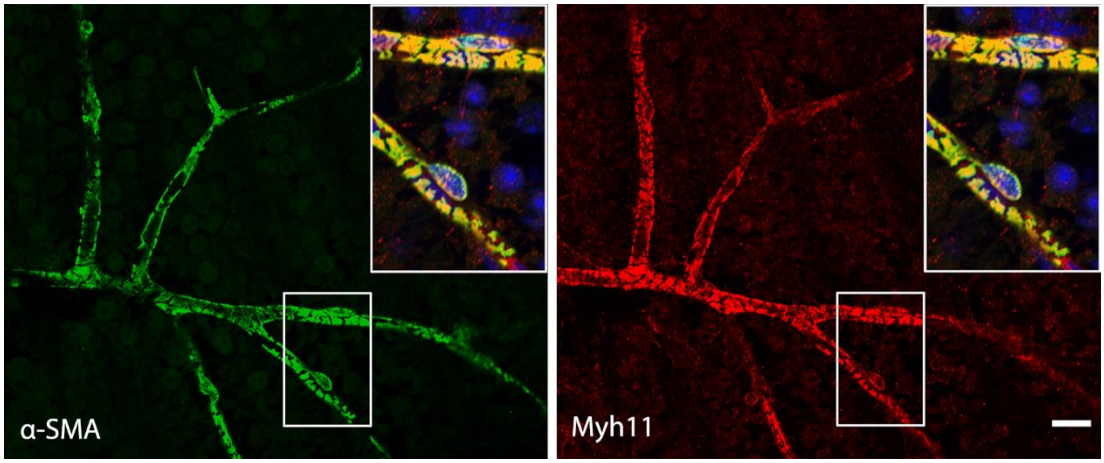

Figure 4.3. Myh11 immunolabeling closely follows that of α-SMA in retinal microvessels. Retinal pericytes in zoomed insets are on the 4th order branches. The intense yellow color indicates the tight overlap between the two proteins labeled green (α-SMA) and red (Myh11). Zoomed insets are 2x magnified and display merged images of the green and red channels along with Hoechst nuclear labeling in blue. Scalebar: 20 µm.

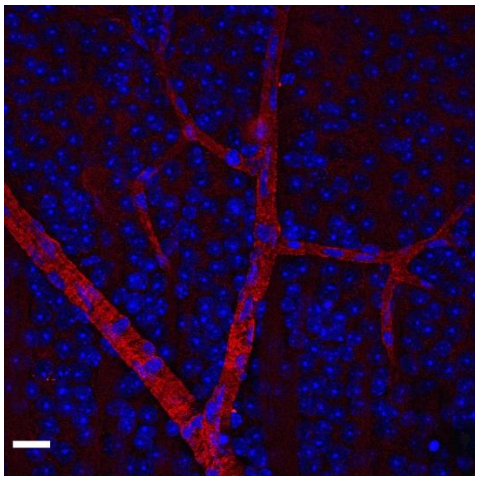

Figure 4.4. Myh11 negative control. Retinal vasculature was labeled with phalloidin (red) and nuclei with Hoechst (blue). Primary antibody against Myh11 was omitted from the staining to attain a negative control. Green channel reveals no signal with the same imaging parameters as the counterpart with primary antibody use, showing the specificity of Myh11 labeling. Scalebar: 20 µm.

Super-Resolution Techniques Better Clarify the α-SMA-Myh11 Overlap

Co-labeling of stress fibers filling the pericyte soma and processes was better visualized with superresolution microscopy techniques such as Lightning (HyVolution) (Figure 4.5.) and STED (Figure 4.6.) Use of nanosecondary antibodies,

which provide superior tissue penetration and higher resolution even with the use of standard confocal microscopy also clearly delineated the actomyosin bundles in pericyte processes and soma (Figure 4.7.).

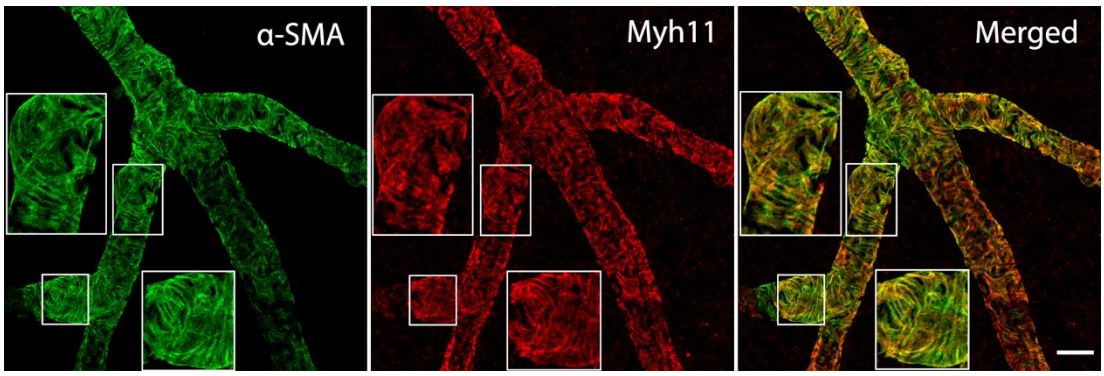

Figure 4.5. Demonstration of α-SMA and Myh11 with deconvolution. α-SMA and Myh11 proteins are highly colocalized and form circular string-like bundles reminiscent of a contractile stress fiber organization. Images were acquired with the deconvolution technique "Lightning". Insets: 2x magnified. Retinal vascular branch order is undetermined. We thank Jens Peter Gabriel for his valuable expertise in image acquisition. Scalebar: 10 µm.

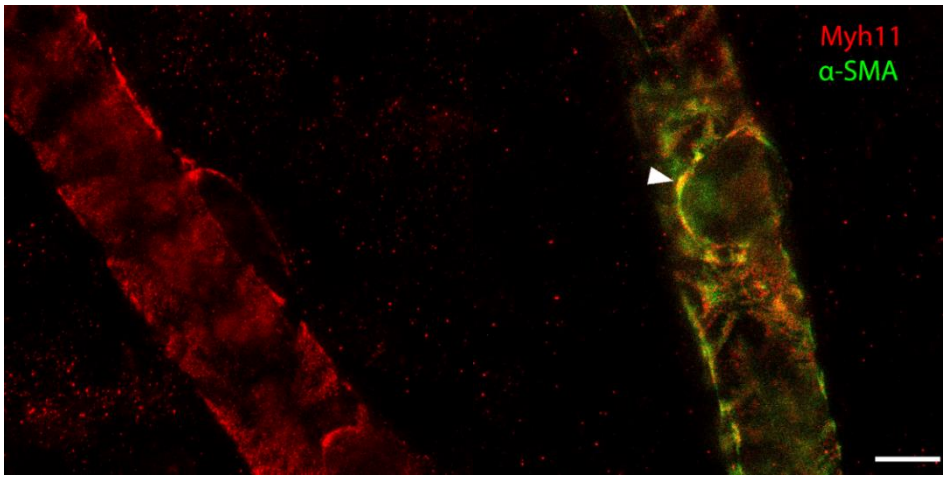

Figure 4.6. Demonstration of α-SMA and Myh11 with STED. The distribution of Myh11 follows a compatible pattern to the known morphology of pericyte soma and extensions in the image acquired with STED technology (left). Higher resolution provided by STED shows close association of Myh11 labeling with that of α-SMA around a pericyte nucleus (arrowhead, right). Scalebar: 5 µm. We thank Ulf Schwarz for his valuable expertise in image acquisition.

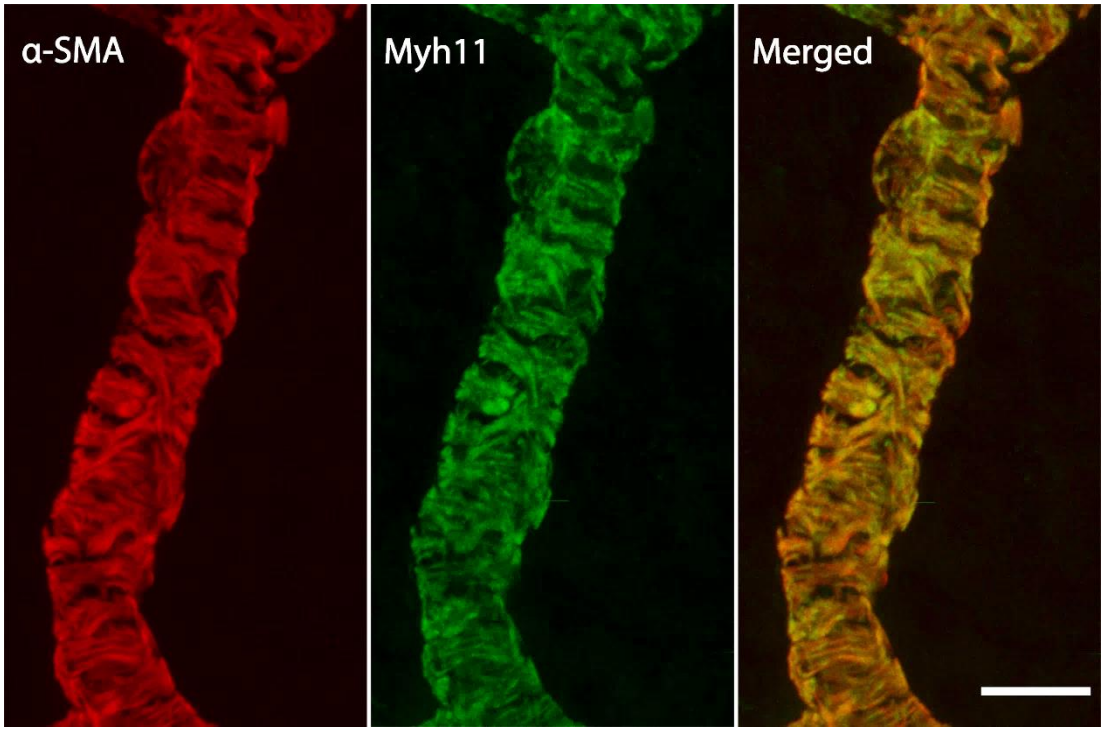

Figure 4.7. Demonstration of α-SMA and Myh11 with nanobodies. Use of nanosecondaries to label Myh11 provides better resolution and delineation of the fibers by standard confocal microscopy compared to the images (c.f. Figure 4.2, 4.3 and 4.12.) obtained with conventional secondary antibodies. The tight overlap between α-SMA and Myh11 proteins is illustrated on a third branch order retinal vessel display the organization of fibrillary bundles in pericyte processes suggestive of tension generating stress fibers. Scalebar: 10 µm. Z-stack maximum projection images of 13 µm thick vascular sections, respectively.

4.3.2. Myh11 Expression is Independent from Retinal Vascular Order, Fixative Type and α-SMA Staining Pattern

Due to rapid depolymerization of α-SMA, tracing the protein in midcapillary segments, where it is expressed in low quantities, is limited with routine immunolabeling techniques. In contrast, Myh11 could be uninterruptedly traced along the microvasculature (Figure 4.8, 4.9.), including the intermediate and deep retinal vascular layers (Figure 4.10.).

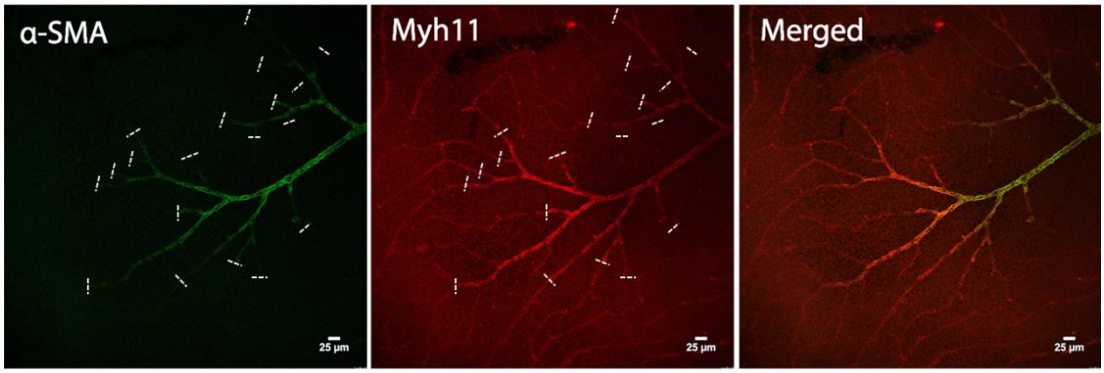

Figure 4.8. Despite gradual tapering in α-SMA labeling (indicated with dashed lines) toward downstream capillaries, Myh11 labeling covers all microvasculature in the superficial retinal vascular layer. The image was captured by LasX Navigator. We thank Jens Peter Gabriel for his valuable expertise in image acquisition.

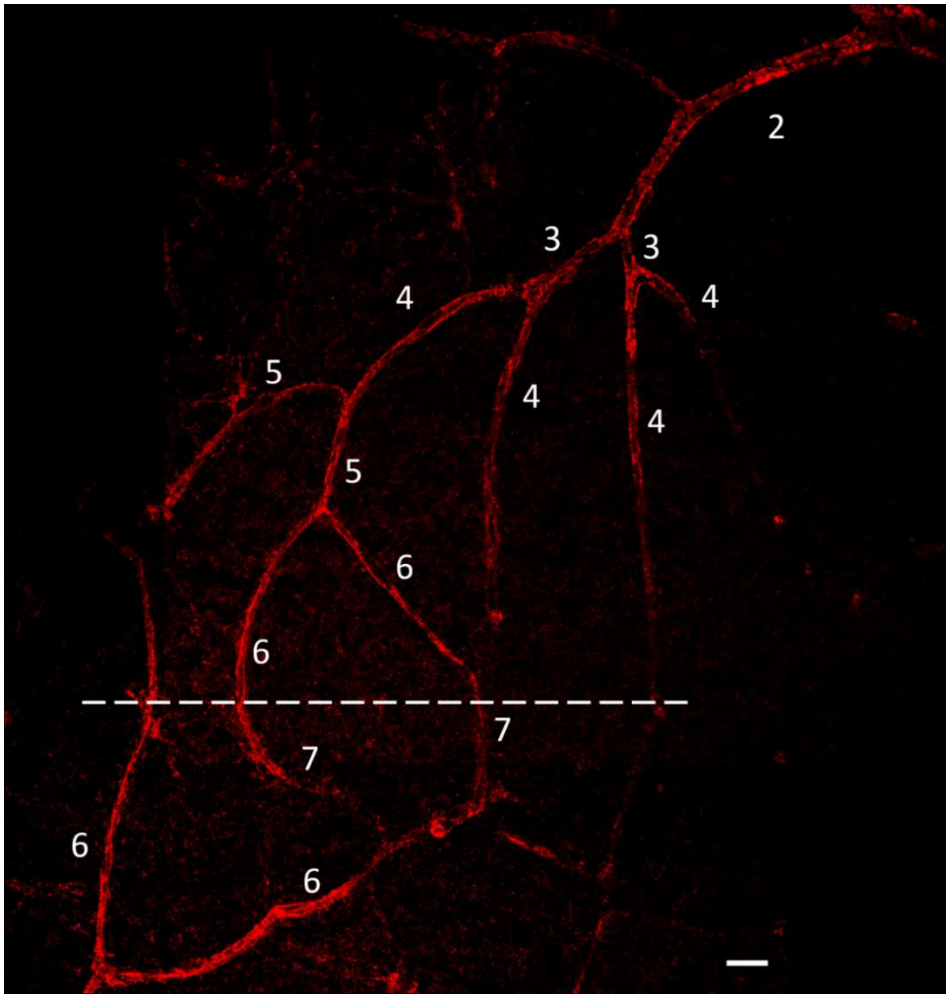

Figure 4.9. Myh11 labeling continues all along the superficial layer, revealing the capillary loops. Dashed line represents where the capillary branches dive deeper to form the intermediate vascular layer. Z-stack maximum projection image. Scalebar: 20 µm.

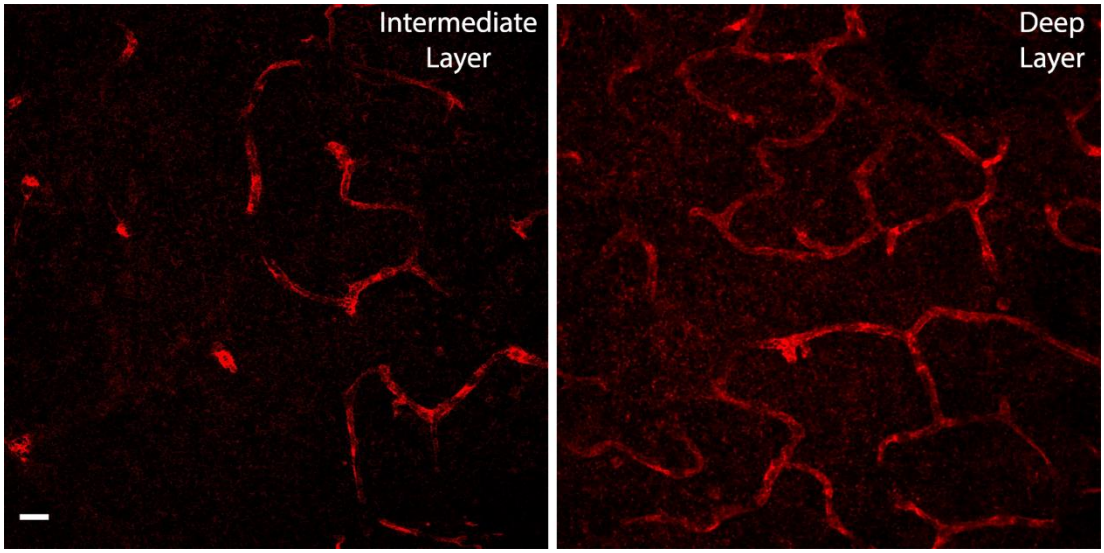

Figure 4.10. Myh11 labeling uninterruptedly continues in the intermediate and deep layers of retinal vasculature. Scalebar: 20 µm. Z-stack maximum projection images of 8.88 and 8.45 µm thick vascular sections, respectively.

α-SMA filaments are constantly de- and repolymerized like all other filamentous actin isoforms in almost all sorts of cells. It has recently been shown that this limits detection of small amounts of α-SMA in downstream pericytes because α-SMA is rapidly depolymerized but cannot be repolimerized in the abscense of ATP during tissue fixation (39). Accordingly, rapid fixation with methanol is required to prevent α-SMA depolymerization during tissue processing; which results in a significant increase in the extent of α-SMA labeling in downstream pericytes compared to PFA fixed tissues (36). Such a discrepancy was not observed for Myh11 (Figure 4.11.), as expected from a globular protein that does not require polymerization to be functional.

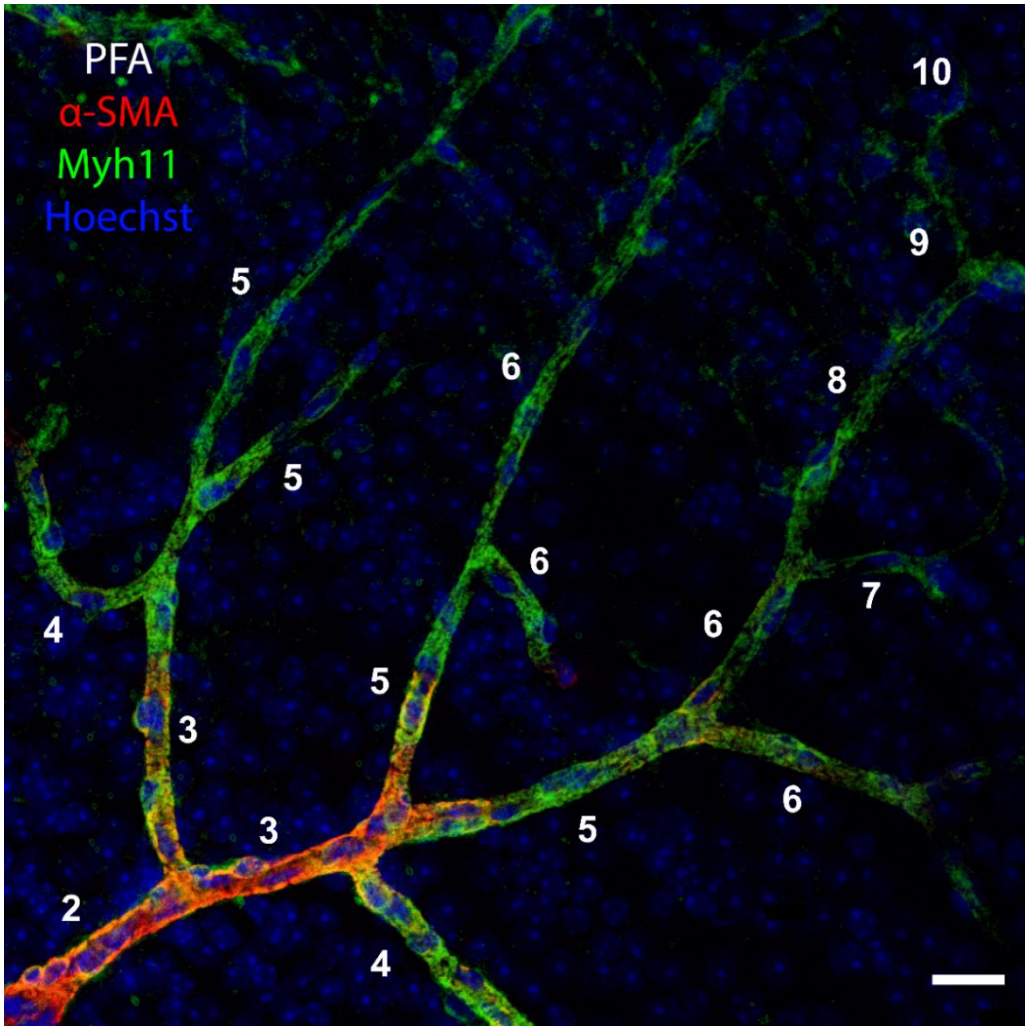

Figure 4.11. Myh11 labeling is unaffected by fixation method. Despite gradual tapering in α-SMA signal towards downstream branches, Myh11 labeling continued all along the whole vascular tree regardless of the fixation method. Here, the tissue was fixed with PFA unlike 4,8, 4.9 and 4.10 that were fixed with methanol. Scalebar: 20 µm.

Actomyosin fibers are organized around the skeleton formed by α-SMA filaments; myosin globular heads are attached to these spirals (Figure 2.6.). Accordingly, we asked whether Myh11 organization would be altered in pericytes where α-SMA expression was knocked down. We found that siRNA targeted against Acta2 transcript knocked down α-SMA protein expression especially in downstream pericytes in a patchy pattern as previously reported (36). In regions where α-SMA expression was partially or totally lost, Myh11 expression uninterruptedly continued (Figure 4.12.), suggesting that Myh11 expression and its organization within the actomyosin bundles is independent from that of α-SMA.

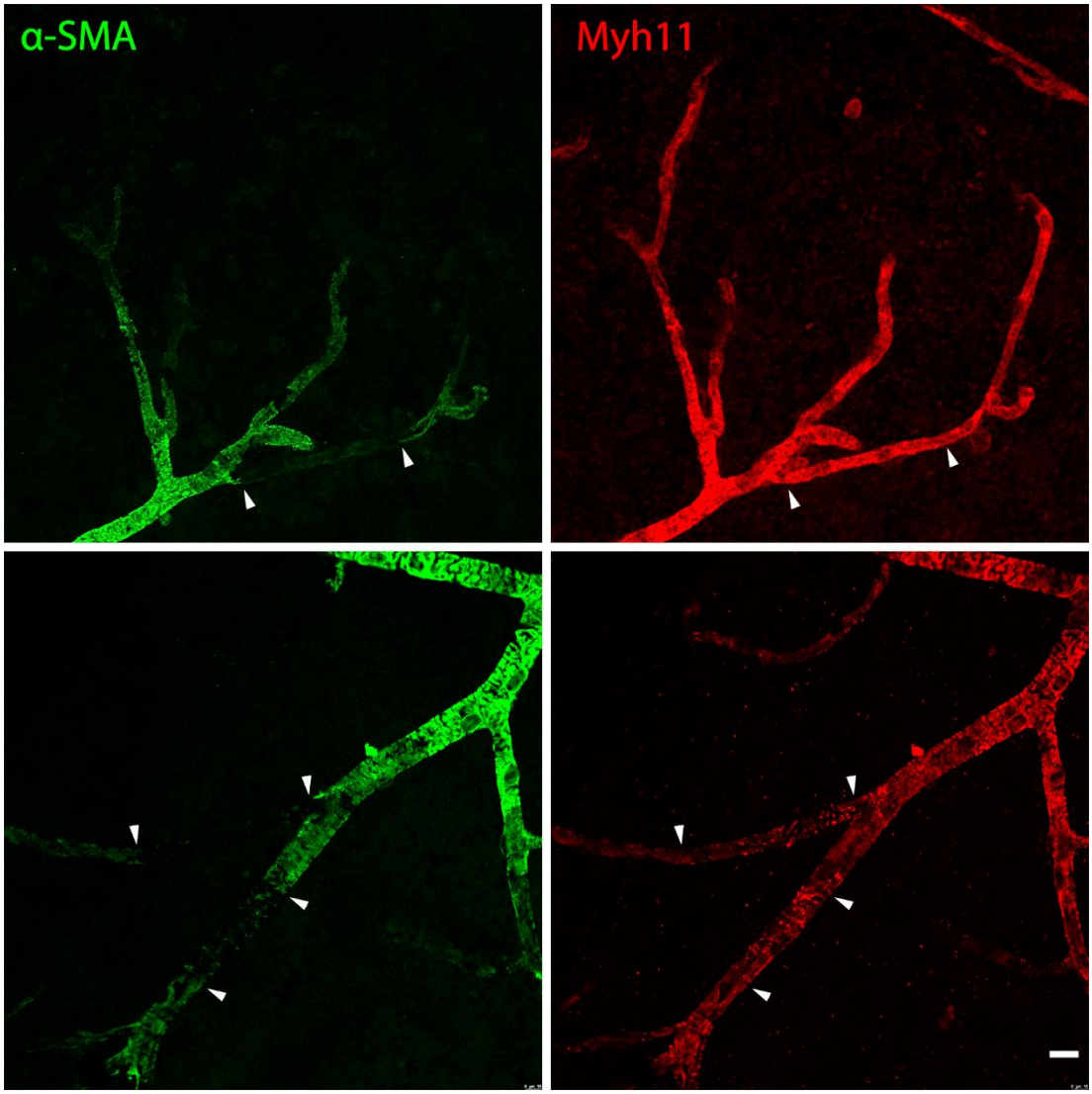

Figure 4.12. Knocking down α-SMA expression did not modify Myh11 organization. α-SMA labeling was discontinuous (arrowheads on 4th order branches) 48 hours after intravitreal injection of siRNA against Acta2 transcript in the superficial vascular layer, whereas Myh11 labeling remained unaffected. Scalebar: 20 µm.

4.3.3. Blebbistatin Disrupts Actomyosin Mediated Constriction in Retinal Microvascular Segments

Next, we tested whether actomyosin bundles detected in pericytes mediate their contraction by inhibiting actomyosin cross-bridge cycling with blebbistatin. Blebbistatin inhibits the activity of myosin ATPase that is indispensable for actomyosin coupling. Intravitreal injection of blebbistatin 40 minutes prior to NA injection significantly reduced the number of contracted capillaries. With the dose

we used, NA significantly reduced capillary luminal diameter assessed by lectin labeling in downstream vessels without affecting upstream capillaries, which allowed us to evaluate the downstream diameter changes independently of changes in blood volume regulated by upstream pericytes or vSMCs.

Blebbistatin significantly prevented NA-induced contraction when all microvascular segments were pooled, compared to vehicle (n=757 vs n=770 vessels, 4 retinas per group) as assessed by JNDR (means: 0.78 vs. 0.74; SDs: 0.19 vs. 0.17, $p<0.001$). When vascular orders were separately analyzed, JNDR was higher in blebbistatin treated group compared to vehicle treated group in downstream vascular orders 5 (means: 0.81 vs. 0.75; SDs: 0.19 vs. 0.18, $p=0.001$, n=197 vs. 217) and 7 (means: 0.79 vs. 0.75; SDs: 0.18 vs. 0.15, $p=0.03$, n=88 vs. 100). Although insignificant, a trend of higher JNDR was observed for all orders (Figure 4. 13.).

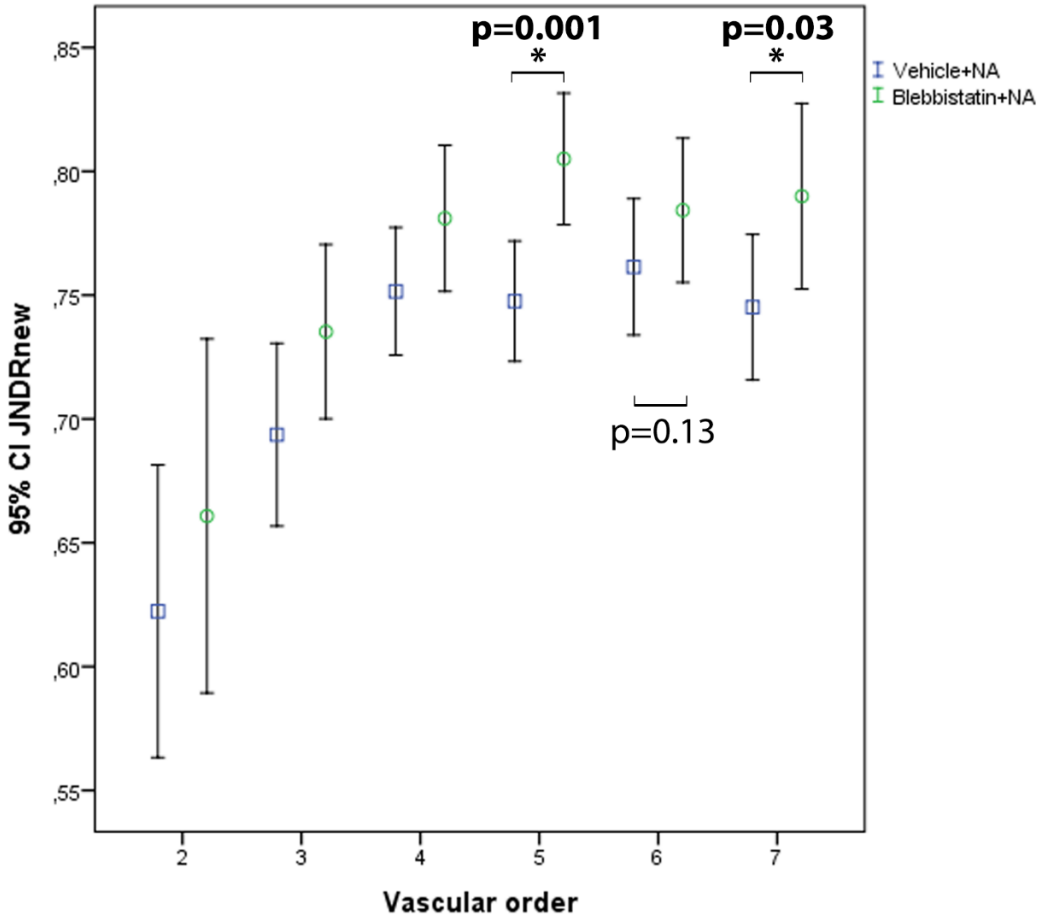

Figure 4.13. Blebbistatin prevents NA-induced vasoconstrictions in downstream retinal vascular branches. The effect was prominent in downstream orders because the NA dose used mainly constrict downstream pericytes. Graph displays juxtanuclear ratio (JNDRs) means with their confidence intervals for each vessel order. Vessel diameters were measured from retinas treated with vehicle (blue squares) or blebbistatin (green circles) prior to NA.

4.3.4. Analysis of α-SMA and Myh11 Interaction in Pericytes with FRET

By spectral unmixing approach, FRET between Cy3 labeled anti-α-SMA and Alexa Fluor-488-nanosecondary labeled anti-Myh11 antibodies was evaluated in retinal pericytes (Figure 4.14.).

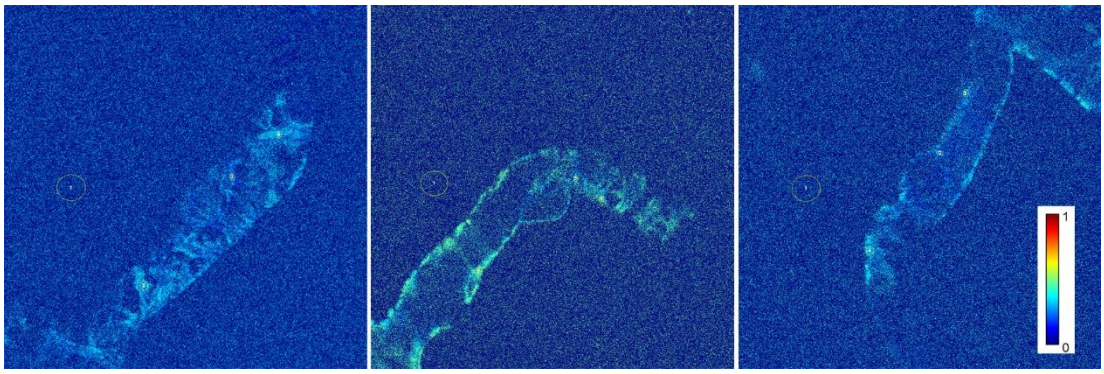

ROI \ Orders	2	3	4
1	0.33	0.44	0.34
2	0.29	0.41	0.27
3	0.33	0.42	0.34

Figure 4.14. FRET efficiency between antibodies against α-SMA and Myh11 in retinal pericytes. FRET colormap image of pericytes from 2-4th order vessels of a retinal sample produced with a spectral unmixing approach, showing close interaction of α-SMA and Myh11 in pericyte processes. Three ROI's are selected from an upstream process, a position near nucleus, and a downstream process, respectively. Efficiency values and colormap are corrected by background value subtraction. Warmer colors indicate higher efficiency values on the colormap.

4.4. Role of Actin Polymerization in Pericyte Contraction

By strengthening the cytoskeletal organization and hence forming a more rigid cellular scaffold, actin polymerization is known to contribute to vSMC contraction. It augments the force generated by actin-myosin cross bridge cycling and mediate transfer of this force to the extracellular matrix (10, 118). We explored this auxiliary mechanism in pericytes, by use of selective markers against monomeric and polymerized states of actin.

4.4.1. Actin Isoforms in Pericytes

Pericytes express constitutional actin isoforms along with α-SMA. Phalloidin is a marker for the filamentous state of actin, not differentiating between isoforms.

F-actin labeling of mouse retinas with phalloidin was continuous along the entire retinal vascular tree. F-actin in nonvascular cells was also labeled. Phalloidin labels not only α-SMA in pericytes but also the other two constitutive actin isoforms (β- and γ-actin), however, α-SMA labeling could be inferred by fibers running circumferential (or twisting at varying angles) to the vessel longitudinal axis in wrapping-type pericytes or filling in the thin processes of downstream mid-capillary pericytes (Figure 4.15.A). This pattern highly overlapped with α-SMA immunostaining, whereas the non-α-SMA F-actin labeling with phalloidin generally ran parallel to the longitudinal axis (including typical submembranous –i.e. cortical- labeling for β-actin), giving rise to long lines (filaments) (Figure 4.15.B). The α-SMA in helical strand-like pericyte processes could be distinguished by its spiraling course eccentrically over the capillary wall unlike endothelial F-actin labeling that runs parallel to the lumen creating a pseudo image of a lumen in the middle of the vessel (Figure 4.15.C).

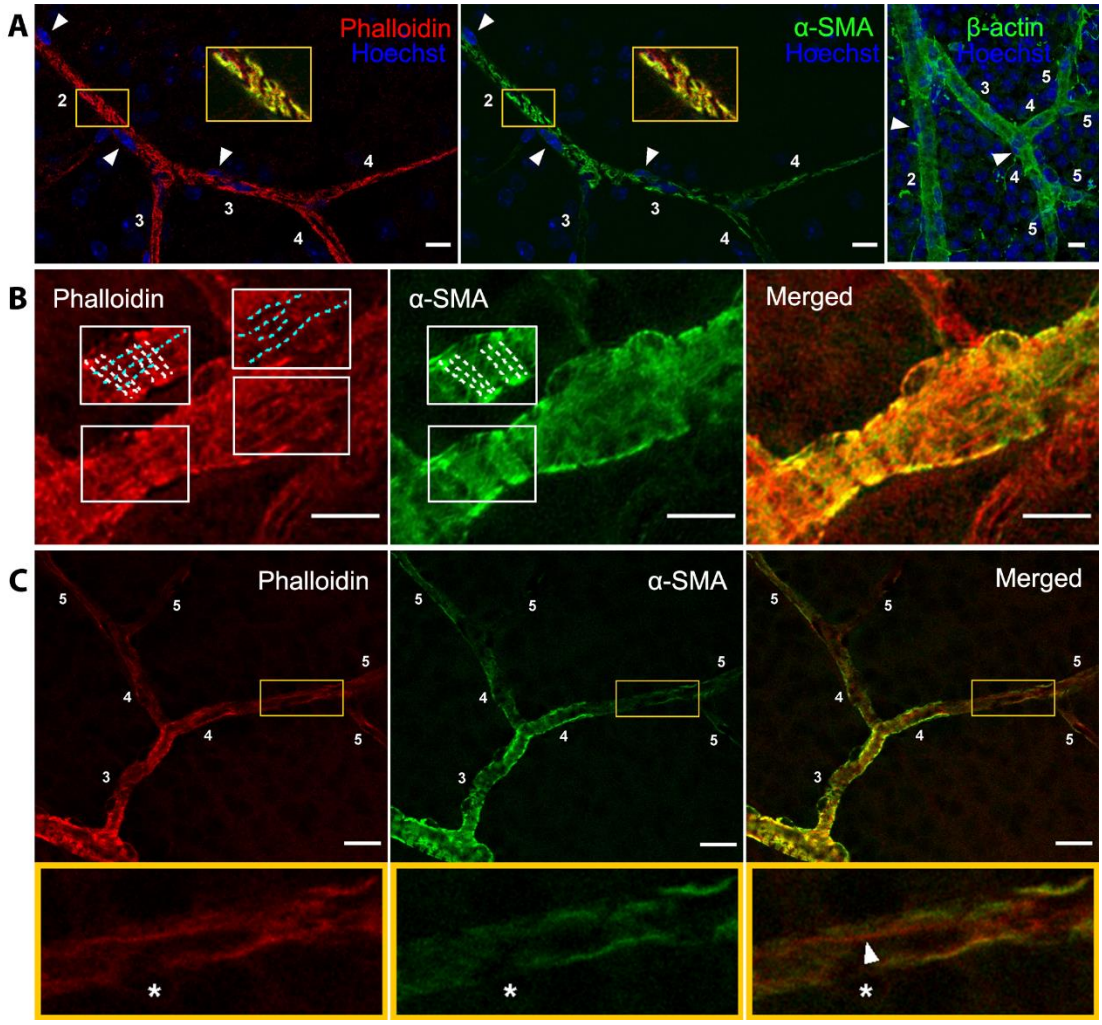

Figure 4.15. Phalloidin labeling largely overlaps with α-SMA immunostaining. A. The phalloidin labeling of α-SMA can be traced and differentiated from other actin isoforms by its pattern overlapping with that of α-SMA immunostaining in wrapping-type pericytes (see 2x zoomed inset for detail of the overlap, i.e. yellow color). Arrowheads point to pericyte somas identified by labeling of nuclei with Hoechst. Note that as pericyte coverage decreases in higher order branches so do α-SMA immunostaining and phalloidin labeling, illustrating that majority of the phalloidin labeling in pericytes displays the α-SMA isoform. The image on the right shows labeling for β-actin, which runs along the cortex of the vessel in addition to slight diffuse labeling. Scalebar: 10 µm. B. α-SMA in the processes of a pericyte on the third order retinal vessel runs around the vascular axis (white dashed lines), whereas non-α-SMA isoforms of actin can be traced along the longitudinal axis of the vessel (cyan dashed lines). Note the absence of α-SMA immunostaining of the phalloidin-positive longitudinal filaments in contrast to circular ones in inset. Scalebar: 10 µm. C. α-SMA in the helical processes follows the vascular wall starting from the boxed area on the distal part of a 4th order branch. Bottom row shows the boxed area at higher magnification. Note that α-

SMA and corresponding phalloidin-staining overlap over the vessel wall, whereas the red-filamentous staining running parallel and closer to the lumen is α-SMA-negative (arrowhead). Phalloidin labeling largely corresponds to the α-SMA isoform even in helical pericytes. Upstream to the box, α-SMA labeling is of wrapping type. *: pericyte soma. Scalebar: 20 µm

4.4.2. Phalloidin and DNase I Labeling as Indicators of Actin Polymerization State

DNase I labeling disclosing actin monomers was evident in the vessel wall as well as throughout the tissue, regardless of cell type. Although G-actin staining delineated the outline of the vascular tree, this was more like a “vascular silhouette” in contrast to phalloidin labeling, which sharply outlined the vessels. When retinas were treated with NA, F-actin staining became more pronounced especially in downstream pericytes, whereas vascular silhouette formed by G-actin labeling was attenuated and became hardly discernable from the background formed by nonvascular cells (Figure 4.16.A). Reduction in DNase I staining was also evident in some low order capillaries without obvious contracted segments (Figure 4.16.B). However, the number of such upstream capillaries did not reach a statistically significant difference compared to vehicle-treated retinas unlike high order capillaries as we detail in the next section (Figure 4.17.C).

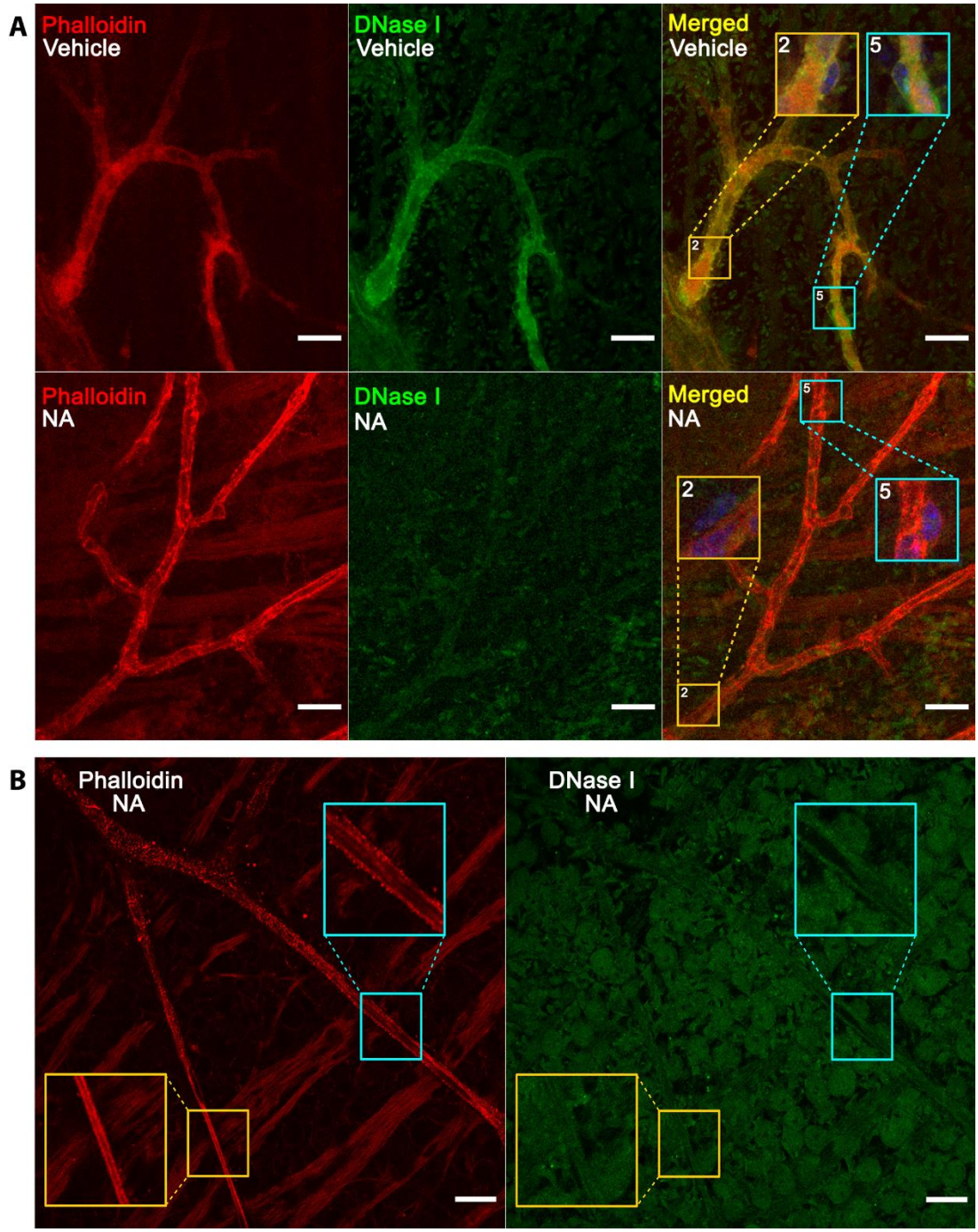

Figure 4.16. Noradrenaline stimulation induces actin polymerization in microvessels. A. Images from vehicle-treated (upper row) and noradrenaline-treated (lower row) retinas were obtained from the same vascular orders (2-5) and all imaging parameters were kept identical. Background signal intensities were matched for illustrative purposes. Yellow and cyan boxes display pericytes on the second and fifth order retinal microvessels, respectively. Blue indicates Hoechst-labeled nuclei. B. Intensely (yellow inset) and partially constricted (cyan inset) segments of retinal capillaries from an NA-treated retina display different F-actin staining patterns. Phalloidin labeled F-actin appears more condensed at the segment where

microvascular constriction is more pronounced. In both instances, however, DNase I staining was noticeably reduced so that vascular outline is barely discernable from the background. Insets are 2x magnified. Scalebars: 20 µm.

4.4.3. NA Induces Actin Polymerization in Retinal Pericytes

We calculated F/G-actin ratios from ROIs placed over pericytes identified by morphological criteria. The balance between monomeric and polymeric forms of actin shifted towards the polymerized (F) actin side in pericytes from the NA-treated retinas compared to the pericytes of the vehicle-treated retinas, as revealed by significantly increased F/G-actin signal ratios (medians: 4.2 vs. 3.5; IQRs: 3.1 vs. 2.1, $p=0.006$, n=108 vs. 83 pericytes, 6 retinas per group; due to the skewed distribution of values, non-parametric tests were used)(Figure 4.17.B). Because double labeling with α-SMA showed that majority of phalloidin labeling in pericytes corresponds to α-SMA, we presume that this rapid shift induced by NA within 2 minutes may involve increased α-SMA polymerization. A similar shift in other isoforms is also likely as seen in aortic vSMCs, but this cannot be easily distinguished in small pericytes *in vivo* with the available techniques and severely limited by rapid depolymerization of small F-actin pool in pericytes during tissue preparation for *ex vivo* investigation unlike vSMCs (16). The pattern of intensified phalloidin signal overlapped with α-SMA immunostaining, however, the present microscopic resolutions do not allow whether α-SMA or adjacent non-α-SMA F-actin filaments were more polymerized (Figure 4.17.B). Pharmacological or genetic inhibitors of polymerization processes also do not differentiate between polymerization of F-actin isoforms. Importantly, however, an increasing F/G-actin signal ratio was observed towards downstream branches when the analyses were performed per retinal vascular order. In fact, the increase was statistically significant only for orders five ($p=0.038$) and six ($p<0.001$) (Figure 4.17.C).

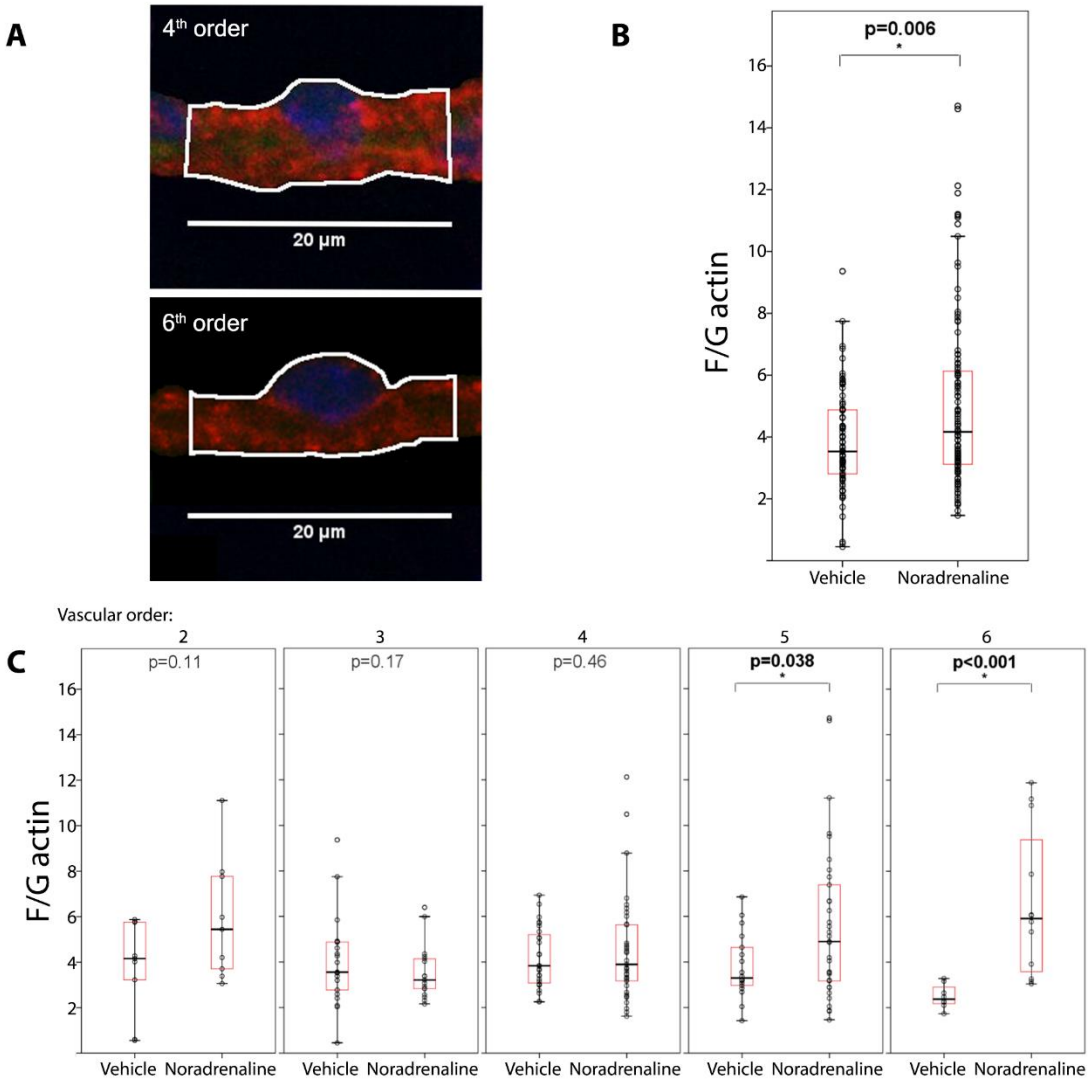

Figure 4.17. Noradrenaline induces F-actin polymerization in downstream retinal pericytes. A. Images illustrate ROI placement over a fourth (upper) and a sixth (lower) order retinal microvessel, representing wrapping and helical pericytes, respectively. B-C. NA treatment promotes F-actin polymerization as suggested by increases in F/G-actin signal ratios. Scatter dot-box plot graphs illustrate F/G-actin signal ratios in individual pericytes from noradrenaline (n=97) or vehicle-treated (n=84) retinas for all orders from 2-6 (B) and by each vascular order (C) (n=6 mice retinas per group).

Although the group differences were statistically significant, considering the high variability and skewed distribution of values as well as the possibility that all downstream pericytes may not be equally responsive to NA, we assessed the presence of a subgroup of pericytes that did not contract within the 5th and 6th order

populations. We found that a threshold F/G ratio value of 5 was able to separate the two populations by ROC analysis of vehicle and NA-treated groups (false positivity rate was accepted as 15%, AUCOR=0.742, p=0.001). This threshold also conformed to the mean $\pm$ 1SD value of 4.8 for the vehicle-treated pericytes. When values above and below the threshold for the 5^{th} and 6^{th} order NA-treated pericyte populations were separately analyzed, the median F/G was 7.6 (IQR=4.7) vs. 3.2 (IQR=1.2) (p<0.001) (n=45). Supporting the idea that the NA-responsive pericytes increased their tonus (contracted); the corresponding ratios [median (IQR)] of the capillary diameter change measured adjacent to the pericyte nucleus divided by the diameter at the branch origin were 0.67 (0.14) vs. 0.81 (0.34), respectively (p=0.005), whereas the median for vehicle treated group was 0.85 (IQR=0.32) (n=25, p<0.001 compared to NA-responsive group)(Figure 4.18.C). We did not measure the diameter under the soma but just next to nucleus (juxtanuclear) because under-soma measurements were confounded by location of the pericyte nucleus relative to the scanning angle (Figure 4.18.A). In response to NA, downstream pericytes generally did not show nodal constrictions but a tide-like diameter decrease, reaching a maximum near soma (Fig 4.18.B). Accordingly, we assessed the diameter change relative to the diameter at the origin of the capillary segment as described in the methods.

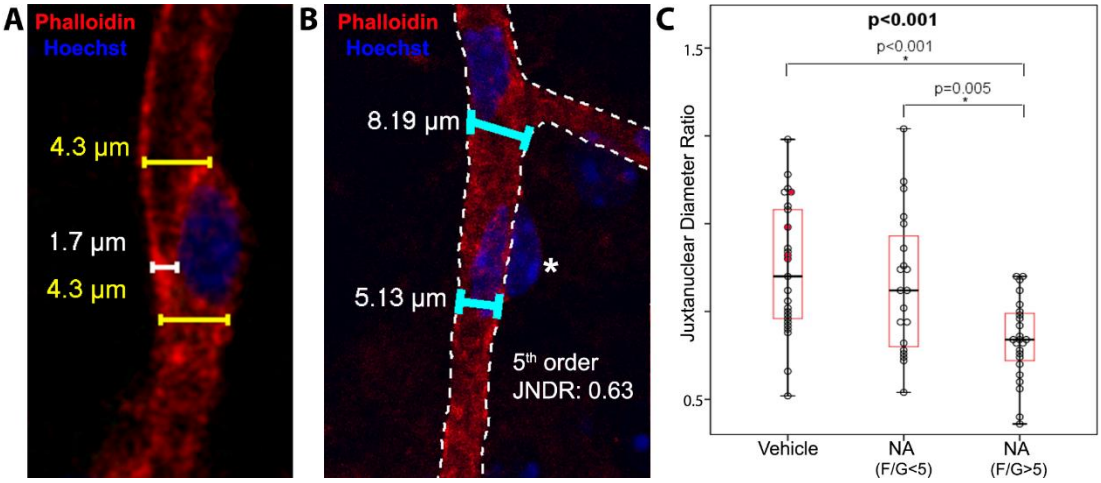

Figure 4.18. High F/G signal ratio is associated with decreased capillary diameter. A. Image illustrates how juxtanuclear capillary diameter was measured. Measurements under the soma (white) were not preferred because they give misleading values in some instances where the pericyte nucleus is superimposed on vessel lumen in maximum projection images. Juxtanuclear values were then divided by the initial diameter of each capillary segment at the proximal branching point to yield juxtanuclear diameter ratio. B. The ratio of diameter near pericyte soma to the diameter at the branch origin is defined as juxtanuclear diameter ratio. Image illustrates how these diameters are measured in a 5^{th} order pericyte with F/G-actin signal ratio above 5. Asterisk shows the index pericyte's soma. JNDR: Juxtanuclear Diameter Ratio. C. In vascular orders of 5 and 6, which had significantly increased F/G-actin signal ratio values, a cutoff F/G value of 5 was able to differentiate NA and vehicle treated groups. This value was used to separate NA responsive and unresponsive pericytes on 5^{th} and 6^{th} order capillaries in NA-treated retinas. The group with high F-actin polymerization index, therefore considered as NA responsive, displayed significantly decreased vascular diameters compared to both NA-unresponsive and vehicle groups. The comparison of three groups by Kruskal-Wallis test yielded a p value less than 0.001. Only 4 of the vehicle treated pericytes had F/G-actin signal ratio values above 5, which are shown with red-filled circles.

5. DISCUSSION

Although it is now generally accepted that pericytes can contract and relax in response to physiological and pharmacological stimuli as well as microvascular pathological processes, the underlying mechanism of this contraction remains underexplored. Actomyosin coupling and F-actin polymerization was previously demonstrated to be involved in pericyte contractility under *in vitro* experimental conditions (8); however, its *in vivo* correspondence is unclear because pericytes exhibit different contractile phenotypes along the microvasculature. An actomyosin-mediated contraction is generally regarded as a putative mechanism for upstream pericytes rich in α-SMA, whereas the presence of a similar mechanism in downstream pericytes expressing low amounts of α-SMA is in question (2, 4, 7, 73). The controversies have been rekindled by recent single cell transcriptomic studies, which could only detect low levels of α-SMA-mRNA in dissociated pericytes (51, 119).

In smooth muscle cells, the prototypical contractile cells in vertebrates, actin alone cannot carry out motor function but acts as a guide for myosin motor protein to slide on. Among the 6 isoforms of actin, α-SMA is the contractility-associated isoform in majority of the smooth muscle cells. The forces exerted by these motor proteins in vSMCs deform the cell, which leads to narrowing of the lumen with help of the connections to the extracellular matrix proteins in the vessel wall. At the microcirculatory level, luminal diameter changes have been shown to be the result of pericyte contraction. By analogy, pericytes may also exploit the actomyosin based contractile system used by vSMCs. A few studies performed on cultured pericytes support this hypothesis (8). However, *in vivo* evidence is lacking for the presence of a functional actomyosin complex in pericytes.

Alarcon-Martinez et al. (18) clearly showed that retinal capillary pericytes express the α-SMA isoform by preventing actin depolymerization using a rapid fixation process. This finding was functionally correlated to the colocalization of capillary constrictions with α-SMA expressing pericytes (37). The anti α-SMA

antibodies used in these studies, and also in the present study, are raised using the synthetic NH2 terminal decapeptide of α-SMA coupled to keyhole limpet hemocyanin (KLH) as the immunogen (120). They do not cross-react with other actin isoforms. Therefore, the immunofluorescent signal observed is considered specific to α-SMA. However, α-SMA labeling was limited in pericytes on 5^{th}-8^{th} downstream orders despite rapid fixation. Mouse Acta2 gene has two splice variants resulting in two proteins sharing similar amino acid sequences at their N terminals (121). Therefore, the alternative splice variant might take over in downstream pericytes that have scarce or no labeling. However, because the anti-α-SMA antibodies used in this study recognize the protein at its N terminal, they are expected to recognize both splice variants, hence, excluding this possibility. Alternatively, some actin binding proteins complexing with stress fibers of downstream pericytes might lead to epitope masking and difficulty in immunolabeling of α-SMA fibers (42); however, there is no evidence as yet supporting this speculative possibility. So, we conclude that the inefficient labeling is likely to be a result of rapid depolymerization of a small pool of α-SMA in downstream capillaries during tissue processing.

The other component of the actomyosin system, the myosin II motor protein, has been far less studied in pericytes. In our study, relying on the expression data and the presence of α-SMA in pericytes, Myh11 was chosen as the MHC isoform of interest. Immunofluorescent labeling against Myh11 revealed an uninterrupted labeling all along the retinal vasculature, from superficial to deep layer. We consider this labeling specific even though the immunogen of Myh11 antibody used in this study shares 82% homology with Myh9 because no experimental cross-reactivity has been reported in the literature and, we used of a rather low concentration of primary antibody (1:400). Moreover, coupling Myh11 with α-SMA is more advantageous for smooth muscle contraction because the smooth muscle isoforms of myosin II have faster kinetics compared to non-muscle isoforms such as Myh9 (122). ECs might be another source of Myh11 signal, since they were reported to express Myh11 transcripts (52). However, the close association with α-SMA is able to unambiguously discriminate pericytic staining. Moreover, the significance of transcriptomic findings

should be treated cautiously because isolation of ECs from pericytes for single-cell studies is very difficult due to the firmly attached basement membrane between cells.

After demonstrating the colocalization of α-SMA and Myh11, we used blebbistatin, a myosin II inhibitor to confirm the presence of a functional actomyosin complex in retinal pericytes. The concentration of blebbistatin was determined based on the cell culture study by Lee et al. (8), with optimization modifications considering the vitreous volume. Blebbistatin application prior to NA inhibited vasoconstriction, particularly in downstream vessels, which preferentially constrict with the NA dose we used. This finding strongly suggests that NA-induced vasoconstriction in retinal microvasculature involves actomyosin coupling. As also suggested by their morphology, capillary/thin-strand pericytes are thought to maintain the capillary tonus, rather than acting like a vascular sphincter. The function of this tonal regulation might be to modify vascular resistance, hence, the flux of RBCs through a narrow lumen (109). As an analogy, smooth muscle layers are organized in circular, longitudinal and sometimes oblique orientations within the walls of hollow organs (i.e. those with a lumen) such as esophagus, stomach, intestines, colon, bladder and ureter. Combined action of these varying orientations provides propulsive movement of the content. For instance, the longitudinal muscle layer shortens the related segment bringing circular forces together and intensifying the overall effect on luminal diameter (123). Besides organization of stress fibers in 3 directions, perhaps creating a propulsive force in addition to tonus, higher basal calcium levels in downstream pericytes (73) suggests a dynamic regulation of contraction in downstream capillaries.

Another approach we used to assess the close association of α-SMA with Myh11 was the FRET technique. FRET pairs are ideally formed by direct fluorescent tagging of proteins at appropriate amino acids. However, synthesis of these labeled proteins requires an extensive work, hence, is not time and cost-effective. Labeling of the targets with fluorescently conjugated antibodies can practically be achieved

under routine laboratory conditions. When these fluorescent-tagged antibodies are used as FRET pairs, sufficient FRET distance (i.e < 10 nm) can potentially be obtained despite spatial limitations imposed by the large size and dipole orientation of antibodies. The interfilament distance between actin and myosin backbones reportedly ranges between 8-14 nm depending on the muscle type although the distance is affected by angular position of the myosin head and the state of power-stroke (124). Therefore, it is reasonable to expect that some of the myosin heads are within the FRET distance of actin. In this study, the antibody against Myh11 was chosen because its epitope is close to the myosin head-actin interaction site whereas the anti α-SMA antibody targets the N-terminal, the site interacting with myosin (125). Additionally, to avoid the distance due to large size of the secondary antibodies, Cy3 fluorophore was directly attached to α-SMA primary antibody, and a nanosecondary antibody was used to label Myh11 with Alexa-Fluor 488, which allowed us to obtain high FRET efficiencies, pointing to a tight colocalization (< 10 nm) of the two motor proteins. Of note, as FRET is an all-or-none phenomenon, the efficiency values obtained only represent the ratio of positive occasions within a defined region. Therefore, higher or lower efficiency values do not correspond to closer or more distant localization of proteins, but only the ratio of pairs showing FRET to total number of pairs within an ROI. Further studies are required to see whether stimulation of actin-myosin interaction increases FRET occurrences.

The present study also shows that F-actin polymerization can be promoted in retinal 5^{th} and 6^{th} order downstream pericytes briefly stimulated *in vivo* with a vasoconstrictive neuromodulator. This is accompanied by a reduction in diameter of 5^{th} and 6^{th} order capillaries, suggesting that F-actin polymerization is involved in pericyte contraction. Previous studies from our laboratory using agents that inhibit F-actin depolymerization such as phalloidin and jasplakinolide as well as short interfering α-SMA-RNA suggested that pericytes on high branch order retinal capillaries had a rapidly (de/re) polymerizing small pool of α-SMA, mediating pericyte contraction (36, 37). Combining these previous and the present observations, we hypothesize that existing α-SMA filaments may be further polymerized on

vasoconstrictive stimulation, providing additional sites for actomyosin coupling along with strengthening the submembranous lattice by β-actin polymerization. The induction of actin polymerization by NA and other vasoconstrictive agents or intraluminal pressure is well documented for vSMCs (1, 126-128). Upon agonist stimulation, monomeric actin in vSMC is readily added to the existing F-actin filaments and elongates them (55). Polymerization is thought to function as an independent but parallel mechanism to actomyosin-mediated contraction by providing cellular stiffness against mechanical deformation of vSMCs during contraction and a lattice between contracting fibers and extracellular matrix to transform the tension developed by actomyosin cross bridge cycling to vessel constriction (10, 118). In freshly dissociated aortic vSMCs, phenylephrine increased F/G ratio and, an isoform specific analysis showed that this increase was caused by polymerization of γ- but not β or α-SMA (16). However, γ-actin could not be detected downstream to 4th order retinal pericytes by immunohistochemistry (36) and, according to recent single cell transcriptomics studies, pericytes express very little smooth muscle - γ actin (Actg2) mRNA unlike vSMCs (52). Contribution of a similar G to F shift in β-actin isoform within pericytes to the increased F/G signal is also likely, which may contribute to contractility by reorganization of the pericyte cytoskeleton, especially the submembranous β-actin lattice as seen in isolated large cerebral arteries (1, 126, 129) and cultured pericytes (8). Unfortunately, as elaborated in the Results section, it is technically challenging to differentiate the relative contributions of each actin isoform in small capillary pericytes *in vivo* as well as to separate the potential (possibly minor) contribution by the endothelial F-actin labeling with phalloidin. However, suppression of the contraction of downstream pericytes with α-SMA-siRNA in our previous studies using the same retina preparation, point to the α-SMA-mediated mechanisms as the main source of contractile force production (37). Supporting this, jasplakinolide, which promotes F-actin polymerization, increased the number of 5th and 6th order α-SMA-immunopositive retinal pericytes about three times more compared to phalloidin, which only stabilizes actin filaments, strongly suggesting that F-actin fibers forming α-SMA is actively (de/re) polymerized in situ in

downstream pericytes (36). However, despite technical shortcoming precluding direct evidence, based on the rich data from vSMCs, we conclude that α-SMA-mediated contraction in downstream pericytes can be complemented with the supplementary force generated by polymerization of submembranous β-actin cytoskeleton connecting to the extracellular matrix (8, 128).

A significant F/G-actin signal ratio increase in retinal high order capillaries, which are only partly covered by pericyte soma and their thin processes, can be explained by dependence of their contractile force generation to *de novo* F-actin polymerization in addition to the contraction of α-SMA fibers existing in low quantities. This formulation is consistent with difficulty in detecting α-SMA protein in pericytes in high order capillaries as well as low α-SMA-mRNA levels (51) and more effective knockdown by RNA interference relatively to the upstream pericytes (36, 37). As previously suggested (73), the downstream pericytes may contribute to regulation of the capillary flow by maintaining a modifiable elasticity (stiffness, tonus) of the capillary wall rather than by focal constriction (28). Peppiatt et al. (30) originally proposed this possibility to explain the lack of nodal capillary constriction under the pericyte soma on stimulation with NA in their study using whole-mount retina. Altogether these observations are in line with the proposal of two different contractile phenotypes of retinal pericytes, one inducing node-like/phasic and the other tide-like/tonic constrictions (117). Therefore, in contrast to the higher-pressurized proximal segments where strong actomyosin bridging is needed for reducing the capillary diameter, in distal capillaries, the lower tension generated by small amounts of α-SMA filaments can be distributed by way of F-actin lattice along the pericyte cortex to provide a modifiable but sustained tonus (stiffness) to the capillary. The continual basal contractile state (tonus) may require relatively higher steady-state intracellular calcium (as suggested by high frequency of spontaneous calcium transients observed by Rungta et al. (73) compared to the upstream temporarily contracting/relaxing enwrapping type pericytes, thereby, increasing their sensitivity to vasoconstrictive stimuli. Also, a small amount of α-SMA fibrils (36) may require polymerization to generate the necessary force in response to

vasoconstrictive stimulation, which, under resting conditions, might be driven by mechanical stress-induced F-actin polymerization triggered by transiting blood cells that are squished in narrow lumina of downstream capillaries (56). In summary, (de/re) polymerization of cytoskeletal F-actin and α-SMA may be a dynamic mechanism regulating stiffness (tonus) and contractility of downstream pericytes. Future studies are needed to gain insight to these mechanisms *in vivo* though it is technically challenging.

Another explanation for differential sensitivity of down and upstream pericytes to NA might be the presence of different densities or subtypes of adrenergic receptors along the retinal vascular tree, with varying sensitivities and downstream signaling pathways; however, this idea remains speculative, as the subject is not sufficiently explored. The vasoconstrictive action of NA is generally associated with α_1-adrenoceptor subtype and, transcriptomic studies consistently show that pericytes express α_1-adrenergic receptors (9, 52), although *in vivo* distribution of the receptor in pericytes along the microvasculature is not clear. Similarly, there are PCR studies supporting the presence of mRNAs belonging to all three α_1-adrenoceptor subtypes (A, B and D) in the rabbit (130) and mouse (131) retina, yet, differential expression of these subtypes regarding the position along the vascular axis has not been investigated. There are a few functional correlation studies between murine α_1-adrenoceptor subtypes and NA response. However, these studies were conducted without any specification of ocular vascular tissue (132) or focused only to the arteriolar level (133). Additionally, administration route of NA was either systemic (133) or topical application over the *ex vivo* retina preparation (132). Compared to the previous administration routes, we presume that, in our model, NA must have preferentially acted on receptors located on pericytes rather than endothelia (134) as the intravitreally administered NA gains access to capillaries from the abluminal side unlike systemically injected NA first reaching to endothelial receptors from the blood. In a study on isolated pig retinal arteries, vasoconstrictive effect of NA was higher when microperfused intraluminally, compared to extraluminal application (135). This finding supports the view that direction of NA access to vessel affects its

mechanism of action. Additionally, to achieve intraluminal access in an *in vivo* study, systemic administration of NA would affect circulation dynamics in a complicated way, because of its positive inotropic/chronotropic effects. Contrary to our results, in a study on rat retinas, intravitreal injection of NA only affected the diameter of larger caliber arterioles but not the capillaries (136). This discrepancy might be a result of the 15 minutes-long incubation period, beyond the half-life of NA, and the change in arterioles might be a secondary effect. Besides, as it was shown in rabbit eyes that intraocular NA increases trabecular outflow, clearance of NA might be increased as well (137).

The finding of NA-responsive and unresponsive populations within NA-treated pericytes of 5th and 6th vascular orders is in line with the recent findings by Alarcon-Martinez et al. (138). They identified interpericyte tunneling nanotubes connecting two retinal pericytes and mediating simultaneous but opposite actions in vascular segments (constriction vs. dilation) that they are associated with. This means that a vasoconstrictive agent may not result in a homogenous constrictive response along the entire retinal vascular network.

Most of the noradrenergic innervation in central nervous system terminates around capillaries, rather than larger caliber vessels (30). Although retina is devoid of sympathetic innervation (95, 139), retinal vascular mural cells harbor adrenergic receptors as discussed above (for review, 31). From an evolutionary point of view, this discrepancy might serve to protect retina from the temporary changes in systemic sympathetic nervous system tonus. Such that, in case of an adrenergic spillover into circulation during a full-blown fight-or-flight response, the blood flow can be redistributed [perhaps toward the intermediate layer where the demand is higher (94)] by adrenaline accessing vessels via putative catecholamine transport mechanisms across blood-retinal barrier (140). However, for validating this idea, we need information on distribution of adrenergic receptors in a layer- and branch order-specific way. Unfortunately, the intermediate and deep layers were not included in

this study due to limitations in penetration of the antibodies and fixatives as well as laser beam used for staining and confocal imaging.

When signal transduction pathways are considered, both effects observed by NA application in this study, actin polymerization and actomyosin coupling, merge on RhoA/Rho kinase pathway. The mechanism of action of NA on α_1-adrenergic receptors in vSMCs is through two different G proteins: G_q, which increases intracellular calcium via phospholipase C mediated inositol triphosphate production pathway; and $G_{12/13}$, which activates Rho-GEF and hence Rho-kinase pathway (141, 142). Rho-kinase inhibits MLCP or activates MLCK by phosphorylation, enhancing actomyosin interaction. Rho-kinase pathway also increases actin filament polymerization (82), assembly (143) and membrane association (144). Therefore, activation of adrenergic receptors triggers a cascade of events that collectively lead to cellular contraction (see Figure 5.1. for a summary), as also suggested by the findings in our study.

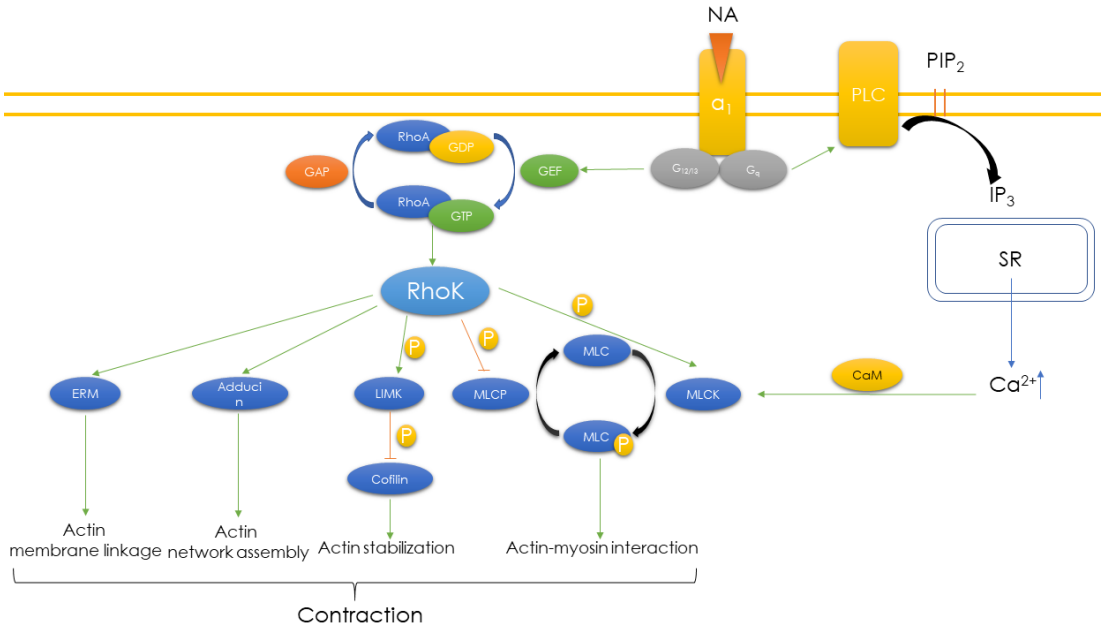

Figure 5.1. Activation of α_1-adrenergic receptors triggers a cascade of events that lead to cellular contraction.

6. CONCLUSION AND REMARKS

In conclusion, retinal microcirculatory pericytes express Myh11 isoform colocalized with α-SMA, suggesting an actomyosin complex based contractile mechanism. This colocalization is functionally relevant to microvessel diameter regulation because pharmacological inhibition of the actomyosin coupling with blebbistatin prevented capillary vasoconstriction. Noradrenergic stimulation of the retinal microcirculatory pericytes also promotes F-actin polymerization, supporting the view that pericytes contract by way of α-SMA-mediated and F-actin supported cytoskeletal mechanisms. Shift from G-actin monomers to polymerized F-actin was more pronounced in high order distal capillaries, possibly due to their dependence on de novo F-actin polymerization for contractile force generation because α-SMA exists in low quantities in these pericytes. These *in vivo* findings clarify that microvascular pericytes share common mechanisms of contractility with upstream vSMCs despite adaptive modifications to meet the local requirements imposed by the function of the microvascular segment that they are located on.

7. REFERENCES

1. Yamin R, Morgan KG. Deciphering actin cytoskeletal function in the contractile vascular smooth muscle cell. J Physiol. 2012;590(17):4145-54.
2. Hill RA, Tong L, Yuan P, Murikinati S, Gupta S, Grutzendler J. Regional Blood Flow in the Normal and Ischemic Brain Is Controlled by Arteriolar Smooth Muscle Cell Contractility and Not by Capillary Pericytes. Neuron. 2015;87(1):95-110.
3. Wei HS, Kang H, Rasheed ID, Zhou S, Lou N, Gershteyn A, et al. Erythrocytes Are Oxygen-Sensing Regulators of the Cerebral Microcirculation. Neuron. 2016;91(4):851-62.
4. Grutzendler J, Nedergaard M. Cellular Control of Brain Capillary Blood Flow: In Vivo Imaging Veritas. Trends Neurosci. 2019;42(8):528-36.
5. Fernandez-Klett F, Offenhauser N, Dirnagl U, Priller J, Lindauer U. Pericytes in capillaries are contractile in vivo, but arterioles mediate functional hyperemia in the mouse brain. Proc Natl Acad Sci U S A. 2010;107(51):22290-5.
6. Kur J, Newman EA, Chan-Ling T. Cellular and physiological mechanisms underlying blood flow regulation in the retina and choroid in health and disease. Prog Retin Eye Res. 2012;31(5):377-406.
7. Grant RI, Hartmann DA, Underly RG, Berthiaume AA, Bhat NR, Shih AY. Organizational hierarchy and structural diversity of microvascular pericytes in adult mouse cortex. J Cereb Blood Flow Metab. 2019;39(3):411-25.
8. Lee S, Zeiger A, Maloney JM, Kotecki M, Van Vliet KJ, Herman IM. Pericyte actomyosin-mediated contraction at the cell-material interface can modulate the microvascular niche. J Phys Condens Matter. 2010;22(19):194115.
9. Hertz L, Lovatt D, Goldman SA, Nedergaard M. Adrenoceptors in brain: cellular gene expression and effects on astrocytic metabolism and [Ca(2+)]i. Neurochem Int. 2010;57(4):411-20.
10. Gunst SJ, Zhang W. Actin cytoskeletal dynamics in smooth muscle: a new paradigm for the regulation of smooth muscle contraction. Am J Physiol Cell Physiol. 2008;295(3):C576-87.
11. Rouget C-MB. Sur la contractilité capillaires sanguins. Comptes rendus de l'Académie des. Sciences 1879;88:916–918
12. Zimmermann K. Der feinere Bau der Blutkapillaren. Z Anat Entwicklungsgesch. 1923;68:29–109.
13. Trost A, Lange S, Schroedl F, Bruckner D, Motloch KA, Bogner B, et al. Brain and Retinal Pericytes: Origin, Function and Role. Frontiers in Cellular Neuroscience. 2016Apr;10. endnote

14. Armulik A, Genové G, Betsholtz C. Pericytes: Developmental, Physiological, and Pathological Perspectives, Problems, and Promises. Developmental Cell. 2011;21(2):193–215.

15. Armulik A, Abramsson A, Betsholtz C. Endothelial/Pericyte Interactions. Circulation Research. 2005;97(6):512–23.

16. Kim HR, Gallant C, Leavis PC, Gunst SJ, Morgan KG. Cytoskeletal remodeling in differentiated vascular smooth muscle is actin isoform dependent and stimulus dependent. Am J Physiol Cell Physiol. 2008;295(3):C768-78.

17. Armulik A, Genové G, Mäe M, Nisancioglu MH, Wallgard E, Niaudet C, et al. Pericytes regulate the blood–brain barrier. Nature. 2010;468(7323):557–61.

18. Dalkara T. Pericytes: A Novel Target to Improve Success of Recanalization Therapies. Stroke. 2019;50(10):2985-91.

19. Sweeney MD, Ayyadurai S, Zlokovic BV. Pericytes of the neurovascular unit: key functions and signaling pathways. Nat Neurosci. 2016;19(6):771-83.

20. Joyce NC, Haire MF, Palade GE. Contractile proteins in pericytes. I. Immunoperoxidase localization of tropomyosin. J Cell Biol. 1985;100(5):1379-86.

21. He L, Vanlandewijck M, Raschperger E, Andaloussi Mae M, Jung B, Lebouvier T, et al. Analysis of the brain mural cell transcriptome. Sci Rep. 2016;6:35108.

22. Krueger M, Bechmann I. CNS pericytes: Concepts, misconceptions, and a way out. Glia. 2010Jan;58(1):1–10.

23. Frank RN, Dutta S, Mancini MA. Pericyte coverage is greater in the retinal than in the cerebral capillaries of the rat. Invest Ophthalmol Vis Sci. 1987;28(7):1086-91.

24. Hamilton NB, Attwell D, Hall CN. Pericyte-mediated regulation of capillary diameter: a component of neurovascular coupling in health and disease. Front Neuroenergetics. 2010;2.

25. Mishra A, Reynolds JP, Chen Y, Gourine AV, Rusakov DA, Attwell D. Astrocytes mediate neurovascular signaling to capillary pericytes but not to arterioles. Nat Neurosci. 2016;19(12):1619-27.

26. Hall CN, Reynell C, Gesslein B, Hamilton NB, Mishra A, Sutherland BA, et al. Capillary pericytes regulate cerebral blood flow in health and disease. Nature. 2014;508(7494):55-60.

27. Rungta RL, Chaigneau E, Osmanski BF, Charpak S. Vascular Compartmentalization of Functional Hyperemia from the Synapse to the Pia. Neuron. 2018;99(2):362-75 e4.

28. Blinder P, Tsai PS, Kaufhold JP, Knutsen PM, Suhl H, Kleinfeld D. The cortical angiome: an interconnected vascular network with noncolumnar patterns of blood flow. Nat Neurosci. 2013;16(7):889-97.

29. Kureli G, Yilmaz-Ozcan S, Erdener SE, Donmez-Demir B, Yemisci M, Karatas H, et al. F-actin polymerization contributes to pericyte contractility in retinal capillaries. Exp Neurol. 2020;332:113392.

30. Peppiatt CM, Howarth C, Mobbs P, Attwell D. Bidirectional control of CNS capillary diameter by pericytes. Nature. 2006;443(7112):700-4.

31. Kisler K, Nelson AR, Montagne A, Zlokovic BV. Cerebral blood flow regulation and neurovascular dysfunction in Alzheimer disease. Nat Rev Neurosci. 2017;18(7):419-34.

32. Durham JT, Dulmovits BM, Cronk SM, Sheets AR, Herman IM. Pericyte chemomechanics and the angiogenic switch: insights into the pathogenesis of proliferative diabetic retinopathy? Invest Ophthalmol Vis Sci. 2015;56(6):3441-59.

33. Dalkara T, Arsava EM. Can restoring incomplete microcirculatory reperfusion improve stroke outcome after thrombolysis? J Cereb Blood Flow Metab. 2012;32(12):2091-9.

34. Erdener ŞE, Dalkara T. Small Vessels Are a Big Problem in Neurodegeneration and Neuroprotection. Frontiers in Neurology. 2019;10.

35. Yemisci M, Gursoy-Ozdemir Y, Vural A, Can A, Topalkara K, Dalkara T. Pericyte contraction induced by oxidative-nitrative stress impairs capillary reflow despite successful opening of an occluded cerebral artery. Nature Medicine. 2009;15(9):1031–7.

36. Alarcon-Martinez L, Yilmaz-Ozcan S, Yemisci M, Schallek J, Kilic K, Can A, et al. Capillary pericytes express alpha-smooth muscle actin, which requires prevention of filamentous-actin depolymerization for detection. Elife. 2018;7.

37. Alarcon-Martinez L, Yilmaz-Ozcan S, Yemisci M, Schallek J, Kilic K, Villafranca-Baughman D, et al. Retinal ischemia induces alpha-SMA-mediated capillary pericyte contraction coincident with perivascular glycogen depletion. Acta Neuropathol Commun. 2019;7(1):134.

38. Lee SH, Dominguez R. Regulation of actin cytoskeleton dynamics in cells. Mol Cells. 2010;29(4):311-25.

39. Pollard TD. Actin and Actin-Binding Proteins. Cold Spring Harbor Perspectives in Biology. 2016;8(8).

40. Condeelis J, Singer RH. How and why does beta-actin mRNA target? Biol Cell. 2005;97(1):97-110.

41. Dugina VB, Shagieva GS, Kopnin PB. Biological Role of Actin Isoforms in Mammalian Cells. Biochemistry (Mosc). 2019;84(6):583-92.

42. Perrin BJ, Ervasti JM. The actin gene family: function follows isoform. Cytoskeleton (Hoboken). 2010;67(10):630-4.

43. Crawford K, Flick R, Close L, Shelly D, Paul R, Bove K, et al. Mice lacking skeletal muscle actin show reduced muscle strength and growth deficits and die during the neonatal period. Mol Cell Biol. 2002;22(16):5887-96.

44. Kumar A, Crawford K, Close L, Madison M, Lorenz J, Doetschman T, et al. Rescue of cardiac alpha-actin-deficient mice by enteric smooth muscle gamma-actin. Proc Natl Acad Sci U S A. 1997;94(9):4406-11.

45. Shawlot W, Deng JM, Fohn LE, Behringer RR. Restricted beta-galactosidase expression of a hygromycin-lacZ gene targeted to the beta-actin locus and embryonic lethality of beta-actin mutant mice. Transgenic Res. 1998;7(2):95-103.

46. Schildmeyer LA, Braun R, Taffet G, Debiasi M, Burns AE, Bradley A, et al. Impaired vascular contractility and blood pressure homeostasis in the smooth muscle alpha-actin null mouse. FASEB J. 2000;14(14):2213-20.

47. Bunnell TM, Ervasti JM. Delayed embryonic development and impaired cell growth and survival in Actg1 null mice. Cytoskeleton (Hoboken). 2010;67(9):564-72.

48. Yao J, Sasaki Y, Wen Z, Bassell GJ, Zheng JQ. An essential role for beta-actin mRNA localization and translation in Ca2+-dependent growth cone guidance. Nat Neurosci. 2006;9(10):1265-73.

49. Herman IM, D'Amore PA. Microvascular pericytes contain muscle and nonmuscle actins. J Cell Biol. 1985;101(1):43-52.

50. Nehls V, Drenckhahn D. Heterogeneity of microvascular pericytes for smooth muscle type alpha-actin. J Cell Biol. 1991;113(1):147-54.

51. Vanlandewijck M, He L, Mae MA, Andrae J, Ando K, Del Gaudio F, et al. A molecular atlas of cell types and zonation in the brain vasculature. Nature. 2018;554(7693):475-80.

52. Mouse Brain Atlas [Internet]. [cited 2020Sep22]. Available from: http://mousebrain.org/

53. Boels PJ, Pfitzer G. Relaxant effect of phalloidin on Triton-skinned microvascular and other smooth muscle preparations. J Muscle Res Cell Motil. 1992;13(1):71-80.

54. Wegner A. Head to tail polymerization of actin. J Mol Biol. 1976;108(1):139-50.

55. Skruber K, Read TA, Vitriol EA. Reconsidering an active role for G-actin in cytoskeletal regulation. J Cell Sci. 2018;131(1).

56. Ohanian J, Pieri M, Ohanian V. Non-receptor tyrosine kinases and the actin cytoskeleton in contractile vascular smooth muscle. J Physiol. 2015;593(17):3807-14.

57. Kassianidou E, Kumar S. A biomechanical perspective on stress fiber structure and function. Biochim Biophys Acta. 2015;1853(11 Pt B):3065-74.

58. Kolyada AY, Riley KN, Herman IM. Rho GTPase signaling modulates cell shape and contractile phenotype in an isoactin-specific manner. Am J Physiol Cell Physiol. 2003;285(5):C1116-21.

59. DeNofrio D, Hoock TC, Herman IM. Functional sorting of actin isoforms in microvascular pericytes. J Cell Biol. 1989;109(1):191-202.

60. Tomasek JJ, Haaksma CJ, Schwartz RJ, Vuong DT, Zhang SX, Ash JD, et al. Deletion of smooth muscle alpha-actin alters blood-retina barrier permeability and retinal function. Invest Ophthalmol Vis Sci. 2006;47(6):2693-700.

61. Holzinger A, Blaas K. Actin-Dynamics in Plant Cells: The Function of Actin-Perturbing Substances: Jasplakinolide, Chondramides, Phalloidin, Cytochalasins, and Latrunculins. Methods Mol Biol. 2016;1365:243-61.

62. Coue M, Brenner SL, Spector I, Korn ED. Inhibition of actin polymerization by latrunculin A. FEBS Lett. 1987;213(2):316-8.

63. Flanagan MD, Lin S. Cytochalasins block actin filament elongation by binding to high affinity sites associated with F-actin. J Biol Chem. 1980;255(3):835-8.

64. Brown SS, Spudich JA. Mechanism of action of cytochalasin: evidence that it binds to actin filament ends. J Cell Biol. 1981;88(3):487-91.

65. Dancker P, Low I, Hasselbach W, Wieland T. Interaction of actin with phalloidin: polymerization and stabilization of F-actin. Biochim Biophys Acta. 1975;400(2):407-14.

66. Oda T, Namba K, Maeda Y. Position and orientation of phalloidin in F-actin determined by X-ray fiber diffraction analysis. Biophys J. 2005;88(4):2727-36.

67. Sawitzky H, Liebe S, Willingale-Theune J, Menzel D. The anti-proliferative agent jasplakinolide rearranges the actin cytoskeleton of plant cells. Eur J Cell Biol. 1999;78(6):424-33.

68. De La Cruz EM, Pollard TD. Transient kinetic analysis of rhodamine phalloidin binding to actin filaments. Biochemistry. 1994;33(48):14387-92.

69. Hitchcock SE. Actin deoxyroboncuclease I interaction. Depolymerization and nucleotide exchange. J Biol Chem. 1980;255(12):5668-73.

70. Odronitz F, Kollmar M. Drawing the tree of eukaryotic life based on the analysis of 2,269 manually annotated myosins from 328 species. Genome Biol. 2007;8(9):R196.

71. Sellers J. Myosins: OUP Oxford; 1999.

72. Heissler SM, Sellers JR. Various Themes of Myosin Regulation. J Mol Biol. 2016;428(9 Pt B):1927-46.

73. Rauscher AA, Gyimesi M, Kovacs M, Malnasi-Csizmadia A. Targeting Myosin by Blebbistatin Derivatives: Optimization and Pharmacological Potential. Trends Biochem Sci. 2018;43(9):700-13.

74. Lee KH, Sulbaran G, Yang S, Mun JY, Alamo L, Pinto A, et al. Interacting-heads motif has been conserved as a mechanism of myosin II inhibition since before the origin of animals. Proc Natl Acad Sci U S A. 2018;115(9):E1991-E2000.

75. Rawal L, Ali S, SpringerLink (Online service). Genome Analysis and Human Health. Available from: https://yale.idm.oclc.org/login?URL=http://dx.doi.org/10.1007/978-981-10-4298-0.

76. Vicente-Manzanares M, Ma X, Adelstein RS, Horwitz AR. Non-muscle myosin II takes centre stage in cell adhesion and migration. Nat Rev Mol Cell Biol. 2009;10(11):778-90.

77. Bandopadhyay R, Orte C, Lawrenson JG, Reid AR, De Silva S, Allt G. Contractile proteins in pericytes at the blood-brain and blood-retinal barriers. J Neurocytol. 2001;30(1):35-44.

78. Marieb EN, Hoehn K. Human Anatomy & Physiology: Pearson; 2013.

79. Somlyo AP, Somlyo AV. Signal transduction by G-proteins, rho-kinase and protein phosphatase to smooth muscle and non-muscle myosin II. J Physiol. 2000;522 Pt 2:177-85.

80. Kimura K, Ito M, Amano M, Chihara K, Fukata Y, Nakafuku M, et al. Regulation of myosin phosphatase by Rho and Rho-associated kinase (Rho-kinase). Science. 1996;273(5272):245-8.

81. Amano M, Ito M, Kimura K, Fukata Y, Chihara K, Nakano T, et al. Phosphorylation and activation of myosin by Rho-associated kinase (Rho-kinase). J Biol Chem. 1996;271(34):20246-9.

82. Maekawa M, Ishizaki T, Boku S, Watanabe N, Fujita A, Iwamatsu A, et al. Signaling from Rho to the actin cytoskeleton through protein kinases ROCK and LIM-kinase. Science. 1999;285(5429):895-8.

83. Kutcher ME, Herman IM. The pericyte: cellular regulator of microvascular blood flow. Microvasc Res. 2009;77(3):235-46.

84. Deng M, Deng L, Xue Y. MAP Kinase-Mediated and MLCK-Independent Phosphorylation of MLC20 in Smooth Muscle Cells, Current Basic and Pathological Approaches to the Function of Muscle Cells and Tissues - From Molecules to Humans, Haruo Sugi, IntechOpen, 2012, DOI: 10.5772/47732.

85. Lodish H, Berk A, Zipursky SL, et al. Molecular Cell Biology. 4th edition. New York: W. H. Freeman; 2000. Section 18.4, Muscle: A Specialized Contractile Machine. Available from: https://www.ncbi.nlm.nih.gov/books/NBK21670/

86. Huber F, Schnauss J, Ronicke S, Rauch P, Muller K, Futterer C, et al. Emergent complexity of the cytoskeleton: from single filaments to tissue. Adv Phys. 2013;62(1):1-112.

87. Zhang HM, Ji HH, Ni T, Ma RN, Wang A, Li XD. Characterization of Blebbistatin Inhibition of Smooth Muscle Myosin and Nonmuscle Myosin-2. Biochemistry. 2017;56(32):4235-43.

88. Kovacs M, Toth J, Hetenyi C, Malnasi-Csizmadia A, Sellers JR. Mechanism of blebbistatin inhibition of myosin II. J Biol Chem. 2004;279(34):35557-63.

89. Shu S, Liu X, Korn ED. Blebbistatin and blebbistatin-inactivated myosin II inhibit myosin II-independent processes in Dictyostelium. Proc Natl Acad Sci U S A. 2005;102(5):1472-7.

90. Bond LM, Tumbarello DA, Kendrick-Jones J, Buss F. Small-molecule inhibitors of myosin proteins. Future Med Chem. 2013;5(1):41-52.

91. Xiong Y, Wang C, Shi L, Wang L, Zhou Z, Chen D, et al. Myosin Light Chain Kinase: A Potential Target for Treatment of Inflammatory Diseases. Front Pharmacol. 2017;8:292.

92. Rucker HK, Wynder HJ, Thomas WE. Cellular mechanisms of CNS pericytes. Brain Res Bull. 2000;51(5):363-9.

93. Powner MB, Vevis K, McKenzie JA, Gandhi P, Jadeja S, Fruttiger M. Visualization of gene expression in whole mouse retina by in situ hybridization. Nat Protoc. 2012;7(6):1086-96.

94. Kornfield TE, Newman EA. Regulation of blood flow in the retinal trilaminar vascular network. J Neurosci. 2014;34(34):11504-13.

95. Schmetterer L, Kiel J. Ocular blood flow. New York: Springer; 2012.

96. Yu DY, Cringle SJ, Yu PK, Balaratnasingam C, Mehnert A, Sarunic MV, et al. Retinal capillary perfusion: Spatial and temporal heterogeneity. Prog Retin Eye Res. 2019;70:23-54.

97. Biesecker KR, Srienc AI, Shimoda AM, Agarwal A, Bergles DE, Kofuji P, et al. Glial Cell Calcium Signaling Mediates Capillary Regulation of Blood Flow in the Retina. J Neurosci. 2016;36(36):9435-45.

98. Chiu K, Chang RC, So KF. Intravitreous injection for establishing ocular diseases model. J Vis Exp. 2007(8):313.

99. Kaplan HJ, Chiang C-W, Chen J, Song S-K. Vitreous Volume of the Mouse Measured by Quantitative High-Resolution MRI. Investigative Ophthalmology & Visual Science. 2010;51(13):4414-.

100. Tremblay M, Lessard MR, Trepanier CA, Nicole PC, Nadeau L, Turcotte G. Stability of norepinephrine infusions prepared in dextrose and normal saline solutions. Can J Anaesth. 2008;55(3):163-7.,

101. Walker SE, Law S, Garland J, Fung E, Iazzetta J. Stability of norepinephrine solutions in normal saline and 5% dextrose in water. Can J Hosp Pharm. 2010;63(2):113-8.

102. Beloeil H, Mazoit JX, Benhamou D, Duranteau J. Norepinephrine kinetics and dynamics in septic shock and trauma patients. Br J Anaesth. 2005;95(6):782-8.

103. Straight AF, Cheung A, Limouze J, Chen I, Westwood NJ, Sellers JR, et al. Dissecting temporal and spatial control of cytokinesis with a myosin II Inhibitor. Science. 2003;299(5613):1743-7.

104. Wieland T. Peptides of poisonous Amanita mushrooms. New York: Springer-Verlag; 1986. xiv, 256 p. p.

105. Cramer LP, Briggs LJ, Dawe HR. Use of fluorescently labelled deoxyribonuclease I to spatially measure G-actin levels in migrating and non-migrating cells. Cell Motil Cytoskeleton. 2002;51(1):27-38.

106. Cinar O, Semiz O, Can A. Carbofuran Alters Centrosome and Spindle Organization, and Delays Cell Division in Oocytes and Mitotic Cells. Toxicological Sciences. 2015May;144(2):298–306.

107. Muyldermans S. Nanobodies: natural single-domain antibodies. Annu Rev Biochem. 2013;82:775-97.

108. Konig P, Krasteva G, Tag C, Konig IR, Arens C, Kummer W. FRET-CLSM and double-labeling indirect immunofluorescence to detect close association of proteins in tissue sections. Lab Invest. 2006;86(8):853-64.

109. Attwell D, Mishra A, Hall CN, O'Farrell FM, Dalkara T. What is a pericyte? J Cereb Blood Flow Metab. 2016;36(2):451-5.

110. Snapp EL, Hegde RS. Rational design and evaluation of FRET experiments to measure protein proximities in cells. Curr Protoc Cell Biol. 2006;Chapter 17:Unit 17 9.

111. Okamoto K-I, Hayashi Y. Visualization of F-actin and G-actin equilibrium using fluorescence resonance energy transfer (FRET) in cultured cells and neurons in slices. Nature Protocols. 2006;1(2):911–9.

112. Shrestha D, Jenei A, Nagy P, Vereb G, Szöllősi J. Understanding FRET as a Research Tool for Cellular Studies. International Journal of Molecular Sciences. 2015;16(12):6718–56.

113. Chen T, He B, Tao J, He Y, Deng H, Wang X, et al. Application of Forster Resonance Energy Transfer (FRET) technique to elucidate intracellular and In Vivo biofate of nanomedicines. Adv Drug Deliv Rev. 2019;143:177-205.

114. Black J, Dykes A, Thatcher S, Brown D, Bryda EC, Wright GL. FRET analysis of actin-myosin interaction in contracting rat aortic smooth muscle. Can J Physiol Pharmacol. 2009;87(5):327-36.

115. Kenworthy AK. Imaging Protein-Protein Interactions Using Fluorescence Resonance Energy Transfer Microscopy. Methods. 2001;24(3):289–96.

116. Mustafa S, Hannagan J, Rigby P, Pfleger K, Corry B. Quantitative Forster resonance energy transfer efficiency measurements using simultaneous spectral unmixing of excitation and emission spectra. J Biomed Opt. 2013;18(2):26024.

117. Ivanova E, Kovacs-Oller T, Sagdullaev BT. Vascular Pericyte Impairment and Connexin43 Gap Junction Deficit Contribute to Vasomotor Decline in Diabetic Retinopathy. J Neurosci. 2017;37(32):7580-94.

118. Tang DD. Critical role of actin-associated proteins in smooth muscle contraction, cell proliferation, airway hyperresponsiveness and airway remodeling. Respir Res. 2015;16:134.

119. Search gene expression in vascular single cells [Internet]. Single Cell RNA-seq Gene Expression Data. [cited 2020Sep22]. Available from: http://betsholtzlab.org/VascularSingleCells/database.html

120. Skalli O, Ropraz P, Trzeciak A, Benzonana G, Gillessen D, Gabbiani G. A monoclonal antibody against alpha-smooth muscle actin: a new probe for smooth muscle differentiation. The Journal of Cell Biology. 1986Jan;103(6):2787–96.

121. Splice variants - Mus_musculus - Ensembl genome browser 101. [cited 2020Sep22]. Available from: https://www.ensembl.org/Mus_musculus/Gene/Splice?db=core%3Bg

122. Lofgren M, Ekblad E, Morano I, Arner A. Nonmuscle Myosin motor of smooth muscle. J Gen Physiol. 2003;121(4):301-10.

123. Ravi Kant Avvari (June 14th 2019). Biomechanics of the Small Intestinal Contractions, Digestive System - Recent Advances, Xingshun Qi and Sam Koruth, IntechOpen, DOI: 10.5772/intechopen.86539. Available from: https://www.intechopen.com/books/digestive-system-recent-advances/biomechanics-of-the-small-intestinal-contractions

124. Redaelli A, Soncini M, Montevecchi FM. Myosin cross-bridge mechanics: geometrical determinants for continuous sliding. J Biomech. 2001;34(12):1607-17.

125. Rubenstein PA, Wen KK. NATure of actin amino-terminal acetylation. Proc Natl Acad Sci U S A. 2018;115(17):4314-6.

126. Cipolla MJ, Gokina NI, Osol G. Pressure-induced actin polymerization in vascular smooth muscle as a mechanism underlying myogenic behavior. FASEB J. 2002;16(1):72-6.

127. Tang DD, Tan J. Role of Crk-associated substrate in the regulation of vascular smooth muscle contraction. Hypertension. 2003;42(4):858-63.

128. Walsh MP, Cole WC. The role of actin filament dynamics in the myogenic response of cerebral resistance arteries. J Cereb Blood Flow Metab. 2013;33(1):1-12.

129. Moreno-Dominguez A, El-Yazbi AF, Zhu HL, Colinas O, Zhong XZ, Walsh EJ, et al. Cytoskeletal reorganization evoked by Rho-associated kinase- and protein kinase C-catalyzed phosphorylation of cofilin and heat shock protein 27, respectively,

contributes to myogenic constriction of rat cerebral arteries. J Biol Chem. 2014;289(30):20939-52.

130. Suzuki F, Taniguchi T, Nakamura S, Akagi Y, Kubota C, Satoh M, et al. Distribution of alpha-1 adrenoceptor subtypes in RNA and protein in rabbit eyes. Br J Pharmacol. 2002;135(3):600-8.

131. Bohmer T, Manicam C, Steege A, Michel MC, Pfeiffer N, Gericke A. The alpha(1)B -adrenoceptor subtype mediates adrenergic vasoconstriction in mouse retinal arterioles with damaged endothelium. Br J Pharmacol. 2014;171(16):3858-67.

132. Gericke A, Kordasz ML, Steege A, Sanbe A, Goloborodko E, Vetter JM, et al. Functional role of alpha1-adrenoceptor subtypes in murine ophthalmic arteries. Invest Ophthalmol Vis Sci. 2011;52(7):4795-9.

133. Mori A, Hanada M, Sakamoto K, Nakahara T, Ishii K. Noradrenaline contracts rat retinal arterioles via stimulation of alpha(1A)- and alpha(1D)-adrenoceptors. Eur J Pharmacol. 2011;673(1-3):65-9.

134. Sorriento D, Trimarco B, Iaccarino G. Adrenergic mechanism in the control of endothelial function. Transl Med UniSa. 2011;1:213-28.

135. Yu DY, Alder VA, Cringle SJ, Su EN, Yu PK. Vasoactivity of intraluminal and extraluminal agonists in perfused retinal arteries. Invest Ophthalmol Vis Sci. 1994;35(12):4087-99.

136. Butryn RK, Ruan H, Hull CM, Frank RN. Vasoactive agonists do not change the caliber of retinal capillaries of the rat. Microvasc Res. 1995;50(1):80-93.

137. Sears ML, Sherk TE. The Trabecular Effect of Noradrenalin in the Rabbit Eye. Investigative Ophthalmology & Visual Science. 1964;3(2):157-63.

138. Alarcon-Martinez L, Villafranca-Baughman D, Quintero H, Kacerovsky JB, Dotigny F, Murai KK, et al. Interpericyte tunnelling nanotubes regulate neurovascular coupling. Nature. 2020;585(7823):91-5.

139. Puro DG. Physiology and pathobiology of the pericyte-containing retinal microvasculature: new developments. Microcirculation. 2007;14(1):1-10.

140. Andre P, Saubamea B, Cochois-Guegan V, Marie-Claire C, Cattelotte J, Smirnova M, et al. Transport of biogenic amine neurotransmitters at the mouse blood-retina and blood-brain barriers by uptake1 and uptake2. J Cereb Blood Flow Metab. 2012;32(11):1989-2001.

141. Cotecchia S, Del Vescovo CD, Colella M, Caso S, Diviani D. The alpha1-adrenergic receptors in cardiac hypertrophy: signaling mechanisms and functional implications. Cell Signal. 2015;27(10):1984-93.

142. Shimokawa H, Rashid M. Development of Rho-kinase inhibitors for cardiovascular medicine. Trends Pharmacol Sci. 2007;28(6):296-302.

143. Fukata Y, Oshiro N, Kinoshita N, Kawano Y, Matsuoka Y, Bennett V, et al. Phosphorylation of adducin by Rho-kinase plays a crucial role in cell motility. J Cell Biol. 1999;145(2):347-61.

144. Oshiro N, Fukata Y, Kaibuchi K. Phosphorylation of moesin by rho-associated kinase (Rho-kinase) plays a crucial role in the formation of microvilli-like structures. J Biol Chem. 1998;273(52):34663-6.